

Hubbard and Kondo lattice models in two dimensions: A QMC study

Von der Fakultät für Physik der Universität Stuttgart
zur Erlangung der Würde eines
Doktors der Naturwissenschaften (Dr. rer. nat.)
genehmigte Abhandlung

Vorgelegt von

Martin Feldbacher

aus Graz (Österreich)

Hauptberichter: Prof. Dr. Fakher F. Assaad

Mitberichter: Prof. Dr. Roland Zeyher

Tag der mündlichen Prüfung: 11. September 2003

Institut für Theoretische Physik der Universität Stuttgart

2003

Contents

Abstract	IV
Zusammenfassung	VII
Introduction	1
1 Auxiliary field Quantum Monte Carlo	11
1.1 Introduction	11
1.2 Auxiliary field algorithm	13
1.3 Single particle Formalism	24
1.4 MC algorithm	33
1.5 Numerical stabilization	40
1.6 The Sign Problem	44
2 Kondo-Hubbard model	47
2.1 Introduction	47
2.2 Model	53
2.3 QMC	57
2.4 Mean-field approach	58
2.5 Magnetic Phase Diagram	65
2.6 Single particle spectral function.	67
2.7 Conclusion	71
3 Coexistence of s-wave SC and Antiferromagnetism	73
3.1 Introduction	73
3.2 Organic Superconductors	73

3.3	Model	77
3.4	Symmetries	79
3.5	QMC	82
3.6	Results	83
3.7	Conclusion	96
Conclusion		97
	Auxiliary field Quantum Monte Carlo	98
	Kondo-Hubbard model	98
	Coexistence of <i>s</i> -wave SC and Antiferromagnetism	99
A	QMC: Proofs	101
A.1	Scalar Product	101
A.2	Grand canonical Trace	102
A.3	$\det(1 + AB) = \det(1 + BA)$	103
B	QMC vs. Diagrams	105
C	Path integrals to Green's function	107
C.1	Grassmann variables	107
C.2	Finite temperature	110
C.3	Zero temperature limit	112
C.4	Generating functional at zero temperature	113
C.5	Wick theorem	114
D	Thermodynamics	117
D.1	Introduction	117
D.2	Convexity of a General Free Energy	118
D.3	Comments	120
E	Spin-Wave Theory	125
E.1	Easy axis	125
E.2	Easy Plane	126
Bibliography		128

Publications	139
Curriculum Vitae	140
Acknowledgments	141

Abstract

This thesis discusses mainly two Fermionic lattice systems, first a Kondo lattice with additional Hubbard interaction and second a Hubbard Hamiltonian augmented with additional spin and charge interactions.

The first chapter introduces the Quantum Monte Carlo technique, which is then employed to study the two respective systems. We present an innovation that allows to calculate time displaced Greens functions more efficiently. The calculation of imaginary-time-displaced correlation functions with the auxiliary-field projector quantum Monte Carlo algorithm provides valuable insight (such as spin and charge gaps) into the model under consideration. Assaad et al. [8] proposed a numerically stable method to compute those quantities. Although precise, their method is expensive in CPU time. Here we present an alternative approach which is an order of magnitude quicker, just as precise, and very simple to implement. The method is based on the observation that for a given auxiliary field the equal-time Green-function matrix G is a projector: $G^2 = G$.

In the second chapter we consider the Kondo lattice model in two dimensions at half filling. In addition to the Fermionic hopping integral t and the superexchange coupling J the role of a Coulomb repulsion U in the conduction band is investigated. We find the model to display a magnetic order-disorder transition in the U - J plane with a critical value of J_c which is decreasing as a function of U . The single-particle spectral function $A(\vec{k}, \omega)$ is computed across this transition. For all values of $J > 0$, and apart from shadow features present in the ordered state, $A(\vec{k}, \omega)$ remains insensitive to the magnetic phase transition with the first low-energy hole states residing at momenta $\vec{k} = (\pm\pi, \pm\pi)$. As $J \rightarrow 0$ the model maps onto the Hubbard Hamiltonian. Only in this limit does the low-energy spectral weight at $\vec{k} = (\pm\pi, \pm\pi)$ vanish such that the lowest energy hole states reside at wave vectors on the magnetic Brillouin-zone boundary. Thus we conclude that (i) the local screening of impurity spins determines the low-energy behavior of the spectral function and (ii) one cannot deform continuously the spectral function of the half-filled Hubbard model at $J = 0$ to that of the Kondo insulator at $J > J_c$. Our results are based on both $T = 0$ Quantum Monte-Carlo simulations and a bond-operator mean-field theory.

In the third chapter we investigate the phase diagram of a new model that exhibits a first order transition between s -wave superconducting and antiferromagnetic phases. The model, a generalized Hubbard model augmented with competing spin-spin and pair-pair interactions, was investigated using the projector quantum Monte Carlo method. Upon varying the Hubbard U from attractive to repulsive, we find a first order phase transition between superconducting and antiferromagnetic states.

Zusammenfassung

Die vorliegende Arbeit beschäftigt sich mit ausgewählten Themen zum Problem der stark wechselwirkenden Elektronensysteme. Genauer untersuchen wir Kondo- und Hubbard-Gittermodelle mit Quanten-Monte-Carlo (QMC) Methoden. Somit haben wir es im wesentlichen mit den folgenden drei Konzepten zu tun: starke Elektron-Elektron Korrelation, Gittermodelle und der Quanten-Monte-Carlo Technik als nicht perturbative Methode zur Berechnung von Korrelationsfunktionen auf endlichen Gittern.

Der bei weitem schwierigste der oben genannten Begriffe sind die elektronischen Korrelationseffekte bei starker Wechselwirkung. Der erste große Erfolg in der Festkörpertheorie kam in den frühen Tagen der Quantenmechanik mit dem Pauli-Prinzip und der Fermi-Dirac Verteilung. Daraus entwickelte sich eine einfache Theorie für nicht wechselwirkende Systeme mit dem Fermisee als Grundzustand und wohldefinierten Einteilchenanregungen. Der Fermisee beschreibt schon nicht triviale Korrelationen, da er das Pauli-Prinzip berücksichtigt, demzufolge zwei Elektronen nicht am gleichen Ort sein dürfen. Moderne Bandstrukturechnungen, der Struktur nach auch nur effektive Einteilchenmodelle, werden mit erstaunlichem Erfolg angewandt. Man kann Bandstrukturechnungen sogar noch so anpassen, dass sie Supraleitung und Bandmagnetismus korrekt wiedergeben, was nahelegt, daß auch diese Korrelationen mit dem Einteilchenbild verträglich sind. Wie ist das aber möglich, wenn im nackten Hamiltonoperator die Coulombabstoßung der Elektronen so groß ist? Und wie ist der Zusammenhang zwischen dem so erfolgreichen Quasiteilchenbild und dem ursprünglichen, stark wechselwirkenden System? Anders gefragt, was unterscheidet Systeme, die dem Quasiteilchenbild entsprechen, von jenen, die es verletzen? Die Fermiflüssigkeitstheorie [59] sucht eine Antwort vom störungstheoretischen Blickwinkel aus. Für dreidimensionale Systeme mit abgeschirmter Coulombwechselwirkung gilt dann laut Fermiflüssigkeitstheorie, daß das niederenergetische Spektrum gut durch ein System von schwach wechselwirkenden Quasiteilchen beschrieben wird. Die

Einelektron-Greensfunktion für k Zustände nahe der Fermifläche ist dann durch

$$G^{ret}(k, \omega) = \frac{Z_k}{\omega - \varepsilon_k - i\gamma_k} + G_{\text{incoh}}(k, \omega)$$

gegeben, wobei Z_k das Quasiteilchengewicht und γ_k die Dämpfung bezeichnen

$$\gamma_k(\omega) \propto (\omega - \varepsilon_k)^2 + \mathcal{O}(\omega^3). \quad (1)$$

Der inkohärente Hintergrund G_{incoh} ist eine glatte Funktion in ω mit verschwindendem Beitrag nahe der Fermifläche. Die Aussage (1) spiegelt die Tatsache wieder, daß der Phasenraum für die Coulombstreuung nahe der Fermifläche wie $(\omega - \mu)^2$ verschwindet. Die Fermiflüssigkeitstheorie demonstriert, daß die obige Quasiteilchenbeschreibung konsistent mit der diagrammatischen Störungstheorie ist [67, 21]. Weiters beweist das Luttinger Theorem [66], dass das Fermi-Volumen in jeder Ordnung Störungstheorie invariant ist. Daraus folgt, daß das Fermiflüssigkeitsverhalten garantiert ist, solange die Störungstheorie konvergiert. Umgekehrt ist es natürlich möglich Fermiflüssigkeitsverhalten zu beobachten, auch wenn die Störungstheorie nicht konvergiert. D.h. Fermiflüssigkeitsverhalten ist viel allgemeiner als Störungstheorie um den Grenzfall freier Elektronen.

Die wesentlichen Aussagen der Fermiflüssigkeitstheorie sind direkt mit der Phasenraumeinschränkung verbunden. Jedoch verbleibt eine möglicherweise große Entartung, die mit den k -Zuständen an der Fermifläche verbunden ist, und zu Fermiflächeninstabilitäten führen kann. Falls eine Zweiteilchenwechselwirkung systematisch Elektronenpaare an der Fermifläche koppelt, wird die Störungstheorie zusammenbrechen. Beispiele für solche Instabilitäten sind die Cooper-Instabilität, das sogenannte “nesting”, die Kohn-Luttinger Instabilität und die $2k_F$ Instabilität von eindimensionalen Systemen, die der Phänomenologie der Luttingerflüssigkeit zugrunde liegt. Diese Instabilitäten können zu geordneten Tieftemperaturphasen führen, wobei die Ordnungstemperatur drei oder vier Größenordnungen kleiner ist als die Fermitemperatur. Diese subtile Umordnung des Niederenergiebereichs hin zu einem geordneten Zustand ist sowohl für analytische als auch numerische Methoden eine Herausforderung.

Typischerweise wird der Begriff “stark korreliert” für Systeme gebraucht, die mit Bandstrukturmethoden nur schlecht zu beschreiben sind. Eine Liste von typischen, stark korrelierten Materialien und Phänomenen enthält jedenfalls:

- Übergangsmetalloxide und den Mott-Übergang

- Selten-Erd Verbindungen und Kondo-Physik
- Fraktionale Quanten-Hall Effekt
- Luttinger Flüssigkeiten (Eindimensionale Systeme)

Als Prototyp für starke Korrelationen kann der Mottisolator gelten. Mott hat schon sehr früh erkannt [77], daß Elektronen, die sich in einem halbgefüllten Band bewegen, sich gegenseitig behindern, was bei starke Coulombabstoßung zu vollständiger Lokalisierung führen kann. Der Wettbewerb zwischen kinetischer Energie (Delokalisierung) und Coulombenergie (Lokalisierung) führt zum Mott-Hubbard Metal-Isolator Übergang. Als Modell für den Mott Übergang formulierte Hubbard [47] das stark vereinfachte Gittermodell

$$H_U = -t \sum_{\langle i,j \rangle, \sigma} \left(c_{i,\sigma}^\dagger c_{j,\sigma} + H.c. \right) + U \sum_{\mathbf{i}} n_{i,\uparrow} n_{i,\downarrow}. \quad (2)$$

Die Freiheitsgrade in der Einheitszelle i werden auf ein einziges Orbital c_i^\dagger eingeschränkt und die kinetische Energie wird durch einen einzigen Parameter t beschrieben. Von der langreichweitigen Coulomb-Wechselwirkung wird ausschließlich die lokale Komponente berücksichtigt. Dieses vereinfachte Gittersystem dient als minimales Modellsystem um das Phasendiagramm des Mottübergangs zu studieren. Der Vorzug einer solchen Vorgehensweise besteht darin, daß man mit Gleichung (2) ein Benchmark System definiert hat. Eine Lösung desselben steht aber immer noch aus! Einige exakte Resultate konnten jedoch für das Hubbard-Modell bewiesen werden. In einer Dimension kann die Hubbardkette mit Betheansatzmethoden exakt gelöst werden [32]. Und in zwei Dimensionen gibt Quanten-Monte-Carlo “numerisch exakte” Resultate für spezielle Punkte im Phasendiagramm, wie z.B. die isolierende Phase bei halber Füllung. Die Einteilchen-Zustandsdichte illustriert den Unterschied zum Quasiteilchenbild. Wird das Hubbard U vergrößert, entwickelt sich die Zustandsdichte in einen Quasiteilchenpeak bei niedriger Energie und die zwei Hubbardbänder bei hohen Energien. Eine komplexe Struktur der Einteilchen-Spektralfunktion ist wesentliches Merkmal von stark korrelierten Systemen. Ein weiteres Beispiel ist das eindimensionale Luttinger Modell [68, 73], bei dem die Quasiteilchenpeaks mit ihrer Polsingularität vollständig verschwinden und in der Greensfunktion zwei separate Potenzsingularitäten für Spin- und Ladungsanregungen zusammen mit einem Anregungskontinuum auftauchen.

Stark korrelierte Systeme können heute allgemein nur durch verschiedene Näherungen behandelt werden. Jenseits der perturbativen Näherungen, die nur für kleine Störungen kontrollierbar sind, benützen alle gebräuchlichen Näherungen selbstkonsistente Schemata. Damit können sie flexibler als reine Störungstheorie eingesetzt werden, sind zugleich aber auch vollkommen unkontrollierte Näherungen und die Struktur der selbstkonsistenten Gleichungen bestimmt in hohem Maße den Charakter der Lösungen. Die Kohn-Sham Gleichungen in der Dichtefunktionaltheorie (LDA) sind wie die Hartree-Fock Gleichungen Beispiele für Theorien, die von Anfang an auf das Quasiteilchenbild eingeschränkt sind. Der Versuch, starke Korrelationen *ad hoc* in Bandstrukturechnungen einzubauen, führt zu LDA+U [5] und LDA + DMFT [4], wobei die dynamische Molekularfeldtheorie (DMFT) die exakte Lösung des Anderson Störstellenproblems mit räumlicher Molekularfeldtheorie verbindet, und im Limes von unendlich vielen Dimensionen exakt wird [35]. Eine andere Möglichkeit sind selbstkonsistente Gleichungen “höherer Ordnung”, wie bei Bickers [13] (FLEX) und Tremblay [2], wobei auf die Einhaltung von Erhaltungssätzen geachtet werden muss. Neue “funktionale” Renormierungsgruppenmethoden erlauben im Regime schwacher Kopplung auch *kontrollierte* Näherungen [39]. Andere Versuche, starke Korrelationseffekte im Hubbard Modell zu beschreiben, umfassen die Gutzwiller Methode [38, 15] und “slave particle” Rechnungen [19]. Zusammenfassend kann man sagen, daß mit der Ausnahme von Schwachkopplungs RG alle oben genannten Methoden unkontrollierte Näherungen sind. Abgesehen von den wenigen exakt lösbaren Modellen, stellen also die “numerisch exakten” Rechnungen die einzigen verlässlichen Resultate zur Verfügung. Leider muss man aber auch betonen, daß die zwei wichtigsten numerischen Verfahren, nämlich die Dichte-Matrix Renormierungsgruppe (DMRG) und Quanten-Monte-Carlo, unter eigenen schweren Einschränkungen leiden. Beide sind auf relativ kleine Systemgrößen beschränkt. Mit DMRG kann man darüber hinaus nur eindimensionale Systeme behandeln und QMC funktioniert nur für sehr spezielle Wechselwirkungen, die eine vorzeichenfreie Simulation erlauben.

Nun wenden wir uns den Materialien zu. Es wurde schon seit langem erkannt, daß Bandstrukturtheorie nicht in der Lage ist Übergangsmetalloxide und Seltenerdverbindungen korrekt zu beschreiben. Zusammengenommen stellen diese beiden Gruppen die Mehrzahl der stark korrelierten Materialien mit ihren faszinierenden Eigenschaften, wie der großen effektiven Masse, dem Mott-Hubbard Metall-Isolator Übergang, Schwerfermi-

on Verhalten und der Hochtemperatur-Supraleitung. Das generische Bild wird von den stark lokalisierten d -Orbitalen für die Übergangsmetalle und den f -Orbitalen für die Seltenerdverbindungen bestimmt. Für die einfachen Übergangsmetalle wie Kupfer liegen diese lokalisierten Bänder weit unterhalb der Fermienergie und nehmen nicht an niederenergetischen Anregungen teil. Befindet sich das gleiche Kupferatom jedoch in einer Oxidverbindung, so gibt es sein s -Elektron an den Sauerstoff ab und die d -Elektronen befinden sich nun auf Fermienergie und hybridisieren mit den Sauerstoffnachbarn. Somit können die ursprünglich lokalisierten d -Elektronen nun auf die Nachbarplätze hüpfen. Die starken Korrelationen sind Folge dieses Wechselspiels von Coulombabstoßung auf den stark lokalen Orbitalen und der kinetischen Energie, die mit dem Hüpfen zwischen Sauerstoff- und Metallplätzen verbunden ist. Die Elektronen müssen sich bewegen, um ihre kinetische Energie zu minimieren, ein Prozess der mit der Quasiteilchendisipation verbunden ist. Zugleich versuchen dieselben Elektronen, sich auf den stark lokalisierten Orbitalen aus dem Weg zu gehen.

Bei den Übergangsmetallen sind die Kupferoxide (i.e. $\text{La}_{2-x}\text{Sr}_x\text{CuO}_4$) wegen ihrer bekannten Hoch- T_c Supraleitung [11] hervorzuheben; bei den Vanadaten V_2O_3 , das den klassischen Fall eines Hubbard-Mott Isolators darstellt und bei den Manganaten das $\text{Nd}_{1-x}\text{Sr}_x\text{MnO}_3$, ein Doppelaustauschsystem, das orbitale Ordnung entwickeln kann. Die Klasse der Schwerfermionensysteme wird durch das $\text{Ce}_x\text{La}_{1-x}\text{Cu}_6$ sehr gut repräsentiert, wobei das $\text{Ce-}f$ Elektron die wesentliche Rolle spielt. Im Grenzfall hoher Verdünnung und niedriger Cer-Konzentration wird ein Störstellen-Kondoeffekt beobachtet, wohingegen das reine CeCu_6 bei Temperaturen unter 0.1K ein schweres Quasiteilchenband entwickelt.

Eine ganz andere Klasse von Materialien, in denen ebenfalls stark korreliertes Verhalten beobachtet wird, sind die organischen Systeme mit π -Leitungselektronen, wie zum Beispiel die κ -(BEDT-TTF) $_2$ -X, mit ausgeprägt zweidimensionaler Struktur [60]. Den Grundbaustein bilden hier die BEDT-TTF Moleküle und die metallischen Eigenschaften können auf Basis der BEDT-TTF Molekülorbitale gut verstanden werden. Bedenkt man die Komplexität der Moleküle, funktioniert die “tight-binding” Näherung erstaunlich gut und es stellt sich die Frage, ob sich Korrelationseffekte ebenfalls auf solch einfachem Niveau einbauen lassen.

In dieser Arbeit werden einige zweidimensionale fermionische Gittermodelle untersucht, die auf dem Hubbard (2) und dem Kondo-Gittermodell (3) aufbauen. So wie das

Hubbard Modell ursprünglich zur Beschreibung des Metall-Isolator Übergangs entwickelt wurde, dient das Kondo-Gittermodell als generisches Modell für die Schwerfermionsysteme. In dieser Arbeit werden generell zweidimensionale Gitter untersucht. Die Dimensionalität bestimmt besonders die geordneten Tieftemperaturphasen. Zum Beispiel wurde das 2D Hubbard Modell intensiv als Prototyp für die Hoch- T_c Supraleitung untersucht und experimentell zeigen $\text{La}_{2-x}\text{Sr}_x\text{CuO}_4$ oder $\kappa\text{-(BEDT-TTF)}_2\text{-X}$ ausgeprägte Schichtstruktur. Auf der numerischen Seite sind Quanten-Monte-Carlo Techniken besser zum Studium zweidimensionaler als eindimensionaler Systeme geeignet, für die numerische RG Methoden besser geeignet scheinen. Dreidimensionale Systeme sind andererseits für eine QMC Rechnung immer noch eine Herausforderung, da bei fermionischen Monte-Carlo Algorithmen die typische Gittergröße 500 Plätze nicht übersteigt, was in drei Dimensionen maximal ein $8 \times 8 \times 8$ Gitter zuläßt.

Aufbau

Der Hauptteil der Arbeit ist folgendermaßen gegliedert:

- Im ersten Kapitel wird die verwendete Methode, nämlich Determinanten-Quanten-Monte-Carlo im Detail eingeführt. Monte Carlo Techniken haben eine lange Tradition in der klassischen statistischen Physik, wo sie eine stochastische Darstellung der Zustandssumme ermöglichen. Der Grundgedanke besteht darin, daß das Boltzmanngewicht einer einzelnen Konfiguration immer berechenbar ist. Nur die vollständige Summation aller möglichen Konfigurationen wird durch deren Anzahl, die exponentiell mit der Systemgröße wächst, unmöglich. In der Monte-Carlo Simulation ersetzt man nun die exakte Summe durch die Summation einer zufällig gewählten Untermenge. Damit stellen Monte-Carlo Resultate statistische Schätzwerte dar, und die Genauigkeit der Rechnung wird durch einen Fehlerbalken angezeigt. Dieser Fehler skaliert wie $1/\sqrt{\text{CPU-Zeit}}$ was einer systematischen Näherungen der Summe weit überlegen ist. Für *Quanten*-Monte-Carlo gelten die gleichen Überlegungen, nachdem die quantenmechanische Zustandssumme, umgeschrieben als Pfadintegral auf der imaginären Zeitachse, formal equivalent zu einem klassischen statistischen Problem erscheint. Bei fermionischen Problemen taucht dabei aber das schwerwiegende Vorzeichenproblem auf, wonach das statistische Gewicht einzelner Konfigu-

rationen oder Beiträge zum Pfadintegral negativ oder komplex werden. Dann gibt es aber kein Kriterium für wichtige und unwichtige Konfigurationen nach dem Gewicht mehr und die Monte-Carlo Simulation funktioniert nicht länger. Eine spezielle Klasse fermionischer Systeme leidet aber nicht unter diesem Vorzeichenproblem, nämlich Systeme mit attraktiver Wechselwirkung. Weiters muss das Pfadintegral noch mittels Hubbard-Stratonovich Transformation konstruiert werden. Der daraus resultierende BSS Algorithmus [14] basiert auf auf Slaterdeterminanten. Unter speziellen Symmetriebedingungen, nämlich halber Füllung und bipartitem Gitter, ist es möglich das attraktive und repulsive Hubbard Modell aufeinander abzubilden. Damit ist möglich, wenigstens diesen speziellen Punkt des repulsiven Phasendiagramms zu untersuchen. Ein großer Vorzug bei Determinanten-Monte-Carlo ist die Möglichkeit, praktisch jede beliebige Korrelationsfunktion für alle imaginäre Zeiten zu berechnen. Um die gewünschten dynamischen Informationen zu gewinnen, wird mit Hilfe der “Maximum Entropy” Methode noch eine analytische Fortsetzung zu reellen Frequenzen unternommen. Im Detail wird noch eine neue Methode vorgestellt, eben diese zeitabhängigen Greensfunktionen zu “messen” [28]. Assaad et. al. [8] haben ein numerisch stabiles Verfahren zur Berechnung dieser zeitabhängigen Greensfunktionen vorgeschlagen, das jedoch sehr viel CPU-Zeit benötigt. Hier wird eine alternative Methode diskutiert, die eine Größenordnung schneller, ebenso genau und einfacher zu implementieren ist. Die neue Methode beruht auf der Beobachtung, daß bei gegebenen Hubbard-Stratonovich Feld die Matrix der Greensfunktion G die Projektoreigenschaft $G^2 = G$ besitzt. Zuletzt wird noch der Hirsch-Fye Algorithmus und die zugehörige Dyson Gleichung diskutiert, die eine konzeptionelle Vereinigung von BSS und Hirsch-Fye Störstellenalgorithmus erlaubt.

- Im zweiten Kapitel wird zunächst das Kondo-Gittermodell eingeführt

$$H_{KLM} = -t \sum_{\langle i,j \rangle, \sigma} \left(c_{i,\sigma}^\dagger c_{j,\sigma} + H.c. \right) + J \sum_{\mathbf{i}} \vec{S}_{i,c} \vec{S}_{i,f}, \quad (3)$$

das erst seit kurzem mit Determinanten-QMC untersucht werden kann, nachdem eine vorzeichenfreie Formulierung gefunden wurde [7]. Das Kondo-Gittermodell fungiert als das minimale Modell zur Beschreibung von Schwerfermionsystemen und beschreibt die Wechselwirkung des Leitungsbands mit lokalisierten f -Orbitalen. In Folge der starken Coulomb Abstoßung sind die f -Orbitale nur einfach besetzt und

Ladungsfluktuationen werden unterdrückt. Im Grenzfall verbleibt nur der Freiheitsgrad eines f -Spins, der mit antiferromagnetischem Austausch J an die Leitungselektronen ankoppelt. Es wird vermutet, daß ein solches Kondo-Gittermodell verschiedene Aspekte der Schwerfermion-Physik beschreibt. Zuerst wird der Übergang von freien zu abgeschirmten f -Spins bei einer Temperaturskala der Störstellen-Kondotemperatur T_K gefunden. Zum zweiten ist eine effektive Ruderman-Kittel Wechselwirkung zwischen den f -Spins enthalten, die über die Spinsuszeptibilität der Leitungselektronen vermittelt wird, und als verantwortlicher Mechanismus für die vielen magnetisch geordneten Phasen bei den Schwerfermion-Materialien angesehen wird. Drittens nimmt man noch an, daß der Grundzustand des Kondo-Gittermodells eine Fermiflüssigkeit mit extrem schwerem Quasiteilchenband ist, eben das Charakteristikum der schweren Fermionen. Damit verhalten sich die niederenergetischen Anregungen im Kondo-Modell sehr unterschiedlich von jenen im Hubbard-Modell. In diesem Kapitel untersuche wir ein Kondo-Gittermodell mit zusätzlicher Hubbard Wechselwirkung für die Leitungselektronen ($UKLM$), wobei der Schwerpunkt auf der Untersuchung der Dynamik der Einlochbewegung liegt. Um kein Vorzeichenproblem zu bekommen, können wir das Modell nur bei halber Füllung studieren. Auf einem quadratischen Gitter (bipartit) werden aber sowohl das Kondo- als auch das Hubbard-Modell schon bei schwacher Kopplung einen antiferromagnetischen, isolierenden Grundzustand haben. Im Hubbard-Modell kann man von einer Spindichtewelle sprechen und beim Kondo-Gittermodell ist der Ursprung des Antiferromagnetismus die RKKY Wechselwirkung. Aber die Einteilchen-Spektralfunktionen sind sehr unterschiedlich. Ein wichtiges Kriterium bei der Beschreibung der Einteilchendispersion ist der k -Vektor minimaler Energie. Im Hubbard Modell liegt er genau bei $k = (\pi/2, \pi/2)$, beim Kondogitter-Modell wird er jedoch am Zonenrand, also bei $k = (\pi, \pi)$ gefunden. Im $UKLM$ sind beide Wechselwirkungen vorhanden und es ist nicht klar wie sich die zwei vollständig unterschiedlichen Dispersionen von Hubbard und Kondo Modell verbinden. Unser Resultat zeigt, daß sich zwei Bänder ausprägen, von denen das eine der typischen Kondo, das andere der Hubbardform folgt. Bei $k = (\pi, \pi)$ verhalten sich die Gewichte dieser zwei Bänder qualitativ wie die Stärke der Wechselwirkungen J und U . Daraus folgt aber, daß bei endlichen J die Ladungslücke vom kondoartigen Dispersionszweig bestimmt wird. Weiters

zeigt unser Kondogitter-Modell einen quantenkritischen Punkt, der vom Wechselspiel von RKKY Magnetismus und der Ausbildung von lokalen Kondo Singlets bei großen J herrührt. Das zugehörige Phasendiagramm in Abhängigkeit von U und J wurde bestimmt.

- Im dritten und letzten Kapitel untersuchen wir ein attraktives Hubbard-Modell, wieder in der einfachen Geometrie des Quadratgitters. Die lokale Hubbard Wechselwirkung wird durch nächste Nachbar Spin-Spin, Paar-Paar und Dichte-Dichte Wechselwirkung ergänzt. Diese Wechselwirkungen werden durch einen einzigen t_p Term in der Gestalt eines quadrierten Hüpfterms beschrieben. Das Modell hat drei veränderbare Parameter und man kann somit ein reichhaltiges Phasendiagramm erwarten. Wir konzentrieren uns hier auf zwei Quantenphasenübergänge. Erstens finden wir einen Punkt mit Koexistenz von Antiferromagnetismus und Supraleitung. Durch Variation von dem Hubbard Parameter U findet sich diese Koexistenz genau am Phasenübergangspunkt erster Ordnung zwischen Magnetismus und Supraleitung. Vor kurzem wurde ein solcher Übergang erster Ordnung zwischen Antiferromagnetismus und Supraleitung bei dem organischen Supraleiter κ -(BEDT-TTF)-Cl [61] entdeckt. Wir schlagen unser Modell als geeignete Beschreibung dieser Tieftemperaturphasen vor, wobei die Spin und Ladungsterme durch eine Elektron-Phonon Wechselwirkung vom Su-Schrieffer-Heeger Typ [98] erzeugt werden können. Der zweite Quantenphasenübergang beschreibt den Wechsel von einem Zustand mit Ladungsdichtewelle zu einem Supraleiter. In der analogen Formulierung mit Spins bedeutet das den Übergang von “easy axis” zu “easy plane” Ordnung. Beim Übergang durch den isotropen Heisenberg Punkt beobachten wir das typische Verhalten von einem Übergang zweiter Ordnung, obwohl die Orientierung des Ordnungsparameters diskontinuierlich von der z -Achse in die Ebene wechselt, was normalerweise auf einen Übergang erster Ordnung hinweisen würde.

Introduction

In the present work we will discuss selected topics in the field of strongly correlated electron systems. In particular we will study Kondo and Hubbard lattice models using quantum Monte Carlo (QMC) methods. Thus we have to introduce three concepts: strong electron-electron correlations, lattice Hamiltonians and quantum Monte Carlo as a non-perturbative approach to calculate correlation functions on finite lattices.

By far the most difficult notion is that of strongly correlated electron systems. The first success in the theory of metals and insulators came in the early days of quantum mechanics with the introduction of the Pauli exclusion principle and Fermi-Dirac statistics. According to these principles the ground state of the non-interacting electron system is described by a Fermi sea in the form of a single Slater determinant with well defined single particle excitations. Such a state includes already many interesting correlations, such as the exchange hole due to the Pauli principle. Band structure calculations, which seek a solution within this single particle picture, have been used with remarkable success. Suitably adapted, they even describe superconductivity and magnetically ordered phases, which implies that all these correlations are compatible with a single particle picture. But certainly the bare Hamiltonian of a highly degenerate electron system is always strongly interacting. Is it possible to understand how the quasiparticle picture emerges from an initially strongly interacting system? This should help to understand what happens in “strongly correlated” that violates the quasi particle picture. Fermi liquid theory [59] addresses this question from a perturbative point of view. For a three dimensional system with a screened Coulomb interaction Fermi liquid theory states that the low lying energy spectrum is well described by system of weakly interacting quasi particles. Then for k states close to the Fermi surface the single electron Green’s function

will be given by

$$G^{ret}(k, \omega) = \frac{Z_k}{\omega - \varepsilon_k - i\gamma_k} + G_{\text{incoh}}(k, \omega) \quad (4)$$

with the quasiparticle weight Z_k and a single particle decay rate γ_k

$$\gamma_k(\omega) \propto (\omega - \varepsilon_k)^2 + \mathcal{O}(\omega^3). \quad (5)$$

The incoherent background G_{incoh} is a smooth function in ω with negligible contribution close to the Fermi surface. The statement (5) reflects the fact that the phase space available for the Coulomb interaction vanishes as $(\omega - \mu)^2$ on approaching the Fermi surface. Fermi liquid theory is able to demonstrate that the above quasi particle description is consistent with perturbation theory [67, 21]. Furthermore the Luttinger theorem [66] proves to all orders in perturbation theory that the Fermi volume does not change. Thus, as long as the perturbation series converges, Fermi liquid behavior is granted. Of course the converse is not true and we may still observe a Fermi liquid when the series does not converge. In this way, Fermi liquid behavior is much more general than the scope of perturbation theory.

The central achievement in Fermi liquid theory was due to the restriction of phase space to states close to the Fermi surface. But there is still a huge degeneracy associated with k -states on the Fermi surface which can give rise to Fermi surface instabilities. When a two particle interaction couples systematically pairs of Fermi surface states, perturbation theory must break down. Examples of such divergencies are the famous Cooper instability, nesting instability, Kohn-Luttinger instability [56] and the $2k_F$ instability of a one dimensional system which causes the transition to the Luttinger liquid. Such instabilities may generate low temperature ordered phases at energy scales which can be three to four orders of magnitude smaller than the Fermi temperature. The subtle rearrangement of the low energy sector into an ordered state is a challenge for both analytical and numerical methods.

One typically reserves the label “strongly correlated” to systems which are not well described by band structure calculations. A list of strongly correlated phenomena includes:

- Transition metal oxides and the Mott transition
- Rare Earth compounds and Kondo physics

- Fractional Quantum Hall effect
- Luttinger liquids (one dimensional systems)

The Mott insulator is the prototype scenario for strong electron correlations. It has been realized early by Mott [77] that electrons moving in half filled bands may be entirely localized when the on-site Coulomb repulsion becomes too strong and blocks electronic motion. The competition between delocalization due to the kinetic energy and localization in order to avoid Coulomb repulsion leads to the Mott-Hubbard metal insulator transition. In order to make any progress Hubbard [47] introduced an oversimplified lattice Hamiltonian

$$H_U = -t \sum_{\langle \mathbf{i}, \mathbf{j} \rangle, \sigma} \left(c_{\mathbf{i}, \sigma}^\dagger c_{\mathbf{j}, \sigma} + H.c. \right) + U \sum_{\mathbf{i}} n_{\mathbf{i}, \uparrow} n_{\mathbf{i}, \downarrow}. \quad (6)$$

The degrees of freedom in the whole unit cell i are restricted to a single orbital c^\dagger and the kinetic energy is modeled by a single tight binding parameter t . Only the local component of the long-range Coulomb interaction, given by $U n_{i, \uparrow} n_{i, \downarrow}$, is retained. Such a simplified lattice Hamiltonian serves as a minimal model to study the phase diagram of the Mott transition. The merit of such a reduced lattice formulation is to define a clear benchmark problem. Unfortunately, the present day status is such that we still fail to solve this benchmark problem. Only a few exact results on the Hubbard model are established. In the one dimensional Hubbard chain the ground state can be constructed with Bethe Ansatz techniques [32]. And in two dimensions quantum Monte Carlo gives “numerically exact” results at some special points in the phase diagram such as the insulating phase at half filling. The single particle spectral function in the Hubbard model illustrates the deviation from the quasi particle picture. Upon increasing U the quasi particle peak develops into a low energy quasiparticle with reduced weight and a high energy incoherent peak. A complex structure in the single particle spectral function is a key feature of strongly correlated systems. Another example is provided by the one dimensional Luttinger model [68, 73] where the quasi particle peaks disappear completely and the pole singularity in the Green’s function is replaced by two separate power law singularities for spin and charge excitations and a continuum with compact support.

In order to resolve the challenging puzzles of strongly correlated systems one usually has to resort to some approximation. Apart from perturbative calculations which

are controlled yet limited to small deviations from the unperturbed solution, the largest number of approximations are self consistent schemes. These are nonperturbative, but uncontrolled approximations and the structure of the self consistent equation imposes to a large degree the character of the possible solutions. The Kohn-Sham equations in local density approximation (LDA) and the Hartree-Fock mean field equations are examples where the solution is naturally restricted to the quasiparticle picture.¹ Some *ad hoc* attempts to include strong correlation effects into the otherwise successful band structure calculations include LDA+U [5] and LDA + DMFT [4], where dynamical mean-field theory (DMFT) combines the exact calculation of a single impurity model with a spatial mean field approach and becomes exact in infinite dimensions [35]. Another possibility is to consider “higher order” self consistent equations. The conserving approximations of Bickers [13] (FLEX) and Tremblay [2] are examples of such an approach. Recently, non-perturbative and *controlled* approximations have been developed in the form of functional RG methods [39]. Other attempts to account for the strong local correlation effects in the Hubbard model include the Gutzwiller approximation [38, 15] and slave particle calculations [19]. To summarize, it is only fair to say that with the exception of weak-coupling RG, all above methods are uncontrolled approximations. Apart from the few exactly solvable models “numerically exact” methods are the only calculations that give reliable results. Unfortunately, the two most prominent numerical techniques, the density-matrix renormalization group (DMRG) and quantum Monte Carlo (QMC), suffer from other severe shortcomings. First, they are restricted to small system sizes. Worse, DMRG works well only for one dimensional systems, and QMC applies only to a few systems which allow a sign free simulation.

Now we turn our attention to materials. It has been long recognized, that band structure theory fails to describe transition metal oxides and rare earth compounds. Taken together these two groups constitute a large class of strongly correlated materials with such diverse properties as large effective mass, a Mott-Hubbard metal insulator transition, heavy fermion behavior and high temperature superconductivity. The generic scenario are well localized d -orbitals in transition metals and similar localized f -orbitals

¹Mean-field theory works well for an ordered ground state, which justifies mean-field decoupling with respect to the order parameter. This is not the case for the generic Mott insulator with no spin or charge order.

in the rare earth compounds. In a simple transition metal such as Cu, these localized bands are well below the Fermi level and do not participate in low energy excitations. But in the transition metal oxides the metal gives up all the s -electrons to the oxygen and the outermost d -orbitals are found at the Fermi level where they also hybridize with their oxygen neighbors. Thus, the originally localized orbitals gained a sizeable hopping amplitude to some neighboring orbitals. Strong correlations arise from the interplay of Coulomb repulsion on the localized orbital and the kinetic energy from hopping between metal and oxygen sites. Electrons have to move around in order to reduce their kinetic energy which generates a quasi particle dispersion. At the same time these electrons try to avoid each other on the localized d -orbitals.

A few prominent examples in the wide class of transition metal compounds include the copper oxides (i.e. $\text{La}_{2-x}\text{Sr}_x\text{CuO}_4$), famous for high temperature superconductivity [11], the vanadate V_2O_3 which provides the classical example for a band width controlled metal-insulator transition and the manganite $\text{Nd}_{1-x}\text{Sr}_x\text{MnO}_3$, a double exchange system which can develop orbital order. An example in the class of heavy fermion systems is provided by the well studied system $\text{Ce}_x\text{La}_{1-x}\text{Cu}_6$ where the Ce f electrons play the crucial role. In the dilute limit of small Cerium concentrations, the single impurity Kondo effect is observed whereas pure CeCu_6 develops a heavy quasi particle band at temperatures below 0.1K.

Quite a different class of materials which shows strongly correlated behavior are the organic systems with π -electron conduction, such as the κ -(BEDT-TTF)₂-X layered materials [60]. The elementary building blocks in these compounds are BEDT-TTF molecules and basic metallic properties are well understood, considering only a single molecular orbital per BEDT-TTF molecule. Given the complexity of the molecule this is a striking simplification and it remains an open question whether subtle correlation effects can be modeled on the same basis.

The subject of this thesis is the study of 2D lattice fermion models, based on two canonical models, the Hubbard (6) and the Kondo lattice model. Whereas the Hubbard model was originally devised as a minimal model for the metal insulator transition, as observed in many of the above mentioned materials, the Kondo lattice model was formulated as the generic model for rare earth compounds which display the heavy fermion behavior. The lattice topology is chosen two dimensional. Dimensionality affects in par-

ticular the low temperature ordered phases, such as superconductivity. For instance the 2D Hubbard model has been intensively studied as a prototype for high temperature superconductivity and on the material side $\text{La}_{2-x}\text{Sr}_x\text{CuO}_4$ or the $\kappa\text{-(BEDT-TTF)}_2\text{-X}$ show a pronounced layered structure. Technically, quantum Monte Carlo techniques are well suited for the study of two dimensional systems as opposed to one dimensional topologies, where it may be favorable to choose numerical RG methods. On the other hand, QMC analysis of three dimensional lattices is still a challenging issue, since the typical lattice size in fermionic QMC calculations is below 500 lattice sites which would amount to a maximum of $8 \times 8 \times 8$ in three dimensions.

Organization

The organization of the main text is as follows:

- In the first chapter we give a detailed account of determinantal quantum Monte Carlo. Monte Carlo techniques have a long tradition in the study of classical statistical physics, where they provide a stochastic representation of the partition sum. The central idea is that the calculation of the Boltzmann weight of a single configuration is always possible. But an exact summation over all possible configurations is prohibited by the number of configurations which grows exponentially with system size. In a Monte Carlo simulation one replaces the exact sum by some randomly chosen subset. Then, Monte Carlo results are a statistical *estimate* to the exact result and the quality of the result is expressed by an error bar. The central observation is that the error of such a simulation scales as $1/\sqrt{\text{CPU-time}}$ which compares favorably with any direct approximation of the sum. In *quantum* Monte Carlo, the same statistical approach is used to estimate the quantum partition function, expressed in the form of a imaginary time path integral. For Fermions, these path integrals are troubled by the so called sign problem, which states that the statistical weight of a single contribution in the path integral may become negative or complex. Then we can no longer select important configurations by there respective weight. Fortunately, a class of fermionic systems with attractive interaction does not suffer from the sign problem when a Hubbard-Stratonovich transformation is used in the construction of the path integral. The resulting BSS algorithm [14] is

based on Slater determinants. Furthermore, under the combined condition of half filling and a bipartite lattice geometry the attractive and repulsive Hubbard models map onto each other which allows to gain insight into the repulsive Hubbard model at least on this special point. A very attractive point in determinantal QMC is the possibility to calculate virtually any correlation function, static and dynamic, where the maximum entropy method [50] is employed for the analytic continuation from imaginary time to real frequencies. Special emphasis is paid to a new method we developed to “measure” these time displaced Green’s functions [28]. Finally, we discuss the Dyson equation in the Hirsch-Fye impurity algorithm, which allows a conceptual unification of the BSS algorithm and the impurity algorithm.

- The second chapter introduces the Kondo lattice model

$$H_{KLM} = -t \sum_{\langle \mathbf{i}, \mathbf{j} \rangle, \sigma} \left(c_{\mathbf{i}, \sigma}^\dagger c_{\mathbf{j}, \sigma} + H.c. \right) + J \sum_{\mathbf{i}} \vec{S}_{\mathbf{i}, c} \vec{S}_{\mathbf{i}, f}, \quad (7)$$

which was only recently studied with determinantal QMC after a sign free formulation was found [7]. The Kondo lattice model is the minimal model for heavy fermion systems and describes the interaction of a conduction band with localized f -orbitals. As a result of strong Coulomb repulsion the f -orbitals are occupied by single electron and charge fluctuations are suppressed. The remaining degree of freedom is a f -spin that couples to the conduction spin via an antiferromagnetic exchange term. The Kondo model is believed to describe many aspects of heavy fermion physics. First it displays a crossover behavior from free to screened f -spins at the temperature scale of the single impurity Kondo temperature T_K . Second, it contains the Ruderman-Kittel effective interaction between f -spins which is mediated by the spin susceptibility of the conduction electrons and is the cause of many magnetically ordered phases in heavy fermion compounds. Finally, the ground state of the Kondo lattice model is believed to be a Fermi liquid with an extremely heavy band, which is the characteristic feature of the heavy fermion systems. Thus the low energy charge excitations in the Kondo model behave very differently from the Hubbard case. In this chapter we study a Kondo lattice model with an additional Hubbard interaction for the conduction electrons ($UKLM$) with an emphasize on single hole dynamics. Due to the constraint of achieving a sign free simulation, we can only investigate the model at half filling. Even in weak

coupling both the Kondo and the Hubbard model on the square lattice will be insulating antiferromagnets. The Hubbard model has a spin-density-wave ground state and the Kondo model is antiferromagnetic due to the RKKY interaction. But the single hole spectral functions are very different. An important point of the dispersion is the energy minimum which sets the charge gap. For the Hubbard model this happens at $k = (\pi/2, \pi/2)$ but in the Kondo lattice model we observe the charge gap at $k = (\pi, \pi)$. In the UKLM both interactions are present and it is not obvious how the different hole dispersions of the Hubbard and Kondo model can be reconciled. The results we obtain indicate the formation of a two “band” dispersion, one following the shape of a Kondo and the other that of a Hubbard dispersion. The weight of these two structures at $k = (\pi, \pi)$ is roughly proportional to the relative weight of the interactions J and U . But this implies that the charge gap for any finite exchange J is set by the Kondo branch of the dispersion. In addition our Kondo lattice model shows a quantum critical point, arising from a competition between long range order induced by the RKKY interaction and the formation of local Kondo singlets for large J . The phase diagram as a function U and J is determined.

- Finally, in the third chapter we investigate a Hubbard model on the simple square lattice topology. To the local Hubbard interaction we add nearest neighbor spin-spin and charge-charge interaction terms. The spin part is in the form of a Heisenberg term whereas for the charge part we consider pair hopping and density-density interactions. With three tunable interaction parameters the model has a rich phase diagram and we choose to concentrate on two particular quantum phase transitions. First, we find a point with coexisting antiferromagnetic and superconducting order. Upon variation of the Hubbard U this point is linked to a first order transition between the two respective phases. Recently, a first order transition between antiferromagnetism and superconductivity has been observed in the organic layered superconductor κ -(BEDT-TTF)-Cl [61]. We speculate, that our model describes these low temperature phases while the nearest neighbor spin and charge interactions are generated by a Su-Schrieffer-Heeger [98] electron-phonon interaction. Second, we study a transition between a charge density wave and superconducting

state. In spin language, the analogy is provided by the transition from an easy axis to an easy plane order. Going across the isotropic Heisenberg point we observe typical behavior of a second order phase transition although the orientation of the order parameter jumps discontinuously from the plane to the axis.

Chapter 1

Auxiliary field Quantum Monte Carlo

1.1 Introduction

A number of well known Quantum Monte Carlo (QMC) techniques, such as stochastic series expansion (SSE), worldline QMC (with loop update) [26, 25] and auxiliary field QMC [14, 64], may be understood as direct implementations of different path integral representations. The common starting point is the thermal average for an observable \mathcal{O}

$$\langle \mathcal{O} \rangle = \frac{\langle e^{-\beta H} \mathcal{O} \rangle}{Z} = \frac{\text{Tr} e^{-\beta H} \mathcal{O}}{\text{Tr} e^{-\beta H}}, \quad (1.1)$$

where H is a Hamiltonian for a finite size system.

In a second step we introduce a path integral representation, which approximates the density matrix $e^{-\beta H}$ with a sum of ρ_i

$$e^{-\beta H} \sim \sum_i \rho_i. \quad (1.2)$$

We are only interested in path integrals which allow to calculate the individual “weights” $\text{Tr} \rho_i$ and “observables” $\text{Tr} \rho_i \mathcal{O}$ in a simple numerical way. In auxiliary field QMC this is achieved via a Trotter decomposition of

$$\exp[-\beta(H_0 + H_I)], \quad (1.3)$$

and a subsequent Hubbard-Stratonovich decoupling of the interaction terms as explained in section 1.2. In the SSE procedure, the density matrix (1.3) is expanded in β (similar to

a high temperature expansion), and both H_0 and H_I are broken into a sum of elementary “ladder” operators.

In order to approximate a given observable \mathcal{O} we now have to evaluate

$$\frac{\langle e^{-\beta H} \mathcal{O} \rangle}{Z} \sim \frac{\sum_i \text{Tr} \rho_i \mathcal{O}}{\sum_i \text{Tr} \rho_i} = \sum_i \frac{\text{Tr} \rho_i}{\sum_i \text{Tr} \rho_i} \frac{\text{Tr} \rho_i \mathcal{O}}{\text{Tr} \rho_i}. \quad (1.4)$$

The approximation $\langle \mathcal{O} \rangle$ is non-perturbative and converges for all values of interaction strength. But evaluating the approximation (1.4) poses a fundamental challenge. In order to answer questions about low temperature behavior, long range order and finite size scaling we need to calculate observables with a small error. Unfortunately, sums of type

$$\sum_i \text{Tr} \rho_i \quad (1.5)$$

can not be evaluated term by term since the sum grows exponentially with system size and inverse temperature β . Monte Carlo techniques can provide an estimate for Eq. (1.4) based on a *small, random* subset of the sum $\sum_i \rho_i$. Obviously, for such an estimate to work we need *additional* knowledge about the behavior of $\text{Tr} \rho_i$. First and foremost QMC relies on the positivity

$$\text{Tr} \rho_i > 0, \quad (1.6)$$

otherwise the cancellation of positive and negative contributions in $\sum_i \text{Tr} \rho_i$ would prohibit a stochastic estimate of Eq. (1.5). Given this positivity, a *probability*

$$p_i = \text{Tr} \rho_i / \sum_i \text{Tr} \rho_i \quad (1.7)$$

for every configuration i is introduced. If the observable

$$\langle \mathcal{O} \rangle_i = \frac{\text{Tr} \rho_i \mathcal{O}}{\text{Tr} \rho_i} \quad (1.8)$$

is well behaved we can evaluate stochastically

$$\langle \mathcal{O} \rangle = \sum_i p_i \langle \mathcal{O} \rangle_i, \quad (1.9)$$

using importance sampling of the probability distribution p_i . Importance sampling of this distribution yields a stream of data for every observable $\langle \mathcal{O} \rangle_i$ and the average of

these data is usually taken as an estimator for the observable $\langle \mathcal{O} \rangle$ in Eq. (1.1). Some statistical analysis, as the rebinning technique, will be necessary to estimate an error bar. In the present text, we will not discuss the necessary concepts of sampling and data analysis. A good account of relevant topics in probability theory, such as Markov chains and autocorrelation time of the stochastic process is given in the review by Sokal [94]. As the primary tool to measure autocorrelation time, we use the rebinning technique and variations, as the Jackknife and bootstrap methods [24].

1.2 Auxiliary field algorithm

Our aim is to give a short, but self contained introduction into the various technical aspects of auxiliary field QMC. Other reviews are available from Loh and Gubernatis [64] and Assaad [6].

For sake of clarity the method is first illustrated for an explicit model system, namely the attractive Hubbard model with the Hamiltonian H

$$H = H_0 + H_I \tag{1.10}$$

where H_0 is the usual hopping Hamiltonian and H_I the attractive Hubbard term with $U < 0$

$$H_0 = -t \sum_{\langle \mathbf{i}, \mathbf{j} \rangle, \sigma} c_{\mathbf{i}, \sigma}^\dagger c_{\mathbf{j}, \sigma} + H.c, \tag{1.11}$$

$$H_I = U \sum_{\mathbf{i}} (n_{\mathbf{i}, \uparrow} - 1/2) (n_{\mathbf{i}, \downarrow} - 1/2). \tag{1.12}$$

The sum in the hopping term runs over bonds $\langle \mathbf{i}, \mathbf{j} \rangle$ and the bandwidth is given by $2tD^2$ where D is the dimension.

In the *finite temperature* version of the auxiliary field Monte Carlo (FTQMC) observable averages are taken with respect to the statistical operator

$$\langle \mathcal{O} \rangle = \frac{\text{Tr} e^{-\beta(H-\mu N)} \mathcal{O}}{\text{Tr} e^{-\beta(H-\mu N)}}, \tag{1.13}$$

where the trace runs over the Fock space, $\beta = 1/k_B T$ and μ is the chemical potential. The evaluation of the finite temperature observable (1.13) sets the stage for FTQMC.

Projector quantum Monte Carlo (PQMC) may be viewed as a small modification of FTQMC which was introduced in order to speed up the convergence of FTQMC in the

zero temperature limit $\beta \rightarrow \infty$. The only modification to the average 1.13 is the reduction of the Fock space trace to a specific trial state projector

$$\text{Tr} \rightarrow \text{Tr} |\psi_T\rangle \langle \psi_T|, \quad (1.14)$$

and Eq. 1.13 reduces to the canonical average

$$\langle \mathcal{O} \rangle = \frac{\langle \psi_T | e^{-\theta(H-\mu N)} \mathcal{O} e^{-\theta(H-\mu N)} | \psi_T \rangle}{\langle \psi_T | e^{-2\theta(H-\mu N)} | \psi_T \rangle}, \quad (1.15)$$

which only has a meaning as an approximation of the zero temperature result. The ground state $|GS\rangle$ is projected from $|\psi_T\rangle$ as

$$|GS\rangle = e^{-\theta(H-\mu N)} |\psi_T\rangle, \quad (1.16)$$

thus we require

$$\langle \psi_T | GS \rangle \neq 0. \quad (1.17)$$

It is exactly this non-orthogonality requirement which allows to restrict the projection to a given symmetry sector of the operator $\exp[-\theta(H-\mu N)]$. This is achieved by choosing the symmetry of $|\psi_T\rangle$ as the ground state symmetry. Low lying excitations in other symmetry sectors can then no longer interfere with the projection.

The difference of the two algorithms for $\beta = 2\theta \rightarrow \infty$ is illustrated in Fig. 1.1, where the repulsive Hubbard model was considered. Since we know that the ground state is a total spin singlet [62], we choose as trial state $|\psi_T\rangle$ a filled Fermi sea, which is a spin singlet. Due to long range order we also expect a Goldstone mode of spin one magnons. These low lying excitations need not be filtered out in PQMC which explains the dramatic improvement.

In the following we will concentrate on the finite temperature algorithm since the projection step (1.14) may be applied later.

Trotter product formula

Non-commutativity of $[H_0, H_I]$, which essentially prevents the solution of the many-body problem is the subject of the Trotter product expansion. The Lie-Trotter formula [102] has been used by Nelson [81, 91] to recover the Feynman-Kac path integral and was first

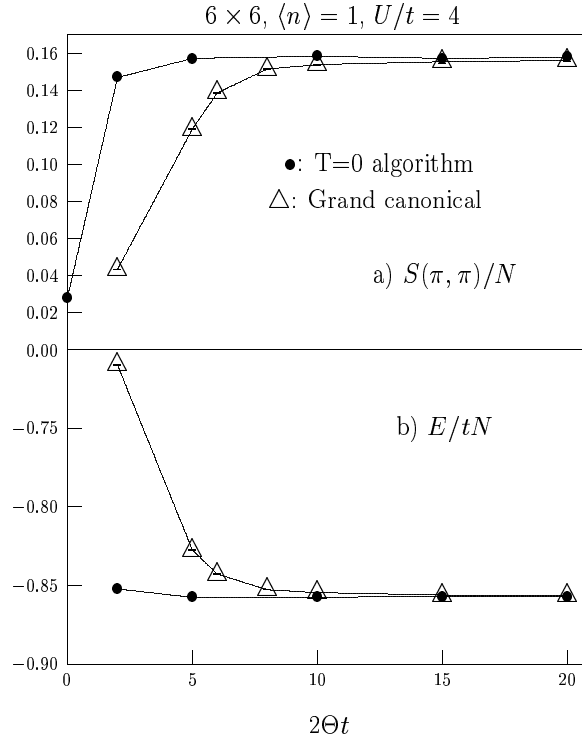


Figure 1.1: A comparison of zero temperature convergence in the case of a half-filled repulsive Hubbard model. ●: PQMC algorithm. △: FTQMC algorithm at $\beta = 2\Theta$
Panel a) Fourier transform of the spin-spin correlation functions at $\vec{Q} = (\pi, \pi)$
Panel b) Ground state energy. (from [6]).

used by Suzuki [100] to introduce the world-line algorithm. The origin of the formula is a statement about Lie groups

$$e^{-\beta H} = \lim_{m \rightarrow \infty} f(\beta/m)^m \quad (1.18)$$

where f is *any* approximation of the short time behavior of the Lee group

$$\lim_{\lambda \rightarrow 0} \frac{\partial f(\lambda)}{\partial \lambda} = -H, \quad (1.19)$$

$$\lim_{\lambda \rightarrow 0} f(\lambda) = 1, \quad (1.20)$$

which just states that up to first order $\exp(-\lambda H)$ and $f(\lambda)$ agree.

For the Trotter product formula¹ we choose

$$f(\lambda) = e^{-\lambda H_0} e^{-\lambda H_I} \quad (1.21)$$

¹Choosing another approximation $f(\lambda) = 1 + \lambda H$, we recover the formula $\exp x = \lim_{n \rightarrow \infty} (1 + x/n)^n$.

which has the *same* derivative as the full $\exp[-\beta H]$. This transforms the initial “propagation” $\exp[-\beta H]$ into a product of short $\Delta\tau = \beta/m$ propagations

$$e^{-\beta(H_0+H_I)} = \lim_{m \rightarrow \infty} (e^{-\Delta\tau H_0} e^{-\Delta\tau H_I})^m \quad (1.22)$$

and becomes exact in the limit $\Delta\tau \rightarrow 0$. Convergence is guaranteed for bounded operators [91].

Let us look at the error we make at a single time step. Expanding exponentials in $\Delta\tau$ we have up to second order

$$e^{-\Delta\tau(H_0+H_I)} - e^{-\Delta\tau H_0} e^{-\Delta\tau H_I} = -\frac{\Delta\tau^2}{2} [H_0, H_I] + \mathcal{O}(\Delta\tau^3). \quad (1.23)$$

Let us plug this into the product

$$\left(e^{-\Delta\tau(H_0+H_I)} + \frac{\Delta\tau^2}{2} [H_0, H_I] + \mathcal{O}(\Delta\tau^3) \right)^m = (e^{-\Delta\tau H_0} e^{-\Delta\tau H_I})^m \quad (1.24)$$

and expand the left side to lowest order in $\Delta\tau$

$$e^{-\beta H} + \frac{\Delta\tau}{2} \int_0^\beta d\lambda e^{-(\beta-\lambda)H} [H_0, H_I] e^{-\lambda H} + \mathcal{O}(\Delta\tau^2) = (e^{-\Delta\tau H_0} e^{-\Delta\tau H_I})^m \quad (1.25)$$

where the integral is a convenient abbreviation for the sum over m parts. For convergence we should require that the correction of order $\Delta\tau$ is a bounded operator

$$\|e^{-(\beta-\lambda)H} [H_0, H_I] e^{-\lambda H}\| < C. \quad (1.26)$$

In fact many Trotter decompositions do better with a leading correction of order $\mathcal{O}(\Delta\tau^2)$. There are two independent ways to ensure zero contribution in order $\mathcal{O}(\Delta\tau)$ [34]:

1. The commutator of two Hermitian operators is antihermitian

$$[H_0, H_I]^\dagger = -[H_0, H_I]. \quad (1.27)$$

The $\Delta\tau$ -coefficient is also antihermitian

$$\left[\int_0^\beta d\lambda e^{-(\beta-\lambda)H} [H_0, H_I] e^{-\lambda H} \right]^\dagger = - \int_0^\beta d\lambda e^{-\lambda H} [H_0, H_I] e^{-(\beta-\lambda)H} \quad (1.28)$$

$$= - \int_0^\beta d\lambda e^{-(\beta-\lambda)H} [H_0, H_I] e^{-\lambda H}, \quad (1.29)$$

where the second line is just a rearrangement of the integrand. Let us assume that both H_0 and H_I are real representable. Then the $\Delta\tau$ -coefficient is also real representable. But the trace of a real, antihermitian operator vanishes!

2. Using a *symmetrized* Trotter decomposition the $\mathcal{O}(\Delta\tau)$ vanishes

$$e^{-\beta H} \sim \left(e^{-\frac{\Delta\tau}{2} H_0} e^{-\Delta\tau H_I} e^{-\frac{\Delta\tau}{2} H_0} \right)^m + \mathcal{O}(\Delta\tau^2), \quad (1.30)$$

which is easily verified comparing orders. For implementation we may continue using the simpler Trotter decomposition (1.22) but measure shifted observables

$$\mathcal{O} \rightarrow e^{-\frac{\Delta\tau}{2} H_0} \mathcal{O} e^{\frac{\Delta\tau}{2} H_0}. \quad (1.31)$$

The different convergence behavior is illustrated in Fig. 1.2 where PQMC results for the repulsive Hubbard model are shown. As apparent the symmetric decomposition (1.30) is much more accurate than the simple decomposition (1.22). In addition and due to the variational principle, the symmetric decomposition also provides an upper bound to the exact energy.

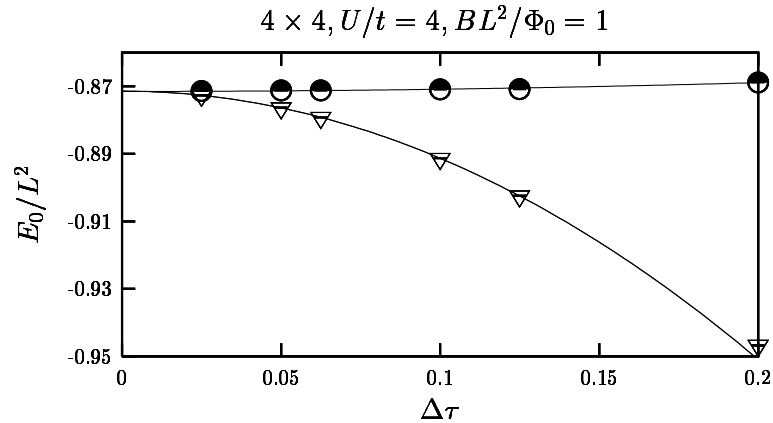


Figure 1.2: Ground state energy of the Half-filled Hubbard model on a 4×4 lattice, $U/t = 4$, $\langle n \rangle = 1$ and $BL^2/\Phi_0 = 1$ as a function of $\Delta\tau$ as obtained with the PQMC. The Trotter decompositions of Eqn. (1.22) (∇) and (1.30) (\circ) are considered. Note that due to the variational principle the Trotter decomposition of Eq. (1.30) yields an upper bound to the energy. The solid lines correspond to least square fits to the form $a + b\Delta\tau^2$. (taken from [6])

Hubbard-Stratonovich

The Trotter decomposition was only the first step towards a path integral. In a second step we will further simplify the interaction term $\exp[-\Delta\tau H_I]$. For instance one could

use the very reasonable approximation

$$e^{-\Delta\tau H_I} \sim 1 - \Delta\tau H_I \quad (1.32)$$

which will generate all Feynman diagrams up to order m (disconnected as well). This close relation between the Trotter product and the diagrammatic expansion raises the question how the first can converge when the latter does not. This is discussed in appendix A.

Auxiliary field QMC is instead based on a Hubbard-Stratonovich (HS) transformation [46] which reduces the interacting term $\exp[-\Delta\tau H_I]$ to a sum of free Fermion propagators. There exists a variety of HS transformations for different interaction terms. In particular the auxiliary field may take discrete or continuous values. In this work we shall only consider some discrete variants and we start with the decoupling of the attractive Hubbard term with $U < 0$ which was introduced by Hirsch [41].

Considering first a single site we can rewrite the Hubbard term into a square form which is the common starting point for all HS transformations

$$(n_\uparrow - 1/2)(n_\downarrow - 1/2) = \frac{1}{2}(n_\uparrow + n_\downarrow - 1)^2 - 1/4 \quad (1.33)$$

and

$$e^{-\Delta\tau U(n_\uparrow - 1/2)(n_\downarrow - 1/2)} = e^{-\Delta\tau U/2(n_\uparrow + n_\downarrow - 1)^2} e^{\Delta\tau U/4}. \quad (1.34)$$

We propose the following decoupling to a sum of two single electron terms

$$e^{-\Delta\tau U/2(n_\uparrow + n_\downarrow - 1)^2} = \frac{e^{\alpha(n_\uparrow + n_\downarrow - 1)} + e^{-\alpha(n_\uparrow + n_\downarrow - 1)}}{2} \quad (1.35)$$

and verify for the four local states:

$$\begin{array}{llll} e^{-\Delta\tau U/2(n_\uparrow + n_\downarrow - 1)^2} & \stackrel{?}{=} & \frac{e^{\alpha(n_\uparrow + n_\downarrow - 1)} + e^{-\alpha(n_\uparrow + n_\downarrow - 1)}}{2} & \\ |0\rangle & e^{-\Delta\tau U/2} & = & \cosh \alpha \\ |\uparrow\downarrow\rangle & e^{-\Delta\tau U/2} & = & \cosh \alpha \\ |\uparrow\rangle & 1 & = & 1 \\ |\downarrow\rangle & 1 & = & 1 \end{array} \quad (1.36)$$

These four equations are solved simultaneously by setting

$$e^{-\Delta\tau U/2} = \cosh \alpha, \quad (1.37)$$

which has a real and positive solution for α when $U < 0$. Thus on a lattice with N sites the HS transformation reads

$$\exp[-\Delta\tau U \sum_{\mathbf{i}} (n_{\mathbf{i},\uparrow} - 1/2)(n_{\mathbf{i},\downarrow} - 1/2)] = C \sum_{s_{\mathbf{i}}=\pm 1} \exp[\sum_{\mathbf{i}} s_{\mathbf{i}} \alpha (n_{\mathbf{i},\uparrow} + n_{\mathbf{i},\downarrow} - 1)], \quad (1.38)$$

where the prefactor C is

$$C = e^{N\Delta\tau U/4}/2^N. \quad (1.39)$$

The auxiliary HS variables $s_{\mathbf{i}}$ are restricted to the Ising values ± 1 . The HS transformation (1.38) is sometimes referred to as *charge* decoupling since the auxiliary Ising spin $s_{\mathbf{i}}$ couples to the local charge operator.

Using the Trotter decomposition (1.22) the finite temperature observable (1.13)

$$\langle \mathcal{O} \rangle = \frac{\text{Tr} e^{-\beta(H-\mu N)} \mathcal{O}}{\text{Tr} e^{-\beta(H-\mu N)}} = \lim_{m \rightarrow \infty} \frac{\text{Tr} \left(e^{-\Delta\tau \tilde{H}_0} e^{-\Delta\tau H_I} \right)^m \mathcal{O}}{\text{Tr} e^{(e^{-\Delta\tau \tilde{H}_0} e^{-\Delta\tau H_I})^m}} \quad (1.40)$$

where the chemical potential term μN was absorbed into \tilde{H}_0

$$\tilde{H}_0 = H_0 - \mu N. \quad (1.41)$$

Decoupling all interaction terms in (1.40) we find the path integral

$$\langle \mathcal{O} \rangle \sim \frac{\sum_{s(\mathbf{i},\tau)} \text{Tr} \left[\prod_{\tau=1}^m e^{-\Delta\tau \tilde{H}_0} e^{\sum_{\mathbf{i}} s(\mathbf{i},\tau) \alpha (n_{\mathbf{i},\uparrow} + n_{\mathbf{i},\downarrow} - 1)} \mathcal{O} \right]}{\sum_{s(\mathbf{i},\tau)} \text{Tr} \left[\prod_{\tau=1}^m e^{-\Delta\tau \tilde{H}_0} e^{\sum_{\mathbf{i}} s(\mathbf{i},\tau) \alpha (n_{\mathbf{i},\uparrow} + n_{\mathbf{i},\downarrow} - 1)} \right]}, \quad (1.42)$$

where we introduced the auxiliary Ising field $s(\mathbf{i}, \tau)$ in space-time and the sum $\sum_{s(\mathbf{i},\tau)}$ runs over all such Ising configurations. Let us further analyze the weight of a single configuration $p[s]$

$$p[s] = \text{Tr} \left[\prod_{\tau=1}^m e^{-\Delta\tau \tilde{H}_0} e^{\sum_{\mathbf{i}} s(\mathbf{i},\tau) \alpha (n_{\mathbf{i},\uparrow} + n_{\mathbf{i},\downarrow} - 1)} \right]. \quad (1.43)$$

This weight has three important properties:

1. the complexity of the interacting problem is reduced to the problem of independent electrons moving through a time dependent field, i.e. the auxiliary field $s(\mathbf{i}, \tau)$. Of course we traded the complex many-body problem for a **sum** of simple problems. The computational cost of integrating the weight (1.43) involves m multiplications of $2N \times 2N$ matrices (for two spin states).

2. since there is no mixing of spin, the propagation is the direct product of an up spin propagation and one for the down spin. Therefore the trace factorizes into up and down components

$$p[s, \uparrow] = \text{Tr}_\uparrow \prod_{\tau=1}^m e^{-\Delta\tau \tilde{H}_{0,\uparrow}} e^{\sum_i s(\mathbf{i},\tau)\alpha(n_{\mathbf{i},\uparrow}-1/2)}, \quad (1.44)$$

$$p[s, \downarrow] = \text{Tr}_\downarrow \prod_{\tau=1}^m e^{-\Delta\tau \tilde{H}_{0,\downarrow}} e^{\sum_i s(\mathbf{i},\tau)\alpha(n_{\mathbf{i},\downarrow}-1/2)}, \quad (1.45)$$

and the weight is the product

$$p[s] = p[s, \uparrow] \times p[s, \downarrow]. \quad (1.46)$$

3. in our particular HS decoupling the up and down factor are *equal* and *real*. Thus the total weight $p[s]$ is positive

$$p[s] \geq 0 \quad (1.47)$$

and a good weight function for MC sampling. As already mentioned one has enough freedom to construct a variety of fermionic path integrals. But only the auxiliary field algorithm gives positive weights in more than one dimension.

4. All possible observables may be constructed from elementary Green's functions using a Wick theorem generally available for all non-interacting Fermion problems.

Repulsive Hubbard model

It is well known that at half filling (or $\mu = 0$) the attractive Hubbard model (1.12) maps onto the repulsive model by a unitary particle-hole transformation. To this end, let us introduce the *canonical* transformation \mathcal{P} (with $\mathcal{P}^2 = 1$)

$$\mathcal{P}c_{\mathbf{i},\downarrow}\mathcal{P} = (-1)^{\mathbf{i}} c_{\mathbf{i},\downarrow}^\dagger, \quad (1.48)$$

which satisfies

$$\mathcal{P}^2 = 1, \quad (1.49)$$

and transforms spin down holes to electrons. The hopping Hamiltonian is invariant

$$\mathcal{P}c_{\mathbf{i},\downarrow}c_{\mathbf{j},\downarrow}^\dagger\mathcal{P} = \underbrace{(-1)^{\mathbf{i}}(-1)^{\mathbf{j}}}_{-1:\text{for bipartite NN hop}} c_{\mathbf{i},\downarrow}c_{\mathbf{j},\downarrow}^\dagger = c_{\mathbf{j},\downarrow}^\dagger c_{\mathbf{i},\downarrow}, \quad (1.50)$$

which holds for bipartite nearest neighbor hopping terms. A density term picks up a minus sign

$$\mathcal{P} \left(c_{i,\downarrow}^\dagger c_{i,\downarrow} - 1/2 \right) \mathcal{P} = - \left(c_{i,\downarrow}^\dagger c_{i,\downarrow} - 1/2 \right), \quad (1.51)$$

which implies the sign change for the Hubbard term. Yet there is the $\mu = 0$ restriction because

$$\mathcal{P} \mu (n_{i,\uparrow} + n_{i,\downarrow} - 1) \mathcal{P} = \mu (n_{i,\uparrow} - n_{i,\downarrow}) = 2\mu S_{\mathbf{i}}^z, \quad (1.52)$$

and the chemical potential gets mapped to a magnetic field.

Since a canonical transformation leaves the trace invariant we know that energies of the half-filled repulsive and attractive Hubbard model are identical

$$\frac{\text{Tr} e^{-\beta H(U)} H(U)}{\text{Tr} e^{-\beta H(U)}} = \frac{\text{Tr} \mathcal{P} e^{-\beta H(U)} H(U) \mathcal{P}}{\text{Tr} \mathcal{P} e^{-\beta H(U)} \mathcal{P}} = \frac{\text{Tr} e^{-\beta H(-U)} H(-U)}{\text{Tr} e^{-\beta H(-U)}}. \quad (1.53)$$

More generally any observable in the attractive model maps to a ‘‘conjugate’’ observable in the repulsive model. Thus solving the attractive case we implicitly also solved the repulsive model at half filling.

Next we apply the particle-hole transformation to the path integral (1.42) where we continue to set $\mu = 0$. The single weight $p[s, \downarrow]$ transforms

$$\text{Tr}_{\downarrow} \mathcal{P} \prod_{\tau=1}^m e^{-\Delta\tau \tilde{H}_{0,\downarrow}} e^{\sum_{\mathbf{i}} s(\mathbf{i},\tau) \alpha (n_{i,\downarrow} - 1/2)} \mathcal{P} = \text{Tr}_{\downarrow} \prod_{\tau=1}^m e^{-\Delta\tau \tilde{H}_{0,\downarrow}} e^{\sum_{\mathbf{i}} -s(\mathbf{i},\tau) \alpha (n_{i,\downarrow} - 1/2)} \stackrel{!}{=} p[s, \downarrow]. \quad (1.54)$$

We observe that the transformation \mathcal{P} induced a flipping of the entire HS configuration. Yet the weight remains invariant

$$p[s, \downarrow] = p[-s, \downarrow], \quad (1.55)$$

and the positivity property (1.47) is conserved. Applying the transformation \mathcal{P} to the HS transformation itself we find the Hirsch decoupling ([41]) for the repulsive case $U > 0$

$$\exp[-\Delta\tau U \sum_{\mathbf{i}} (n_{i,\uparrow} - 1/2) (n_{i,\downarrow} - 1/2)] = C \sum_{s_{\mathbf{i}} = \pm 1} \exp[\sum_{\mathbf{i}} s_{\mathbf{i}} \alpha (n_{i,\uparrow} - n_{i,\downarrow})], \quad (1.56)$$

where α takes the same numerical value as in (1.37) and is given by

$$e^{\Delta\tau U/2} = \cosh \alpha. \quad (1.57)$$

In this HS transformation the field couples to the z -component of the spin $S_{\mathbf{i}}^z = (n_{i,\uparrow} - n_{i,\downarrow})/2$.

Complex HS

The spin decoupling scheme obviously breaks the full spin symmetry of the Hubbard model which eventually will be restored by summing over all HS fields. In practice summing enough contributions for this symmetry restoration may be difficult and a spin symmetric decoupling scheme would be favorable. The charge HS transformation (1.38) is trivially spin symmetric but solving for α when $U > 0$ we find an imaginary solution $\alpha = i\tilde{\alpha}$ ($\tilde{\alpha} \in \mathbb{R}$)

$$e^{-\Delta\tau U/2} = \cosh i\tilde{\alpha} = \cos \tilde{\alpha}. \quad (1.58)$$

The complex decoupling for the repulsive case reads

$$\exp[-\Delta\tau U \sum_{\mathbf{i}} (n_{\mathbf{i},\uparrow} - 1/2)(n_{\mathbf{i},\downarrow} - 1/2)] = C \sum_{s_{\mathbf{i}}=\pm 1} \exp[\sum_{\mathbf{i}} i\tilde{\alpha} s_{\mathbf{i}} (n_{\mathbf{i},\uparrow} + n_{\mathbf{i},\downarrow} - 1)], \quad (1.59)$$

and we should be worried about the positivity of $p[s]$. But the particle-hole transformation \mathcal{P} ensures that $p[s, \downarrow]$ is real! Under the action of \mathcal{P} the external field propagation changes into the conjugate. All other propagations are pure real, so the effect of the \mathcal{P} transformation on $p[s, \downarrow]$

$$p[s, \downarrow] = \text{Tr}_{\downarrow} \mathcal{P} \prod_{\tau=1}^m e^{-\Delta\tau \tilde{H}_{0,\downarrow}} e^{\sum_{\mathbf{i}} i\tilde{\alpha} s(\mathbf{i},\tau)(n_{\mathbf{i},\downarrow}-1/2)} \mathcal{P} = \text{Tr}_{\downarrow} \prod_{\tau=1}^m e^{-\Delta\tau \tilde{H}_{0,\downarrow}} e^{\sum_{\mathbf{i}} -i\tilde{\alpha} s(\mathbf{i},\tau)(n_{\mathbf{i},\downarrow}-1/2)} \quad (1.60)$$

$$= \overline{p[s, \downarrow]}, \quad (1.61)$$

is to enforce $p[s, \downarrow] \in \mathbb{R}$ through $p[s, \downarrow] = \overline{p[s, \downarrow]}$.

The complex decoupling in the attractive case

$$\exp[-\Delta\tau U \sum_{\mathbf{i}} (n_{\mathbf{i},\uparrow} - 1/2)(n_{\mathbf{i},\downarrow} - 1/2)] = C \sum_{s_{\mathbf{i}}=\pm 1} \exp[\sum_{\mathbf{i}} i\tilde{\alpha} s_{\mathbf{i}} (n_{\mathbf{i},\uparrow} - n_{\mathbf{i},\downarrow})], \quad (1.62)$$

leads to complex conjugate weights

$$p[s, \uparrow] = \overline{p[s, \downarrow]}, \quad (1.63)$$

and a positive weight $p[s] \geq 0$.

As long as we insist on sign free simulations for the repulsive Hubbard model it is a matter of taste whether we use the above mentioned decouplings for $U > 0$ or transform

first to an attractive model. However we will have to choose between the inequivalent real and complex decoupling.

In PQMC the “ \mathcal{P} -invariance” of the trace has to be substituted by “ \mathcal{P} -invariant” trial wave functions

$$\mathcal{P} |\psi_T\rangle = |\psi_T\rangle. \quad (1.64)$$

Then the above proofs of positive weights may be repeated accordingly. A particle hole invariant Slater determinant $|\psi_T\rangle$ is naturally generated as the ground state of the hopping Hamiltonian. Of course we have to fill the free Fermi sea with $N_e = N$ electrons.

General HS

We now consider interaction terms of “perfect square” form:

$$H_I = -W \sum_{\mathbf{i}} (O^{(\mathbf{i})})^2 \quad (1.65)$$

where $O^{(\mathbf{i})}$ is a one-body operator. In general, $[O^{(\mathbf{i})}, O^{(\mathbf{j})}] \neq 0$ so that the sum in the above equation has to be split into sums of commuting terms: $H_I = \sum_r H_I^r$, $H_I^r = -W \sum_{\mathbf{i} \in S_r} (O^{(\mathbf{i})})^2$. For \mathbf{i} and \mathbf{j} in the set S_r one requires $[O^{(\mathbf{i})}, O^{(\mathbf{j})}] = 0$. The imaginary time evolution may be written as $e^{-\Delta\tau H_I} \approx \prod_r e^{-\Delta\tau H_I^r}$. Thus we are left with the problem of decoupling $e^{\Delta\tau W O^2}$ where we have omitted the index \mathbf{i} . In principle, one can decouple a perfect square with the canonical HS transformation:

$$e^{\Delta\tau W O^2} = \frac{1}{\sqrt{2\pi}} \int d\Phi e^{-\frac{\Phi^2}{2} + \sqrt{2\Delta\tau W} \Phi O} \quad (1.66)$$

However, this involves a continuous field which renders the sampling hard. An alternative formulation is given by [9]:

$$e^{\Delta\tau W O^2} = \sum_{l=\pm 1, \pm 2} \gamma(l) e^{\sqrt{\Delta\tau W} \eta(l) O} + \mathcal{O}(\Delta\tau^4) \quad (1.67)$$

where the fields η and γ take the values:

$$\begin{aligned} \gamma(\pm 1) &= 1 + \sqrt{6}/3, \quad \gamma(\pm 2) = 1 - \sqrt{6}/3 \\ \eta(\pm 1) &= \pm \sqrt{2(3 - \sqrt{6})}, \quad \eta(\pm 2) = \pm \sqrt{2(3 + \sqrt{6})}. \end{aligned}$$

This transformation is not exact and produces an overall systematic error proportional to $\Delta\tau^3$. However, since we already have a systematic error proportional to $\Delta\tau^2$ from the Trotter decomposition, the transformation is as good as exact. It also has the great advantage of being discrete thus allowing efficient sampling.

1.3 Single particle Formalism

So far we have used the Trotter decomposition together with a HS transformation to convert the interacting many body problem to a sum of independent electron problems. Consequently, we now have to demonstrate, how the latter may be solved on a computer. The central quantity which we need to calculate is the one particle Green's function.

We will review the formalism associated with independent electrons moving in an external time-dependent field. The goal is to numerically evaluate formulas like

$$Z_{\uparrow} = \text{Tr} e^{-\mathbf{c}_{\uparrow}^{\dagger} \mathbf{H}_m \mathbf{c}_{\uparrow}} \dots e^{-\mathbf{c}_{\uparrow}^{\dagger} \mathbf{H}_1 \mathbf{c}_{\uparrow}} = \det(1 + \mathbf{B}_m \dots \mathbf{B}_1) \quad (1.68)$$

where \mathbf{H}_{τ} represents the time-dependent single particle Hamiltonian from Eq. (1.22). An important result is that all relevant quantities such as the partition function and all correlation functions are readily expressed in terms of the single particle propagation matrices

$$\mathbf{B}_{\tau} = e^{-\mathbf{H}_{\tau}}, \quad (1.69)$$

and are thus easily evaluated numerically.

Determinants

From here on we suppress the spin index since it is sufficient to consider a single spin sector. The following formulas may be verified using either operator methods [64, 6] or a coherent state representation for the fermi partition function [10]. Here we rely only on operator methods, for the coherent state formalism see appendix C.

We start with the definition of the N_e electron state

$$|R\rangle = \prod_{i=1}^{N_e} \left(\sum_x c_x^{\dagger} R_{x,i} \right) |0\rangle = \prod_{i=1}^{N_e} (\mathbf{c}^{\dagger} \mathbf{r}_i) |0\rangle, \quad (1.70)$$

where \mathbf{R} is a $N_e \times N$ matrix. The columns of \mathbf{R} denoted by \mathbf{r}_i are the single electron state vectors. The scalar product of two states $|R\rangle$ and $|L\rangle$ evaluates to the determinant

$$\langle L|R\rangle = \det \mathbf{L}^\dagger \mathbf{R} , \quad (1.71)$$

where a proof is found in appendix A. In first quantization the meaning is evident considering the 2 electron case

$$|R\rangle = \frac{1}{\sqrt{2}} (|\mathbf{r}_1\rangle |\mathbf{r}_2\rangle - |\mathbf{r}_2\rangle |\mathbf{r}_1\rangle) , \quad (1.72)$$

$$|L\rangle = \frac{1}{\sqrt{2}} (|\mathbf{l}_1\rangle |\mathbf{l}_2\rangle - |\mathbf{l}_2\rangle |\mathbf{l}_1\rangle) \quad (1.73)$$

and the scalar product is

$$\langle L|R\rangle = \det \begin{pmatrix} \langle \mathbf{l}_1|\mathbf{r}_1\rangle & \langle \mathbf{l}_1|\mathbf{r}_2\rangle \\ \langle \mathbf{l}_2|\mathbf{r}_1\rangle & \langle \mathbf{l}_2|\mathbf{r}_2\rangle \end{pmatrix} . \quad (1.74)$$

Further on we will often need to commute c_x^\dagger with the propagation $\exp[-\mathbf{c}^\dagger \mathbf{H} \mathbf{c}]$ and we get

$$\exp[-\mathbf{c}^\dagger \mathbf{H} \mathbf{c}] \mathbf{c}^\dagger = \mathbf{c}^\dagger \mathbf{B} \exp[-\mathbf{c}^\dagger \mathbf{H} \mathbf{c}] , \quad (1.75)$$

$$c_x^\dagger \exp[-\mathbf{c}^\dagger \mathbf{H} \mathbf{c}] = \sum_{\mathbf{i}} \exp[-\mathbf{c}^\dagger \mathbf{H} \mathbf{c}] c_i^\dagger (B^{-1})_{ix} \quad (1.76)$$

with the propagation matrix $\mathbf{B} = \exp[-\mathbf{H}]$. We proof this by integrating the equation of motion

$$\begin{aligned} \frac{d}{d\tau} e^{-\tau \mathbf{c}^\dagger \mathbf{H} \mathbf{c}} c_l^\dagger e^{\tau \mathbf{c}^\dagger \mathbf{H} \mathbf{c}} &= -e^{-\tau \mathbf{c}^\dagger \mathbf{H} \mathbf{c}} \left[\mathbf{c}^\dagger \mathbf{H} \mathbf{c}, c_l^\dagger \right] e^{\tau \mathbf{c}^\dagger \mathbf{H} \mathbf{c}} \\ &= -e^{-\tau \mathbf{c}^\dagger \mathbf{H} \mathbf{c}} \sum_{i,j} H_{ij} \left(c_i^\dagger \{c_j, c_l^\dagger\} - \{c_i^\dagger, c_l^\dagger\} c_j \right) e^{\tau \mathbf{c}^\dagger \mathbf{H} \mathbf{c}} \end{aligned} \quad (1.77)$$

$$= -e^{-\tau \mathbf{c}^\dagger \mathbf{H} \mathbf{c}} \sum_i c_i^\dagger H_{il} e^{\tau \mathbf{c}^\dagger \mathbf{H} \mathbf{c}} , \quad (1.78)$$

which has the solution

$$e^{-\tau \mathbf{c}^\dagger \mathbf{H} \mathbf{c}} c_l^\dagger e^{\tau \mathbf{c}^\dagger \mathbf{H} \mathbf{c}} = \sum_i c_i^\dagger B_{il} \quad \text{qed.} \quad (1.79)$$

We make a first use of Eq. (1.75) when we proof

$$\langle L|e^{-\mathbf{c}^\dagger \mathbf{H}_m \mathbf{c}} \dots e^{-\mathbf{c}^\dagger \mathbf{H}_1 \mathbf{c}} |R\rangle = \det \mathbf{L}^\dagger \mathbf{B} \mathbf{R} , \quad (1.80)$$

where \mathbf{B} abbreviates the product of single propagations

$$\mathbf{B} = \mathbf{B}_m \dots \mathbf{B}_1. \quad (1.81)$$

We simply commute all the creation operators to the left

$$\begin{aligned} \langle L | e^{-\mathbf{c}^\dagger \mathbf{H}_m \mathbf{c}} \dots e^{-\mathbf{c}^\dagger \mathbf{H}_1 \mathbf{c}} | R \rangle &= \langle L | e^{-\mathbf{c}^\dagger \mathbf{H}_m \mathbf{c}} \dots e^{-\mathbf{c}^\dagger \mathbf{H}_1 \mathbf{c}} \prod_{i=1}^{N_e} (\mathbf{c}^\dagger \mathbf{r}_i) | 0 \rangle \\ &= \langle L | e^{-\mathbf{c}^\dagger \mathbf{H}_m \mathbf{c}} \dots \prod_{i=1}^{N_e} (\mathbf{c}^\dagger \mathbf{B}_1 \mathbf{r}_i) \underbrace{e^{-\mathbf{c}^\dagger \mathbf{H}_1 \mathbf{c}} | 0 \rangle}_{=|0\rangle} \rangle = \\ &= \langle L | \prod_{i=1}^{N_e} (\mathbf{c}^\dagger \mathbf{B}_m \dots \mathbf{B}_1 \mathbf{r}_i) | 0 \rangle = \det \mathbf{L}^\dagger (\mathbf{B}\mathbf{R}) \quad \text{qed.} \end{aligned} \quad (1.82)$$

For the finite temperature grand canonical partition sum we need to perform a trace in the Fock space of zero to N particles

$$Z = \text{Tr} e^{-\mathbf{c}^\dagger \mathbf{H}_m \mathbf{c}} \dots e^{-\mathbf{c}^\dagger \mathbf{H}_1 \mathbf{c}} = \det (1 + \mathbf{B}). \quad (1.83)$$

The proof is deferred to appendix A. But we may understand Eq. (1.83) from applying it to a two site system,

$$\begin{aligned} \det \begin{pmatrix} 1 + B_{11} & B_{12} \\ B_{21} & 1 + B_{22} \end{pmatrix} &= 1 + B_{11} + B_{22} + \det \begin{pmatrix} B_{11} & B_{12} \\ B_{21} & B_{22} \end{pmatrix} \\ &= \text{Tr}_{N=2} e^{-\mathbf{c}^\dagger \mathbf{H}_m \mathbf{c}} \dots e^{-\mathbf{c}^\dagger \mathbf{H}_1 \mathbf{c}}, \end{aligned} \quad (1.84)$$

where the determinant is expanded using the multilinearity property. But the right side of Eq. 1.84 traces over a complete set of states in Fock space. For instance there are only two one particle basis states $|P_1\rangle$ and $|P_2\rangle$

$$\begin{aligned} \mathbf{P}_1^\dagger &= (1, 0), \\ \mathbf{P}_2^\dagger &= (0, 1) \end{aligned} \quad (1.85)$$

and both

$$\begin{aligned} \det \mathbf{P}_1^\dagger \mathbf{B} \mathbf{P}_1 &= B_{11}, \\ \det \mathbf{P}_2^\dagger \mathbf{B} \mathbf{P}_2 &= B_{22}, \end{aligned} \quad (1.86)$$

appear in Eq. (1.84). Finally, in our example the expectation values of the vacuum and the totally filled state are given by one and the determinant which completes the Fock space trace.

Here we want to remark on an interesting interpretation of all these determinants. While the determinant in the scalar product (1.71) is a manifestation of fermionic antisymmetrization, the trace formula (1.83) has another simple interpretation. Assume, that we can diagonalize the entire propagation by a canonical transformation

$$\begin{aligned} \text{Tr}_{\text{fermi}} e^{-\mathbf{c}^\dagger \mathbf{H}_m \mathbf{c}} \dots e^{-\mathbf{c}^\dagger \mathbf{H}_1 \mathbf{c}} &= \text{Tr}_{\text{fermi}} \exp \left(- \sum_k \varepsilon_k c_k^\dagger c_k \right) \\ &= \prod_k (1 + e^{-\varepsilon_k}) = \det(1 + \mathbf{B}). \end{aligned} \quad (1.87)$$

Now the determinant is a basis invariant form of the product. For bosons \mathbf{b}^\dagger the analogous result also involves a determinant (and is also correct for arbitrary propagation)

$$\begin{aligned} \text{Tr}_{\text{bose}} e^{-\mathbf{b}^\dagger \mathbf{H}_m \mathbf{b}} \dots e^{-\mathbf{b}^\dagger \mathbf{H}_1 \mathbf{b}} &= \text{Tr}_{\text{bose}} \exp \left(- \sum_k \varepsilon_k b_k^\dagger b_k \right) \\ &= \prod_k (1 + e^{-\varepsilon_k} + e^{-2\varepsilon_k} + \dots) = \det \left(\frac{1}{1 - \mathbf{B}} \right). \end{aligned} \quad (1.88)$$

In this way one may adapt the auxiliary field QMC to a grand canonical simulation for bosons.² Within the coherent state formalism (see appendix C) we can evaluate Fermi and Bose traces on the same level.

Using cyclic rotation under the trace (1.83) (for alternative proof see appendix A) we conclude that

$$\det(1 + \mathbf{B}_2 \mathbf{B}_1) = \det(1 + \mathbf{B}_1 \mathbf{B}_2). \quad (1.89)$$

At the end of this introduction to the determinantal formalism we present the following summary

c, c^\dagger	\longleftrightarrow	matrix	
$ R\rangle$		\mathbf{R}	
$\langle L $		\mathbf{L}	
$\langle L R\rangle$		$\det \mathbf{LR}$	(1.90)
U		\mathbf{B}	
$Z = \langle L U R\rangle$		$\det \mathbf{LBR}$	
$\text{Tr } U$		$\det(1 + \mathbf{B})$.	

²Canonical simulation for bosons as in PQMC is not possible. A zero temperature limit as in 1.3 is not well defined. And a direct implementation for N bosons would involve the calculation of permanents instead of determinants and they have much worse properties.

Green's function

The single particle Green's function is the *central* quantity in the QMC algorithm. For the updating of the HS fields we need the equal time Green's function $\mathbf{G}(\tau)$. Dynamical information, as the spectral function, is contained in the time displaced Green's function $\mathbf{G}^<(\tau_1, \tau_2)$ where a particle is added at time τ_1 and removed at a later time τ_2 . In the next section on the Wick theorem we shall learn how *any* observable is constructed from Green's functions.

In a preliminary step we introduce the notation (with $\tau_1 > \tau_2$)

$$U(\tau_1, \tau_2) = \prod_{\tau=\tau_2+1}^{\tau_1} U(\tau, \tau-1) \quad (1.91)$$

$$U(\tau, \tau-1) = e^{-\mathbf{c}^\dagger \mathbf{H}_\tau \mathbf{c}} \quad (1.92)$$

$$U(\tau_1, \tau_2)^{-1} \equiv U(\tau_2, \tau_1) \quad (1.93)$$

and accordingly for the matrices

$$\mathbf{B}(\tau_1, \tau_2) = \prod_{\tau=\tau_2+1}^{\tau_1} \mathbf{B}(\tau, \tau-1) \quad (1.94)$$

$$\mathbf{B}(\tau, \tau-1) = \mathbf{B}_\tau. \quad (1.95)$$

Since we started with m different propagation matrices \mathbf{B}_τ the τ slots can only take discrete values and may be indexed from $\tau \in 0 \dots m$. In order to simplify some notation we introduce “time-dependent” operators

$$c_l = c_l(\tau_l) \equiv U(0, \tau_l) c_l U(\tau_l, 0), \quad (1.96)$$

$$c_l^\dagger = c_l^\dagger(\tau_l) \equiv U(0, \tau_l) c_l^\dagger U(\tau_l, 0). \quad (1.97)$$

With these abbreviations the commutation rule (1.75) reads

$$U(\tau_1, \tau_2) \mathbf{c}^\dagger = \mathbf{c}^\dagger \mathbf{B}(\tau_1, \tau_2) U(\tau_1, \tau_2). \quad (1.98)$$

The time displaced Green's function is defined as

$$G_{xy}(\tau_1, \tau_2) = \langle \mathcal{T} c_x(\tau_1) c_y^\dagger(\tau_2) \rangle. \quad (1.99)$$

Thus for $\tau_1 \geq \tau_2$ the Green's function is

$$G_{xy}^>(\tau_1, \tau_2) = \frac{\text{Tr} U(\beta, \tau_1) c_x U(\tau_1, \tau_2) c_y^\dagger U(\tau_2, 0)}{Z}, \quad (1.100)$$

and for $\tau_1 < \tau_2$

$$G_{xy}^<(\tau_1, \tau_2) = -\frac{\text{Tr} U(\beta, \tau_1) c_y^\dagger U(\tau_1, \tau_2) c_x U(\tau_2, 0)}{Z}. \quad (1.101)$$

It is notationally more convenient to first calculate

$$G_{xy}^> = \frac{\text{Tr} e^{-\mathbf{c}^\dagger \mathbf{H}_3 \mathbf{c}} c_x e^{-\mathbf{c}^\dagger \mathbf{H}_2 \mathbf{c}} c_y^\dagger e^{-\mathbf{c}^\dagger \mathbf{H}_1 \mathbf{c}}}{Z}, \quad (1.102)$$

where we make use of the commutation rule 1.75

$$\begin{aligned} C_{xy} &= \text{Tr} e^{-\mathbf{c}^\dagger \mathbf{H}_3 \mathbf{c}} c_x e^{-\mathbf{c}^\dagger \mathbf{H}_2 \mathbf{c}} c_y^\dagger e^{-\mathbf{c}^\dagger \mathbf{H}_1 \mathbf{c}} = \sum_k \text{Tr} e^{-\mathbf{c}^\dagger \mathbf{H}_3 \mathbf{c}} c_x c_k^\dagger B_{2,ky} e^{-\mathbf{c}^\dagger \mathbf{H}_2 \mathbf{c}} e^{-\mathbf{c}^\dagger \mathbf{H}_1 \mathbf{c}} \\ &= -\sum_k \text{Tr} e^{-\mathbf{c}^\dagger \mathbf{H}_3 \mathbf{c}} c_k^\dagger c_x B_{2,ky} e^{-\mathbf{c}^\dagger \mathbf{H}_2 \mathbf{c}} e^{-\mathbf{c}^\dagger \mathbf{H}_1 \mathbf{c}} + B_{2,xy} \text{Tr} e^{-\mathbf{c}^\dagger \mathbf{H}_3 \mathbf{c}} e^{-\mathbf{c}^\dagger \mathbf{H}_2 \mathbf{c}} e^{-\mathbf{c}^\dagger \mathbf{H}_1 \mathbf{c}} \\ &= -\sum_{k,l,m} \text{Tr} e^{-\mathbf{c}^\dagger \mathbf{H}_3 \mathbf{c}} c_x e^{-\mathbf{c}^\dagger \mathbf{H}_2 \mathbf{c}} c_m^\dagger e^{-\mathbf{c}^\dagger \mathbf{H}_1 \mathbf{c}} B_{1,ml} B_{3,lk} B_{2,ky} + B_{2,xy} Z. \end{aligned} \quad (1.103)$$

In matrix form this is more transparent

$$\mathbf{C} = -\mathbf{C}\mathbf{B}_1\mathbf{B}_3\mathbf{B}_2 + \mathbf{B}_2Z \quad (1.104)$$

or

$$\mathbf{G}^> = \frac{\mathbf{C}}{Z} = \frac{1}{\mathbf{B}_2^{-1} + \mathbf{B}_1\mathbf{B}_3}. \quad (1.105)$$

In a similar way we obtain the electron removal Green's function $G^<$

$$G_{xy}^< = -\frac{\text{Tr} e^{-\mathbf{c}^\dagger \mathbf{H}_3 \mathbf{c}} c_y^\dagger e^{-\mathbf{c}^\dagger \mathbf{H}_2 \mathbf{c}} c_x e^{-\mathbf{c}^\dagger \mathbf{H}_1 \mathbf{c}}}{Z}. \quad (1.106)$$

The result from cyclically commuting c_y^\dagger to the left is

$$\mathbf{G}^< = -\frac{1}{(\mathbf{B}_1\mathbf{B}_3)^{-1} + \mathbf{B}_2}. \quad (1.107)$$

Without ambiguity we may translate Eqs. 1.101 and 1.100

$$\mathbf{G}^>(\tau_1, \tau_2) = \frac{1}{\mathbf{B}^{-1}(\tau_1, \tau_2) + \mathbf{B}(\tau_2, 0)\mathbf{B}(\beta, \tau_1)} \quad (1.108)$$

and

$$\mathbf{G}^<(\tau_1, \tau_2) = -\frac{1}{(\mathbf{B}(\tau_1, 0)\mathbf{B}(\beta, \tau_2))^{-1} + \mathbf{B}(\tau_2, \tau_1)}. \quad (1.109)$$

Wrapping equal time Green's function

At equal time $\tau_1 = \tau_2$ we need an additional definition for G

$$G_{xy}(\tau) \equiv \frac{\text{Tr } U(\beta, \tau) c_x c_y^\dagger U(\tau, 0)}{Z} \quad (1.110)$$

$$\mathbf{G}(\tau) = \frac{1}{\mathbf{1} + \mathbf{B}(\tau, 0) \mathbf{B}(\beta, \tau)}. \quad (1.111)$$

We will see that the Monte Carlo algorithm provides at every step the equal time $\mathbf{G}(\tau)$. In order to obtain the general time displaced $G_{xy}^>(\tau_1, \tau_2)$ for $\tau_1 > \tau_2$ we may “wrap” with the correct propagation matrix

$$\mathbf{G}^>(\tau_1, \tau_2) = \mathbf{B}(\tau_1, \tau) \mathbf{G}(\tau) \mathbf{B}(\tau, \tau_2). \quad (1.112)$$

The electron removal Green's function $\tau_1 < \tau_2$ may equally be obtained from the equal time $\mathbf{G}(\tau)$

$$\begin{aligned} \mathbf{G}^<(\tau, \tau) &= \mathbf{G}(\tau) - 1, \\ \mathbf{G}^<(\tau_1, \tau_2) &= \mathbf{B}^{-1}(\tau, \tau_1) \mathbf{G}^<(\tau, \tau) \mathbf{B}^{-1}(\tau_2, \tau) \\ &= \mathbf{B}^{-1}(\tau, \tau_1) (\mathbf{G}(\tau) - 1) \mathbf{B}^{-1}(\tau_2, \tau). \end{aligned} \quad (1.113)$$

Wick theorem

We also need to calculate spin-spin or density-density correlations which are four fermion observables. On the level of a free electron time evolution we can always build up many electron correlations from products of the Green's functions $G_{xy}(\tau_1, \tau_2)$. Using operator methods the proof relies on the ability to commute U and c as in Eq. (1.98). In the coherent state path integral it is a statement about Gaussian integrals.

We follow the strategy described for instance in [29]. A arbitrary many particle correlation function may take the form

$$\frac{\text{Tr } U(\beta, 0) \dots c_l c_k^\dagger c_j^\dagger c_i \dots}{Z}. \quad (1.114)$$

Time order is not an issue here, since we already start with an ordered sequence $\tau_l > \tau_k > \dots$. The reduction to two point Green's functions is achieved by picking some c_j^\dagger creation operator and commuting it to the left, cycling through the trace and commuting to the

original position. This is the exact same procedure already employed in the evaluation of $G^<$ in Eq. (1.103). The only difference is that here we need more than one commutation of type $\{c_x, c_j^\dagger\}$ which generates the Green's functions. After a complete rotation of c_j^\dagger one obtains a relation between the original expression and a sum of correlation functions with two operators less

$$\frac{\text{Tr } U(\beta, 0) \dots c_l c_k^\dagger c_j^\dagger c_i \dots}{Z} = (-1)^1 \frac{\text{Tr } U(\beta, 0) c_l c_j^\dagger}{Z} \times \frac{\text{Tr } U(\beta, 0) \dots c_k^\dagger c_i \dots}{Z} + \dots + \quad (1.115)$$

$$+ (-1)^2 \frac{\text{Tr } U(\beta, 0) c_j^\dagger c_i}{Z} \times \frac{\text{Tr } U(\beta, 0) \dots c_l c_k^\dagger \dots}{Z}. \quad (1.116)$$

The ‘‘contraction’’ we pulled in front is just the Green's function we would calculate if all other operators were missing. For instance on line (1.115) $\text{Tr } U(\beta, 0) c_l c_j^\dagger / Z$ arises from the commutator $\{c_l, c_j^\dagger\}$ and the same steps used to complete (1.103). In addition a factor $(-1)^c$ accounts for the number of fermion commutations necessary to pair the operators before they are contracted. As promised the recursive application of the procedure (1.116) reduces the original correlation function to products of Green's functions.

Space-time matrix \mathbf{g}

An elegant way to compute the full matrix \mathbf{g}

$$g_{\mathbf{x}'\mathbf{x}} = G_{x',x}(\tau', \tau) \quad (1.117)$$

which contains all possible time dependent Green's functions was used by Hirsch [43] in order to stabilize the calculation of time displaced Green's functions.

Evidently $\mathbf{x} = x_{i,\tau}$ and \mathbf{g} is a space time matrix of dimension $(N - m) \times (N - m)$, where we will only display the time part. The inverse \mathbf{g}^{-1} is directly calculated in the coherent state formalism (appendix C)

$$\mathbf{g}^{-1} = \begin{pmatrix} I & 0 & 0 & \dots & \mathbf{B}_1 \\ -\mathbf{B}_2 & I & 0 & \dots & 0 \\ 0 & -\mathbf{B}_3 & I & 0 & \vdots \\ \vdots & \ddots & & \ddots & 0 \\ 0 & \dots & 0 & -\mathbf{B}_m & I \end{pmatrix}.$$

It may be shown by direct multiplication $\mathbf{g}^{-1}\mathbf{g} = \mathbf{g}\mathbf{g}^{-1} = I$, that it really is the inverse of the matrix

$$\mathbf{g} = \begin{pmatrix} \mathbf{G}^>(1,1) & G^<(1,2) & \dots & G^<(1,m) \\ \mathbf{G}^>(2,1) & \mathbf{G}^>(2,2) & \dots & G^<(2,m) \\ \vdots & \vdots & \ddots & \vdots \\ \mathbf{G}^>(m,1) & \mathbf{G}^>(m,2) & \dots & G^>(m,m) \end{pmatrix}, \quad (1.118)$$

where the definition of the Green's functions follows Eqs. (1.101) and (1.100). The partition function Z is conveniently expressed in terms of \mathbf{g} in (1.118)

$$Z = \det(1 + \mathbf{B}) = \det \mathbf{g}^{-1}. \quad (1.119)$$

Zero temperature limit

Sofar we did not cite results in the PQMC “zero temperature” limit (1.14), where the trace is systematically replaced by a scalar product

$$\text{Tr } X \rightarrow \text{Tr } |R\rangle \langle L| X = \langle L| X |R\rangle. \quad (1.120)$$

In particular we need again the equal-time Green's function which is readily calculated [64]

$$\mathbf{G}(\tau) = \mathbf{G}^>(\tau, \tau) = 1 - \mathbf{B}(\tau, 0) \mathbf{R} \frac{1}{\mathbf{L}^\dagger \mathbf{B}(\beta, 0) \mathbf{R}} \mathbf{L} \mathbf{B}(\beta, \tau) \quad (1.121)$$

$$\mathbf{G}^<(\tau, \tau) = -\mathbf{B}(\tau, 0) \mathbf{R} \frac{1}{\mathbf{L}^\dagger \mathbf{B}(\beta, 0) \mathbf{R}} \mathbf{L} \mathbf{B}(\beta, \tau). \quad (1.122)$$

But in the zero temperature limit we can no longer rotate cyclically under the trace which necessitates entirely new proofs for the Wick theorem and so forth.

But instead of repeating the derivation for the zero temperature formalism, we may obtain every single result by taking the proper limit of the finite temperature version. [6] Additionally, this point of view guarantees a proper zero temperature algorithm whenever we already have a finite temperature version. In appendix C we define an operator $U(E)$ which in the limit $E \rightarrow \infty$ satisfies

$$\lim_{E \rightarrow \infty} U(E) = |R\rangle \langle L|. \quad (1.123)$$

Using this method we recover in app. C the Eq. (1.121) for the Green's function and

$$\langle L|U(\beta, 0)|R\rangle = \lim_{E \rightarrow \infty} \text{Tr} U(E) U(\beta, 0) = \lim_{E \rightarrow \infty} \det [1 + \mathbf{B}(E) \mathbf{B}(\beta, \mathbf{0})] \quad (1.124)$$

$$= \det \mathbf{L}^\dagger \mathbf{B}(\beta, \mathbf{0}) \mathbf{R} \quad (1.125)$$

for the scalar product.

Time displaced Green's functions are again obtained by “wrapping” the equal-time \mathbf{G} .

1.4 MC algorithm

MC scheme

We use the Monte Carlo scheme proposed by Blankenbecler, Sugar and Scalapino [14] to update the HS field and calculate observables. Here we introduce the necessary computational steps and provide a schematic outline of the algorithm.

Let us assume that we have already chosen a particular HS transformation and introduced an approximate path integral as in Eq. (1.42) with m Trotter steps. The path integral is

$$\langle \mathcal{O} \rangle = \sum_{s(\mathbf{i}, \tau)} \frac{p[s(\mathbf{i}, \tau)]}{Z} \frac{\text{Tr}[U(\beta, 0) \mathcal{O}]}{p[s(\mathbf{i}, \tau)]}. \quad (1.126)$$

The weight function

$$\frac{p[s(\mathbf{i}, \tau)]}{Z} \quad (1.127)$$

is naturally normalized to unity and will be sampled with a Metropolis algorithm. The decision to accept or reject the proposed spin flip is based on the *weight ratio*

$$\mathcal{R} = \frac{p[s'(\mathbf{i}, \tau)]}{p[s(\mathbf{i}, \tau)]}. \quad (1.128)$$

We will see that the ratio \mathcal{R} is easily calculated from the equal time Green's function $\mathbf{G}^\sigma(\tau)$. The observable part in

$$\frac{\text{Tr}[U(\beta, 0) \mathcal{O}]}{p[s(\mathbf{i}, \tau)]} \quad (1.129)$$

can be calculated using the Wick theorem. Thus for the moment the only observable we are interested in is the Green's function.

For updating the auxiliary field $s(\mathbf{i}, \tau)$ we propose sequential single spin flips which are accepted by Metropolis rules. The obvious choice for the sequential sweep through the field $s(\mathbf{i}, \tau)$ is to first visit all sites at a given time slice τ , then change over to the adjacent time slice and so forth. At the last time slice m we change direction and propagate back to $\tau = 1$.

On every time slice we need the two matrices $\mathbf{B}_s^\sigma(\beta, \tau)$ and $\mathbf{B}_s^\sigma(\tau, 0)$ which allow immediate calculation of the equal time Greens' function

$$\mathbf{G}_s^\sigma(\tau) = \frac{1}{\mathbf{1} + \mathbf{B}_s^\sigma(\tau, 0) \mathbf{B}_s^\sigma(\beta, \tau)}. \quad (1.130)$$

Moving on from one time slice to the next involves matrix multiplications for the $\mathbf{B}_s(\tau, 0)$ which we have to do m times for a full sweep. Successive multiplication of \mathbf{B}_s matrices has to be *stabilized* and inverse propagation like

$$\mathbf{B}_s^{-1}(\tau, \tau - 1) \mathbf{B}_s(\tau, 0) = \mathbf{B}_s(\tau - 1, 0). \quad (1.131)$$

is only possible over a few time slices. Extensive recalculations are avoided by storing matrices $\mathbf{B}_s(\beta, \tau)$ for all τ . In the next sweep we propagate $\mathbf{B}_s(\tau, 0)$ as we increase τ but take the matrix $\mathbf{B}_s(\beta, \tau)$ from storage.

Weight ratio

The Monte Carlo decision to accept or reject a new HS configuration \mathbf{s}' is based on the weight ratio

$$\mathcal{R}_\uparrow \mathcal{R}_\downarrow = \frac{p[s', \uparrow] p[s', \downarrow]}{p[s, \uparrow] p[s, \downarrow]}. \quad (1.132)$$

It is sufficient to consider the ratio for a single spin sector

$$\mathcal{R} = \frac{\text{Tr } U_{\mathbf{s}'}(\beta, 0)}{\text{Tr } U_{\mathbf{s}}(\beta, 0)}. \quad (1.133)$$

Let us assume a propagation matrix \mathbf{B}_n

$$\mathbf{B}_n = e^{\mathbf{V}_n} e^{-\Delta\tau \mathbf{h}_0} \quad (1.134)$$

where \mathbf{V}_n depends on the given HS configuration \mathbf{s}_n . We further introduce \mathbf{V}'_n for a different HS configuration \mathbf{s}'_n .

It is convenient to introduce the abbreviation Δ

$$\Delta = e^{\mathbf{V}'_n} e^{-\mathbf{V}_n} - 1, \quad (1.135)$$

such that upon updating

$$\mathbf{B}(\tau, 0) \longrightarrow e^{\mathbf{V}'_\tau} e^{-\mathbf{V}_\tau} \mathbf{B}(\tau, 0) = (1 + \Delta) \mathbf{B}(\tau, 0). \quad (1.136)$$

For the case that we make a single HS spin flip, the matrix Δ will be zero almost everywhere. Then we may define a small Δ_s which contains only the nonzero part of Δ

$$\Delta = \mathbf{p} \Delta_s \mathbf{q}, \quad (1.137)$$

where \mathbf{p} and \mathbf{q} are rectangular shaped matrices with only one and zero entries.

The weight ratio

$$\begin{aligned} \mathcal{R} &= \det [1 + (1 + \Delta) \mathbf{B}(\tau, 0) \mathbf{B}(\beta, \tau)] \det \frac{1}{1 + \mathbf{B}(\tau, 0) \mathbf{B}(\beta, \tau)} \\ &= \det \mathbf{G}'(\tau)^{-1} \mathbf{G}(\tau), \end{aligned} \quad (1.138)$$

is thus related to the ratio of the Green's functions \mathbf{G}'/\mathbf{G} . In the next section we obtain a simple expression for the ratio \mathbf{G}'/\mathbf{G} (Eq. 1.142) and \mathcal{R} depends only on the local part of the Green's function $\mathbf{q}(1 - \mathbf{G}(\tau))\mathbf{p}$

$$\mathcal{R} = \det (1 + \Delta (\mathbf{G}(\tau) - 1)) = \det (1_s + \Delta_s \mathbf{q}(1 - \mathbf{G}(\tau))\mathbf{p}). \quad (1.139)$$

Green's function update

We already indicated that for spin flips on a given time slice it is enough to know the Green's function $G(\tau)$. Yet $G(\tau)$ itself changes when a HS spin is flipped. Recalculating $G(\tau)$ using Eq. (1.130) would be extremely expensive. Fortunately there exists an efficient method for the Green's function update.

Again we consider only a single spin sector. Now we calculate the new Green's function \mathbf{G}' from the old \mathbf{G} . The defining equations are best written for \mathbf{G}^{-1}

$$\begin{aligned} \mathbf{G}^{-1}(\tau) &= 1 + \mathbf{B}(\tau, 0) \mathbf{B}(\beta, \tau), \\ [\mathbf{G}'(\tau)]^{-1} &= 1 + (1 + \Delta) \mathbf{B}(\tau, 0) \mathbf{B}(\beta, \tau). \end{aligned} \quad (1.140)$$

The updated inverse \mathbf{G}^{-1} is recast by adding $0 = \Delta - \Delta$

$$[\mathbf{G}']^{-1} = (1 + \Delta) \mathbf{G}^{-1} - \Delta, \quad (1.141)$$

and it is safe to omit the τ index from here on. Taking the inverse we obtain an expression for the *ratio* \mathbf{G}'/\mathbf{G}

$$\mathbf{G}' = \mathbf{G} [1 + \Delta (1 - \mathbf{G})]^{-1}, \quad (1.142)$$

which is a simple rearrangement of the following *Dyson equation*

$$\mathbf{G}' = \mathbf{G} - \mathbf{G}' \Delta (1 - \mathbf{G}). \quad (1.143)$$

In order to obtain the new Green's function we apply the Woodbury-Sherman-Morrison [86] formula ³

$$\frac{1}{(\mathbf{A} - \mathbf{B}\mathbf{C})} = \frac{1}{\mathbf{A}} + \frac{1}{\mathbf{A}} \mathbf{B} \frac{1}{1 - \mathbf{C}\mathbf{A}^{-1}\mathbf{B}} \mathbf{C} \frac{1}{\mathbf{A}} \quad (1.144)$$

to the ratio equation 1.142, using definitions

$$\mathbf{B} = \mathbf{p}, \quad (1.145)$$

$$\mathbf{C} = \Delta_s \mathbf{q} (1 - \mathbf{G}). \quad (1.146)$$

The updated Green's function is then obtained as

$$\mathbf{G}'(\tau) = \mathbf{G}(\tau) - \mathbf{G}(\tau) \mathbf{p} \frac{1}{1 + \Delta_s \mathbf{q} (1 - \mathbf{G}(\tau)) \mathbf{p}} \Delta_s \mathbf{q} (1 - \mathbf{G}(\tau)). \quad (1.147)$$

Dyson equation

First we would like to generalize the updating to the full space-time Green's function \mathbf{g} (1.118). In order to obtain equations that define the updating and are similar to (1.140)

³The Woodbury formula may be viewed as a simple series rearrangement

$$\begin{aligned} \frac{1}{(\mathbf{A} - \mathbf{B}\mathbf{C})} &= \frac{1}{\mathbf{A}} (1 + \mathbf{B}\mathbf{C}\mathbf{A}^{-1} + \mathbf{B}\mathbf{C}\mathbf{A}^{-1}\mathbf{B}\mathbf{C}\mathbf{A}^{-1} + \dots) \\ &= \frac{1}{\mathbf{A}} + \frac{1}{\mathbf{A}} \mathbf{B} (1 + \mathbf{C}\mathbf{A}^{-1}\mathbf{B} + \dots) \mathbf{C} \frac{1}{\mathbf{A}} \\ &= \frac{1}{\mathbf{A}} + \frac{1}{\mathbf{A}} \mathbf{B} \frac{1}{1 - \mathbf{C}\mathbf{A}^{-1}\mathbf{B}} \mathbf{C} \frac{1}{\mathbf{A}}. \end{aligned}$$

we introduce \mathbf{b} as the space-time generalization of the \mathbf{B} matrix

$$\mathbf{b} = \begin{pmatrix} 0 & 0 & 0 & \dots & \mathbf{B}_1 \\ -\mathbf{B}_2 & 0 & 0 & \dots & 0 \\ 0 & -\mathbf{B}_3 & 0 & 0 & \vdots \\ \vdots & & \ddots & \ddots & 0 \\ 0 & \dots & 0 & -\mathbf{B}_m & 0 \end{pmatrix} \quad (1.148)$$

and accordingly for the interaction with the space-time HS field, we generalize \mathbf{V} to a space-time matrix \mathbf{v}

$$e^{\mathbf{v}} = \begin{pmatrix} e^{\mathbf{V}_1} & 0 & 0 & \dots & \mathbf{0} \\ 0 & e^{\mathbf{V}_2} & 0 & \dots & 0 \\ 0 & 0 & e^{\mathbf{V}_3} & 0 & \vdots \\ \vdots & & \ddots & \ddots & 0 \\ 0 & \dots & 0 & 0 & e^{\mathbf{V}_m} \end{pmatrix}. \quad (1.149)$$

We emphasize, that with this notation we reproduce the matrix Eqs. (1.140) for \mathbf{g}^{-1}

$$\begin{aligned} \mathbf{g}^{-1} &= 1 + \mathbf{b}, \\ [\mathbf{g}']^{-1} &= 1 + e^{\mathbf{v}'} e^{-\mathbf{v}} \mathbf{b}. \end{aligned} \quad (1.150)$$

We already encountered two different ways to present the solution of these equations which both must apply again. Either the Dyson form

$$\mathbf{g}' = \mathbf{g} - \mathbf{g}' \delta (1 - \mathbf{g}), \quad (1.151)$$

or in the update form

$$\mathbf{g}' = \mathbf{g} + \mathbf{g} \mathbf{p} \frac{1}{1 + \delta_s \mathbf{q} (1 - \mathbf{g}) \mathbf{p}} \delta_s \mathbf{q} (1 - \mathbf{g}), \quad (1.152)$$

with δ and $\delta_s = \mathbf{p} \delta \mathbf{q}$ also defined on space and time. Using this updating equation for \mathbf{g} , Hirsch [43] was able to stabilize the computation of time displaced Green's functions because the inverse $(1 + \mathbf{b})^{-1}$ is a numerically stable operation⁴. Using the updating scheme (1.152) results in a very elegant formulation which is much easier to implement than the BSS scheme. Yet, there is a major drawback. Solving space-time equation directly for updating \mathbf{g} scales like $(N\beta)^3$ which compares unfavorably with the $N^3\beta$

⁴We will see below that wrapping of the equal-time Green's function (1.112) is very unstable.

behavior of the BSS algorithm. But here *all* possible time displaced Green's functions are calculated. This accounts for the difference of β^2 in two algorithms.

An interesting aspect of Eqs. (1.151) and (1.152) is that they allow to update the Green's function on a restricted set of space-time points. Let us assume that the HS field $s(\mathbf{i}, \tau)$ fluctuates only on a given subset $(\mathbf{i}, \tau) \in \mathcal{S}$ and is frozen everywhere else. Then the difference δ_s is also restricted to \mathcal{S} and Eqs. (1.151) and (1.152) become closed again if we are only interested in \mathbf{g}' , restricted to the same set of points where the HS field fluctuates. Applying this point of view we immediately think of two interesting restrictions \mathcal{S} :

1. Restricting HS fluctuations to a single time slice, we come to the BSS algorithm with sequential updating which is what we use. As long as we stay on a given time slice τ , updating the local HS field, we only need to know $\mathbf{G}(\tau)$ (see Eq. 1.147). The Green's function on other time slices does not enter explicitly!
2. The Hirsch-Fye algorithm [44] for the single impurity problem is based on another restriction of the general Dyson equation (1.151). The impurity is located at site f and we have to update a local HS field $s(f, \tau)$. Accordingly, we obtain closed equations for the impurity Green's function

$$\tilde{\mathbf{g}} = G_{ff}(\tau_1, \tau_2). \quad (1.153)$$

Updating $(\mathbf{LR})^{-1}$

The version of PQMC we use is based on updating the denominator

$$\frac{1}{\mathbf{L}_\tau \mathbf{R}_\tau}. \quad (1.154)$$

We introduced another useful abbreviation

$$\mathbf{L}_\tau = \mathbf{LB}(\beta, \tau), \quad (1.155)$$

$$\mathbf{R}_\tau = \mathbf{B}(\tau, 0) \mathbf{R}. \quad (1.156)$$

Updating $\mathbf{B}(\tau, 0)$ implies

$$\mathbf{R}_\tau \longrightarrow (1 + \mathbf{\Delta}) \mathbf{R}_\tau. \quad (1.157)$$

Finally the PQMC updates

$$(\mathbf{L}_\tau \mathbf{R}_\tau)^{-1} \longrightarrow (\mathbf{L}_\tau (1 + \Delta) \mathbf{R}_\tau)^{-1}, \quad (1.158)$$

not the Green's function. Starting with Eqs. (1.147) and (1.122) we obtain after some manipulations

$$(\mathbf{L}_\tau \mathbf{R}_\tau)^{-1} \longrightarrow (\mathbf{L}_\tau \mathbf{R}_\tau)^{-1} \quad (1.159)$$

$$- (\mathbf{L}_\tau \mathbf{R}_\tau)^{-1} \mathbf{L}_\tau \mathbf{p} \frac{1}{1 + \Delta_s \mathbf{q} \mathbf{B}(\tau, 0) \mathbf{B}(\beta, \tau) \mathbf{G}(\tau) \mathbf{p}} \Delta_s \mathbf{q} \mathbf{R}_\tau (\mathbf{L}_\tau \mathbf{R}_\tau)^{-1}. \quad (1.160)$$

MC summary

In principle, we now have all elements required to carry out the simulations. The equal time Green's function is the central quantity. On one hand it is used to compute all observables. On the other hand, it determines the Monte Carlo dynamics. As already mentioned it is convenient to adopt a sequential upgrading scheme. Given the Green's function at imaginary time τ , one upgrades the HS fields on this time slice deterministically or randomly. In case of acceptance, the Green's function is upgraded after each single spin flip. To reach the next time slice, the relation:

$$\mathbf{G}_s(\tau + \Delta\tau) = \mathbf{B}_s(\tau + \Delta\tau, \tau) \mathbf{G}_s(\tau) (\mathbf{B}_s(\tau + \Delta\tau, \tau))^{-1} \quad (1.161)$$

is used and the procedure is repeated till $\tau = \beta$ (FTQMC) or $\tau = 2\theta$ (PQMC). Having reached $\tau = \beta$ or $\tau = 2\theta$ we propagate the Green's function back to $\tau = 0$ and on the way upgrade the HS fields. The whole procedure may then be repeated. We note that for interactions of the form (1.65) the propagation of the Green's function from time slice τ to time slice $\tau + \Delta\tau$ is split into intermediate steps so as to upgrade the HS fields in the sets S_r successively. The above corresponds precisely to the procedure adopted in the case of the FTQMC. For the PQMC, it is more efficient to keep track of $(\mathbf{L}_\tau \mathbf{R}_\tau)^{-1}$ since (i) it is of dimension $N_e \times N_e$ in contrast to the Green's function which is a $N \times N$ matrix and (ii) it is τ independent. When Green's functions are required - to compute either the ratio \mathcal{R} , or observables - the matrix elements needed are calculated from scratch.

1.5 Numerical stabilization

In the previous section, we have assumed that we are able to compute the Green functions. On finite precision machines this is unfortunately not the case. To understand the sources of numerical instabilities, it is convenient to consider the PQMC. Instabilities in FTQMC will not be discussed but we refer the reader to [6] and references therein.

The rectangular matrix \mathbf{R} is just a set of column orthonormal vectors. Typically for a Hubbard model, at weak couplings, the extremal scales in the matrix $\mathbf{B}_s(2\theta, 0)$ are determined by the kinetic energy and range from $e^{4t\theta}$ to $e^{-4t\theta}$ in the two-dimensional case. When the set of orthonormal vectors in \mathbf{R} are propagated, the large scales will wash out the small scales yielding a numerically ill defined inversion of the matrix $\mathbf{LB}_s(2\theta, 0)\mathbf{R}$. To be more precise consider a two electron problem. The matrix \mathbf{R} then consists of two column orthonormal vectors, $\mathbf{r}(0)_1$ and $\mathbf{r}(0)_2$. After propagation along the imaginary time axis, they will be dominated by the largest scales in $\mathbf{B}_s(2\theta, 0)$ so that $\mathbf{r}(2\theta)_1 = \mathbf{r}(2\theta)_2 + \epsilon$, where $\mathbf{r}(2\theta)_1 = \mathbf{B}_s(2\theta, 0)\mathbf{r}(0)_1$. It is the information contained in ϵ which renders the matrix $\mathbf{LB}_s(2\theta, 0)\mathbf{R}$ non-singular. For large values of θ this information is lost in round-off errors. To circumvent this problem a set of matrix decomposition techniques were developed [95, 96, 107].

In practice one has to address three separate problems, all originating in the aforementioned mixing of large and small scales.

1. The product of many \mathbf{B} matrices is decomposed into UDV form

$$\begin{aligned} \mathbf{B} \dots \mathbf{B}\mathbf{R} &= \mathbf{U}_r \mathbf{D}_r \mathbf{V}_r, \\ \mathbf{L}\mathbf{B} \dots \mathbf{B} &= \mathbf{V}_l \mathbf{D}_l \mathbf{U}_l \end{aligned} \tag{1.162}$$

where \mathbf{U}_r (\mathbf{U}_l) is a $N \times N_e$ ($N_e \times N$) column (row) orthogonal matrix, $\mathbf{D}_{r,l}$ ($N_e \times N_e$) is diagonal and $\mathbf{V}_{r,l}$ ($N_e \times N_e$) is a well conditioned upper triangular matrix.⁵ Shapes of the respective matrices are given in brackets and correspond to the PQMC. The *main* information about the propagated Slater determinant is contained in \mathbf{U}_r which needs to be known with high precision. The scales \mathbf{D}_r and the matrix \mathbf{V}_r together only represent a single numerical prefactor $\det \mathbf{D}_r \mathbf{V}_r$ to the orthogonalized Slater

⁵Alternatively, one can use the singular value decomposition. [86]

determinant given by \mathbf{U}_r . This is illustrated by calculating the overlap

$$\det \mathbf{L}_\tau \mathbf{R}_\tau = \det \mathbf{L} \mathbf{B}(\beta, \tau) \mathbf{B}(\tau, 0) \mathbf{R} \quad (1.163)$$

$$= c \det \mathbf{U}_l \mathbf{U}_r, \quad (1.164)$$

where the prefactor c is given by

$$c = \det \mathbf{D}_r \mathbf{V}_r \times \det \mathbf{D}_l \mathbf{V}_l. \quad (1.165)$$

The calculation of the overlap (1.163) is only possible when $\mathbf{U}_{r,l}$ are known with high accuracy. This is reached by successive UDV decomposition (typically on every 5 or 10 Trotter time slices).

2. The inverse \mathbf{B}^{-1} is ill defined. We can certainly obtain a reasonable representation of matrix elements $(B^{-1})_{ij}$ through

$$\mathbf{B}^{-1} = \mathbf{V}^{-1} \mathbf{D}^{-1} \mathbf{U}^{-1}, \quad (1.166)$$

but as an inverse to \mathbf{B} satisfying

$$\mathbf{B}^{-1} \mathbf{B} = 1, \quad (1.167)$$

this will nevertheless fail. Numerically, even the simple multiplication

$$\mathbf{D} (\mathbf{V} \mathbf{V}^{-1}) \mathbf{D}^{-1} \neq 1 \quad (1.168)$$

does not give unity! Although Green's functions by definition involve some matrix inversion they eventually do not suffer from such instabilities. For the equal-time Green's function (1.122) this is easily verified

$$\mathbf{G}^<(\tau, \tau) = -\mathbf{R}_\tau \frac{1}{\mathbf{L}_\tau \mathbf{R}_\tau} \mathbf{L}_\tau = -\mathbf{U}_r \mathbf{D}_r \mathbf{V}_r \frac{1}{\mathbf{V}_l \mathbf{D}_l \mathbf{U}_l \mathbf{U}_r \mathbf{D}_r \mathbf{V}_r} \mathbf{V}_l \mathbf{D}_l \mathbf{U}_l \quad (1.169)$$

$$= -\mathbf{U}_r \frac{1}{\mathbf{U}_l \mathbf{U}_r} \mathbf{U}_l, \quad (1.170)$$

without explicit multiplications of type (1.168).

3. In order to obtain the time-displaced Green's function through wrapping the equal time $\mathbf{G}^<(\tau, \tau)$

$$\mathbf{G}^<(\tau_1, \tau) = \mathbf{B}^{-1}(\tau, \tau_1) \mathbf{G}^<(\tau, \tau) \quad (1.171)$$

$$= \mathbf{B}^{-1}(\tau, \tau_1) \mathbf{B}(\tau, 0) \mathbf{R} \frac{1}{\mathbf{L}_\tau \mathbf{R}_\tau} \mathbf{L}_\tau \quad (1.172)$$

we should do some “backpropagation” as in

$$\mathbf{B}^{-1}(\tau, \tau') \mathbf{B}(\tau, 0) \mathbf{R} = \mathbf{B}(\tau', 0) \mathbf{R}. \quad (1.173)$$

But this is again ill defined! However $\mathbf{G}^<(\tau_1, \tau)$ is a stable quantity which is apparent after rewriting $\mathbf{G}^<(\tau_1, \tau)$ as

$$\begin{aligned} \mathbf{G}^<(\tau_1, \tau) &= \mathbf{U}_r(\tau_1, 0) \frac{1}{\mathbf{U}_l(\beta, \tau) \mathbf{B}(\tau, \tau_1) \mathbf{U}_r(\tau_1, 0)} \mathbf{U}_l(\beta, \tau) \\ &= \mathbf{U}_r(\tau_1, 0) \mathbf{v}^{-1} \mathbf{d}^{-1} \mathbf{u}^{-1} \mathbf{U}_l(\beta, \tau), \end{aligned} \quad (1.174)$$

where \mathbf{d} will contain only large scales.

Efficient calculation of $\mathbf{G}^<(\tau_1, \tau)$

We conclude this introduction on auxiliary field methods with a detailed review of a stable and *efficient* way of calculating the time-displaced Green’s function $\mathbf{G}^<(\tau_1, \tau)$. [27] We first introduce another way of thinking about the mentioned instability by considering free electrons on a two-dimensional square lattice.

$$H = -t \sum_{\langle \mathbf{i}, \mathbf{j} \rangle} c_{\mathbf{i}}^{\dagger} c_{\mathbf{j}}. \quad (1.175)$$

For this Hamiltonian one has:

$$\langle \Psi_0 | c_{\mathbf{k}}^{\dagger}(\tau) c_{\mathbf{k}} | \Psi_0 \rangle = \langle \Psi_0 | c_{\mathbf{k}}^{\dagger} c_{\mathbf{k}} | \Psi_0 \rangle \exp(\tau(\epsilon_{\mathbf{k}} - \mu)), \quad (1.176)$$

where $\epsilon_{\mathbf{k}} = -2t(\cos(\mathbf{k}\mathbf{a}_x) + \cos(\mathbf{k}\mathbf{a}_y))$, $\mathbf{a}_x, \mathbf{a}_y$ being the lattice constants. We will assume $|\Psi_0\rangle$ to be non-degenerate. In a numerical calculation the eigenvalues and eigenvectors of the above Hamiltonian will be known up to machine precision, ϵ . In the case $\epsilon_{\mathbf{k}} - \mu > 0$, $\langle \Psi_0 | c_{\mathbf{k}}^{\dagger} c_{\mathbf{k}} | \Psi_0 \rangle \equiv 0$. However, on a finite precision machine the later quantity will take a value of the order of ϵ . When calculating $\langle \Psi_0 | c_{\mathbf{k}}^{\dagger}(\tau) c_{\mathbf{k}} | \Psi_0 \rangle$ this roundoff error will be blown up exponentially and the result for large values of τ will be unreliable.

The \mathbf{B}_s matrix plays the role of the exponential factors, and contains exponentially large and small scales whereas $\mathbf{G}_s^<(\theta, \theta)$ contains scales bounded by order unity. Since we equally expect the result $\mathbf{G}_s^<(\theta, \theta + \tau)$ to be bounded by order unity, we will eventually run into numerical problems when τ becomes *large*.

In order to circumvent this problem, Assaad and Imada [8] proposed to do the calculation at finite temperatures and then take the limit to vanishingly small temperatures. For the example of free electrons this amounts in doing calculation via:

$$\langle \Psi_0 | c_{\mathbf{k}}^\dagger(\tau) c_{\mathbf{k}} | \Psi_0 \rangle = \lim_{\beta \rightarrow \infty} \frac{\exp(\tau(\epsilon_{\mathbf{k}} - \mu))}{1 + \exp(\beta(\epsilon_{\mathbf{k}} - \mu))}.$$

Even if the eigenvalues are known only up to machine precision, the right hand side of the above equation for large but finite values of β is a numerically stable operation. To implement this idea in the QMC method, Assaad and Imada considered a single particle Hamilton H_0 which has the trial wave function, $|\Psi_T\rangle$ as non-degenerate ground state and then compute:

$$\mathbf{G}_s^<(\theta, \theta + \tau) \equiv \lim_{\beta \rightarrow \infty} \frac{\text{Tr} (e^{-\beta H_0} U_s(2\theta, \theta + \tau) c_y^\dagger U_s(\theta + \tau, \theta) c_x U_s(\theta, 0))}{\text{Tr} (e^{-\beta H_0} U_s(2\theta, 0))}. \quad (1.177)$$

Although the rhs of the above equation may be computed in a numerically stable way, the approach is cumbersome and numerically expensive. In particular, for each measurement, all quantities have to be computed from scratch since the ad-hoc inverse temperature β has to be taken into account.

The alternative, efficient method may be introduced in a similar intuitive way. We start again with the example of free electrons. Since, $\langle \Psi_0 | c_{\mathbf{k}}^\dagger(\tau) c_{\mathbf{k}} | \Psi_0 \rangle = 1, 0$, we can rewrite Eq. (1.176) as:

$$\langle \Psi_0 | c_{\mathbf{k}}^\dagger(\tau) c_{\mathbf{k}} | \Psi_0 \rangle = \left(\langle \Psi_0 | c_{\mathbf{k}}^\dagger c_{\mathbf{k}} | \Psi_0 \rangle \exp((\epsilon_{\mathbf{k}} - \mu)\tau) \right)^\tau \quad (1.178)$$

which involves only well defined numerical manipulations even in the large τ limit.

The implementation of this idea in the QMC algorithm is as follows. First, one has to notice that the Green function $\mathbf{G}_s^<(\theta, \theta)$ is a projector:

$$\mathbf{G}_s^<(\theta, \theta)^2 = \mathbf{G}_s^<(\theta, \theta). \quad (1.179)$$

Let $\mathbf{G}_s^<(\theta, \theta)$ be given by

$$\mathbf{G}_s^<(\theta, \theta) = \mathbf{R}(\mathbf{LR})^{-1}\mathbf{L}, \quad (1.180)$$

and Eq. (1.179) follows from:

$$\begin{aligned} \mathbf{G}_s^<(\theta, \theta)^2 &= \mathbf{R}(\mathbf{LR})^{-1}\mathbf{LR}(\mathbf{LR})^{-1}\mathbf{L} \\ &= \mathbf{G}_s^<(\theta, \theta). \end{aligned} \quad (1.181)$$

This in turn implies that $\mathbf{G}_s^<(\tau_1, \tau_3)$ obeys a simple composition identity

$$\mathbf{G}_s^<(\tau_1, \tau_2)\mathbf{G}_s^<(\tau_2, \tau_3) = \mathbf{G}_s^<(\tau_1, \tau_3) \quad (1.182)$$

since

$$\begin{aligned} \mathbf{G}_s^<(\tau_1, \tau_3) &= \mathbf{G}_s^<(\tau_1, \tau_1)\mathbf{B}_s^{-1}(\tau_3, \tau_1) = \\ &[\mathbf{G}_s^<(\tau_1, \tau_1)]^2 \mathbf{B}_s^{-1}(\tau_3, \tau_1) = \mathbf{G}_s^<(\tau_1, \tau_1)\mathbf{G}_s^<(\tau_1, \tau_3) \\ &= \mathbf{G}_s^<(\tau_1, \tau_2)\mathbf{G}_s^<(\tau_2, \tau_3). \end{aligned}$$

Using this composition property (1.182) we can break up a large τ interval into a set of smaller intervals of length $\tau = N\tau_1$ so that

$$\mathbf{G}_s^<(\theta, \theta + \tau) = \prod_{n=0}^{N-1} \mathbf{G}_s^<(\theta + [n+1]\tau_1, \theta + n\tau_1) \quad (1.183)$$

The above equation is the generalization of Eq. (1.178). If τ_1 is *small* enough each Green's function in the above product is accurate and has matrix elements bounded by order unity. The matrix multiplication is then numerically well defined.

We conclude this section by comparing both presented approaches for the calculation of time displaced correlation functions in the PQMC. We consider the special case of the Kondo lattice model (see Fig. 1.3). Both methods based on Eq. (1.183) and Eq. (1.177) produce identical results within the error-bars. (Had we used the same series of random numbers, we would have obtained exactly the same values up to roundoff errors which are of the order 10^{-8})

The important point however, is that the method based on Eq. (1.183) is for the considered case an order of magnitude faster in CPU time than the calculation based on Eq. (1.177).

1.6 The Sign Problem

Although the sign problem is the major restriction in QMC, surprisingly little is known why and when a Hamiltonian may in principle have a sign free representation.

Obviously, the first ingredient involved is the spin $\uparrow \Leftrightarrow \downarrow$ symmetry of the Hamiltonian. This is not very restrictive. Second, we regard the attractive Hubbard model as generic

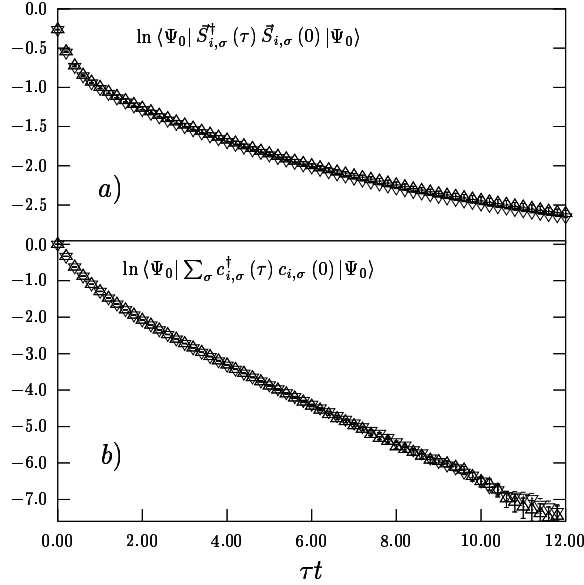


Figure 1.3: Imaginary time displaced on-site spin-spin correlation function (a) and Green's function (b). We consider a 6×6 lattice at half-filling and $J/t = 1.2$. In both (a) and (b) results obtained from Eq. (1.183) (\triangle) and (1.177) (∇) are plotted.

prototype for systems where we can find a sign free simulation. From the PQMC path integral we may immediately deduce the following representation of the ground state $|\Psi_0\rangle$

$$|\Psi_0\rangle = \sum_i c_i |\psi_{i,\uparrow}\rangle \otimes |\psi_{i,\downarrow}\rangle, \quad (1.184)$$

with positive $c_i \geq 0$ and real Slater determinants $|\psi_{i,\uparrow}\rangle = |\psi_{i,\downarrow}\rangle$. Of course, this satisfies the spin $\uparrow \Leftrightarrow \downarrow$ symmetry, but conversely not every symmetric Hamiltonian will have a positive real representation (1.184). An alternative representation of $|\Psi_0\rangle$ is illustrated by the complex decoupling of the attractive U model with complex $|\psi_{i,\uparrow}\rangle = \overline{|\psi_{i,\downarrow}\rangle}$.

The HS decoupling of the repulsive Hubbard model apparently violates condition (1.184). But the repulsive U simulations are only possible due to the accidental particle-hole symmetry that maps $U \leftrightarrow -U$.

When a sign-free simulation is not possible we have to sample the average sign

$$\langle \text{sign} \rangle = \frac{\sum_s p[s]}{\sum_s |p[s]|}, \quad (1.185)$$

in order to calculate observables. For the repulsive U model away from half-filling, the average sign decays quickly as shown in Fig. 1.4. This is most severe at low dopings. In general, when the average sign drops below 0.1 accurate simulations become prohibitively expensive.

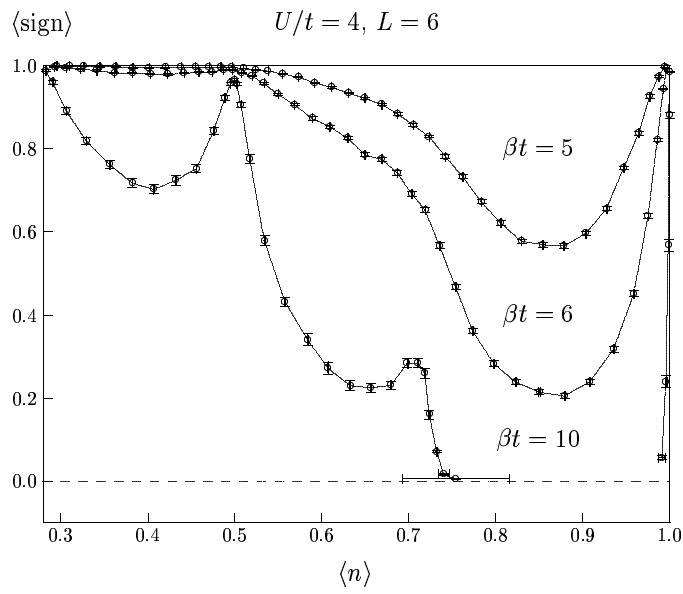


Figure 1.4: Average sign versus band filling $\langle n \rangle$ on a 6×6 lattice at $U/t = 4$. Filled shells are present at $\langle n \rangle = 26/36$ and $\langle n \rangle = 18/36$. As apparent for those band fillings, the decay of the average sign is slow.

Chapter 2

Kondo-Hubbard model

2.1 Introduction

In this chapter we will discuss the single-hole dynamics in the half-filled two-dimensional Kondo-Hubbard model. [28] It is appropriate to start the discussion of Kondo physics with a brief account of the single impurity Kondo effect. At first sight the Kondo Hamiltonian may look simple: free conduction electrons $c_{i,\sigma}^\dagger$ interact with the impurity spin $\vec{S}_{1,f}$ via the local antiferromagnetic interaction J

$$H_K = -t \sum_{\langle i,j \rangle, \sigma} \left(c_{i,\sigma}^\dagger c_{j,\sigma} + H.c. \right) + J \vec{S}_{1,c} \vec{S}_{1,f}. \quad (2.1)$$

The electron spin is given by $\vec{S}_{1,c} = 1/2 \sum_{s,s'} c_{1,s}^\dagger \vec{\sigma}_{s,s'} c_{1,s'}$ with Pauli matrices $\vec{\sigma}$. The longitudinal scattering from $S_{1,c}^z S_{1,f}^z$ is a simple potential scattering that leaves electrons independent. But the impurity has two states and spin flip scattering may change them. This is enough to create effective electron-electron interactions as illustrated in Fig. 2.1. Consider two electrons with spin-up which subsequently scatter from the impurity. If the first electron spin-flip scatters the impurity is left in spin-up state and the second up-electron *cannot* spin-flip scatter. On the other hand the first electron could do a potential scattering that conserves the spin of the impurity thus giving the second electron a chance for spin-flip scattering. In this way electrons interact exchanging information through the impurity spin state and a many-body problem results. In the Kondo problem [57], [3] two interesting things happen upon cooling the system. First one observes a crossover from the high temperature free spin behavior (Fig. 2.2a) to a new low temperature state where conduction electrons screen the magnetic impurity by singlet formation. At

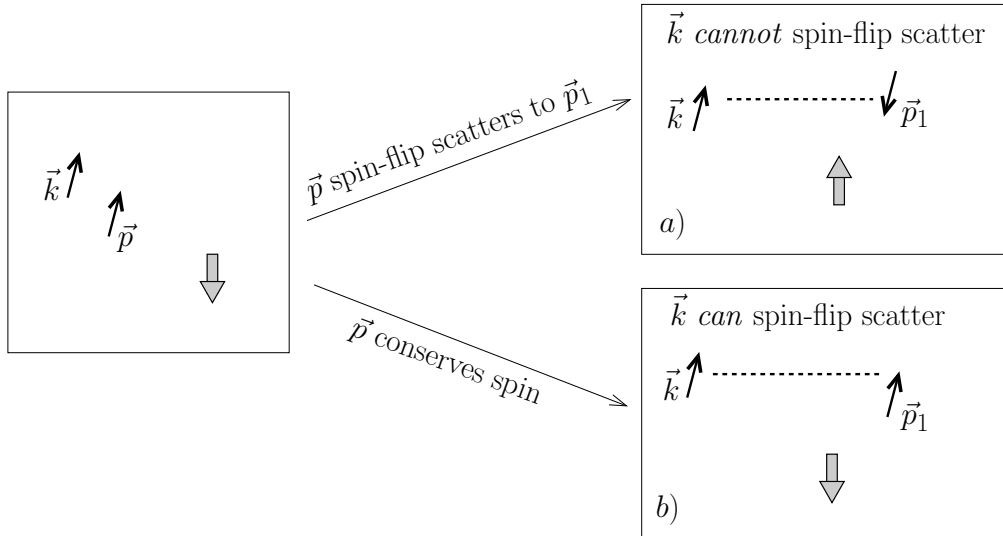


Figure 2.1: In the Kondo problem the magnetic impurity with its two states mediates an effective interaction between the electrons. We consider two up-electrons that subsequently scatter from a down-spin impurity. In case *a*) the first electron \mathbf{p} spin-flip scatters which leaves the impurity in the up state. Then the \mathbf{k} electron *cannot* spin-flip scatter. In case *b*) the first electron scatters and conserves spins. Then the second electron *can* spin-flip scatter. The second scattering process depends on the first which amounts to an effective electron-electron interaction mediated by the magnetic impurity (adapted from [108]).

the same time the impurity resistivity *increases* and a resistivity minimum is measured (Fig.2.2b). It turns out that this crossover happens for arbitrary small couplings J at a temperature T_K . In weak coupling the Kondo temperature is exponentially small

$$T_K = W e^{-1/J\rho_0} \quad (2.2)$$

where the bandwidth W and density of states at the Fermi level ρ_0 are used. The second important question involves the $T \rightarrow 0$ behavior. Wilson [108] found a finite impurity susceptibility $\chi_{\text{imp}}(T=0)$ which indicates that the impurity spin is fully compensated and a large singlet object is formed.¹ Approaching zero temperature the gradual buildup of the perfect singlet is linked to criticality. The diverging length scale is the lifetime of the singlet or the inverse spin-flip scattering rate. This results in universal behavior for

¹The easiest way to understand the formation of a bound singlet object, is the variational calculation due to [112].

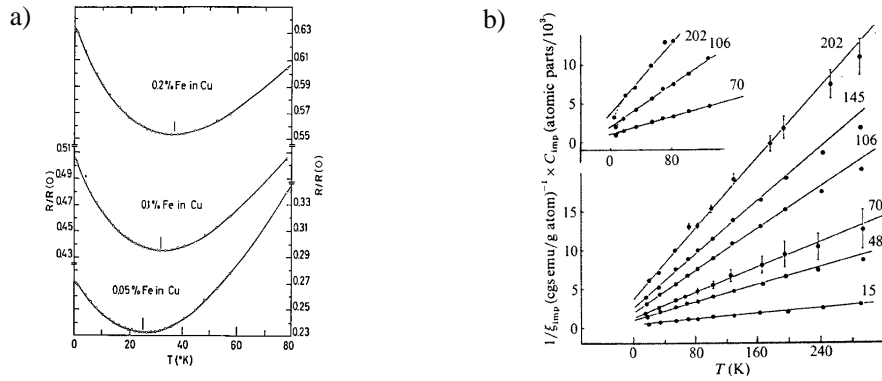


Figure 2.2: Panel a) The resistance as a function of temperature for Cu with Fe as impurity. The resistance minimum is evident. (From [33])

Panel b) The inverse susceptibility follows a Curie-Weiss law at high temperatures. At low T the impurity χ'_{imp} saturates at a finite value. (Reproduced from [48])

$T < T_K$. The Kondo screening cloud is exponentially large

$$\xi_K = ae^{1/J\rho_0} \quad (2.3)$$

where a is the lattice spacing.

In the Kondo model the valence of the impurity site is naturally restricted to one (integral valence). This corresponds to the large U limit in the more general Anderson impurity model which can also describe valence mixing between f^0 and f^1 impurity levels. Further on we restrict our attention to the integral valence regime.

Next, we want to switch attention to lattice models with a periodic arrangement of “impurity” sites. It is interesting to see what happens when we go from the dilute limit of Kondo impurities to a periodic lattice arrangement of the impurity sites. This is realized in $\text{Ce}_x\text{La}_{1-x}\text{Cu}_6$ where the nonmagnetic Lanthanum is gradually substituted by the rare earth Cerium and single impurity Kondo behavior changes to a heavy fermion system (HFS). In Fig.2.3 the molar magnetic resistivity is plotted. Enhancement of electron mass and specific heat coefficient in the HFS CeCu_6 is of order 1000 which sets in at a temperature comparable to the single impurity T_K .² Mass enhancement is due to the formation of a narrow f -band contributing to the Fermi sea. In pure CeCu_6 the resistivity at much lower temperatures $T \sim 0.1\text{K}$ follows the Landau Fermi liquid form $\rho = \rho_0 + AT^2$

²In CeCu_6 the specific heat coefficient $\gamma = 1550 \text{ mJ/molK}^2$. Pure metallic Cu: $\gamma = 0.695 \text{ mJ/molK}^2$.

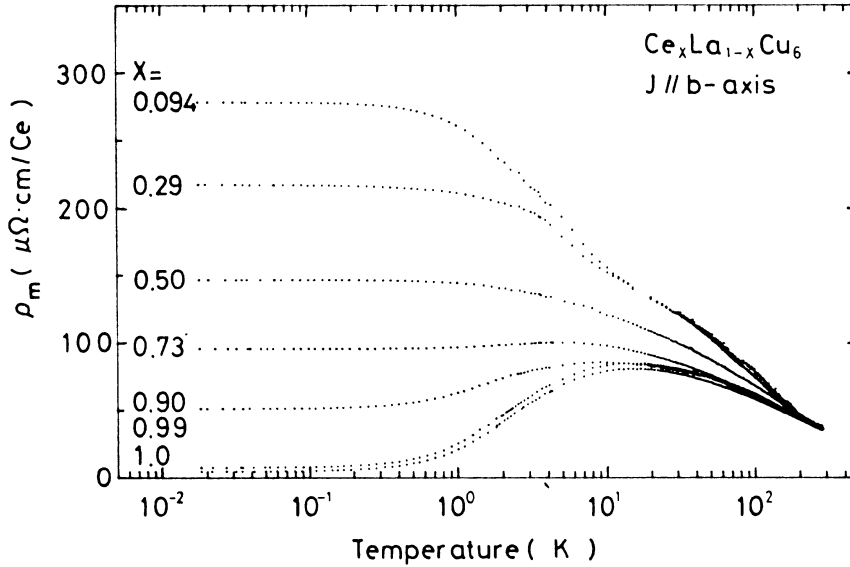


Figure 2.3: Temperature dependence of the magnetic resistivity ρ_m per mole Ce: $\rho_m = \rho_{\text{Ce}_x\text{La}_{1-x}\text{Cu}_6} - \rho_{\text{LaCu}_6}$. Taken from [99]. The Kondo temperature $T_K \sim 10\text{K}$ is robust up to pure CeCu_6 . This is also the temperature where the mass enhancement sets in. On a much lower temperature scale $T \sim 0.1\text{K}$ Fermi liquid behaviour is restored and the resistivity obeys the Landau form $\rho = \rho_0 + AT^2$.

which is interpreted as coherent Kondo singlets forming the narrow band. The CeCu_6 is a prototype heavy-fermion system with a large enhancement factor

$$\frac{A^*}{A} \propto \frac{\gamma^*}{\gamma} \propto \frac{m^*}{m} \propto 1000. \quad (2.4)$$

It is only fair to say that on the theoretical side, HFS need further understanding. Yet a common ingredient in theories for HFS is the integral valence of the rare earth f -orbital. This has led to the study of the Kondo lattice model, where only the f -spin degree of freedom is retained.

In the Kondo lattice model (KLM)

$$H_{KLM} = -t \sum_{\langle i,j \rangle, \sigma} (c_{i,\sigma}^\dagger c_{j,\sigma} + H.c.) + J \sum_{\mathbf{i}} \vec{S}_{\mathbf{i},c} \vec{S}_{\mathbf{i},f} \quad (2.5)$$

the singly occupied f -electron interacts with the conduction electrons via a local anti-ferromagnetic Heisenberg term. Here we only want to list some fundamental questions regarding the KLM 2.5:

1. it is only conjectured that the fixed point of the KLM in more than one dimension is a Fermi liquid³ (FL).
2. when we have a FL, Luttinger's theorem [66, 69, 55] states that the volume of the Fermi surface (i.e. the volume enclosed by the surface) does not change when an interaction is turned on. Since Luttinger's theorem is proven perturbatively, it is only valid as long we do not go through a non-analytic point in the phase diagram. What is the Fermi surface volume in the KLM? In particular, do the f -spins contribute such that we have a "large Fermi surface" [83], or does the Fermi sea contain only conduction electrons.
3. we could easily answer the question about the Fermi surface volume if we can connect the weak coupling periodic Anderson model (PAM) to the KLM on a analytic path in the phase diagram. In the PAM we may choose $V \rightarrow \infty$ and $U \rightarrow \infty$ requiring

$$\frac{V^2}{U} \rightarrow \text{const.} \quad (2.6)$$

which generates a formal Kondo limit [93] for the PAM. Assuming analyticity along such a path, the KLM is a FL with a large Fermi surface volume.

Exactly at half filling a *Kondo insulator* emerges (in accordance with a band picture) with a small gap of the order of T_K in Eq. (2.2). For instance $\text{Ce}_3\text{Bi}_4\text{Pt}_3$ belongs to this class of insulators [1].

Finally the Kondo lattice model contains an additional magnetic interaction which acts between f -spins, namely the Ruderman-Kittel-Kasuya-Yosida (RKKY) interaction. A localized spin will polarize the sea of conduction electrons. This polarization is of oscillating, long range nature and will couple to f -spins in the vicinity of the original polarizing spin. The effective spin-spin interaction is

$$J_{eff}(\mathbf{q}) \propto -J^2 \text{Re} \chi(\mathbf{q}, \omega = 0), \quad (2.7)$$

with $\chi(\mathbf{q}, \omega)$ being the spin susceptibility of the electrons. But with increasing Kondo coupling J the f -spins are screened and become nonmagnetic. In this sense there is

³In one dimension the FL has to be replaced by a Luttinger liquid but questions regarding the volume of the Fermi sea remain [110].

competition between RKKY magnetism and Kondo singlet formation leading to a quantum phase transition. [7] RKKY interaction and singlet formation are visualized⁴ in the caricature plot 2.4. The Doniach phase diagram summarizes this competition in the

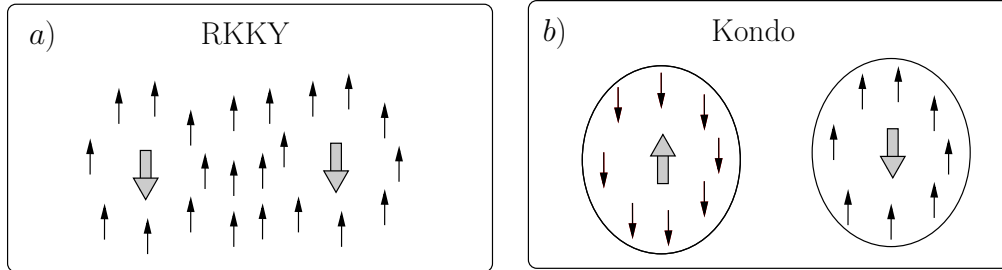


Figure 2.4: Panel a) Polarized conduction electrons mediate an effective interaction between f -spins. The sketch is for ferromagnetic interaction. Panel b) For large J a cloud of localized conduction electrons forms singlets with the f -spin. Singlet formation obviously competes with the magnetic state.

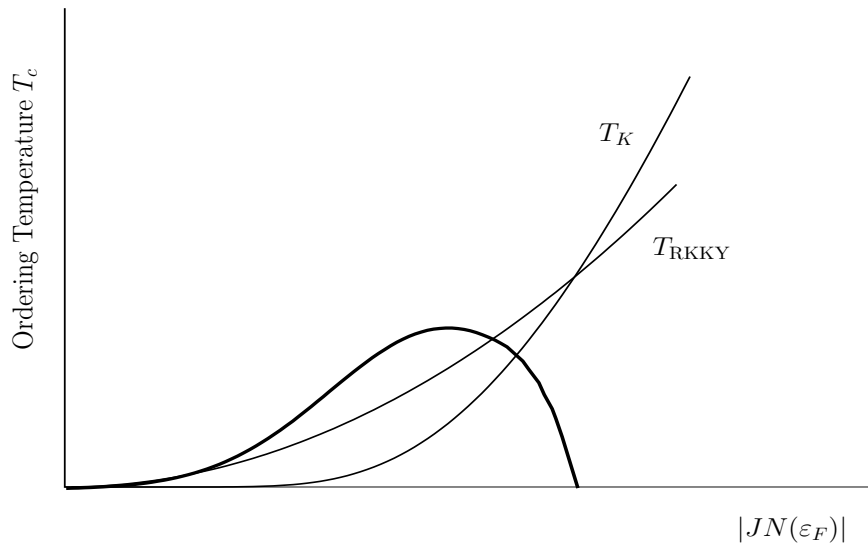


Figure 2.5: The different J dependence of $T_{\text{RKKY}} \sim J^2$ and $T_K \sim W e^{-\frac{W}{J}}$ is summarized in the Doniach diagram where the region of dominant RKKY interaction is identified with the region of the magnetic state.

following way: In the weak coupling regime, the singlet formation is preempted by the

⁴Looking at plot 2.4 b) the problem of exhaustion becomes apparent. In a system with equal number of f -spins and conduction electrons complete localization of the electrons is necessary in order to compensate each f -spin. For weak coupling such a state is prohibited by the large kinetic energy.

larger RKKY scale responsible for a magnetic state. At some critical value J_c the Kondo energy scale starts to dominate and the nonmagnetic heavy fermion state forms. Doniach's Kondo necklace model [20] [113] substantiates this view of a quantum critical point. In the two HFS CePd_2Si_2 [71] and $\text{CeCu}_{6-x}\text{Au}_x$ [65] it is possible to observe this magnetic-paramagnetic transition by tuning pressure or by the chemical substitution with the larger Au atoms, thereby increasing the hybridization and J . Both HFS have a metallic RKKY phase with incommensurate antiferromagnetism.

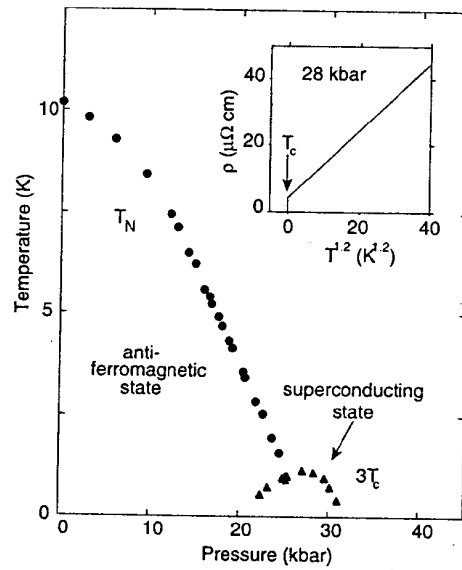


Figure 2.6: The Néel temperature of CePd_2Si_2 decreases when pressure is applied and serves as direct evidence of the Doniach phase diagram. Taken from [71].

Heavy fermion systems give rise to a large variety of questions. In the following we concentrate on a model with a Doniach phase diagram.

2.2 Model

We consider the Kondo lattice model in two dimensions at half filling. The phases of this model are dominated by the competition of the RKKY and Kondo interaction and the general picture of the Doniach phase diagram is realized. A peculiarity of our model are the dominant AF fluctuations in the half filled conduction band. Therefore the RKKY interaction is antiferromagnetic and stabilizes a commensurate insulating AF phase.

In addition to the antiferromagnetic exchange coupling J we investigate the role of a Coulomb repulsion U in the conduction band. Starting from the seminal work of Brinkman and Rice [15] the single-hole dynamics in correlated insulators has remained an intriguing issue with many open questions yet to be clarified. In this respect our Kondo model with the additional Hubbard interaction provides for a case in which the single particle dynamics can be studied continuously across genuinely distinct correlation induced insulating phases, i.e., Mott-Hubbard insulators with long range antiferromagnetic order, magnetic insulators and Kondo insulators. Of particular interest in this situation is to understand i) which properties of the correlated insulator, i.e., long range magnetic order or local effects determine the functional form of the quasiparticle dispersion relation and more specifically ii) if it is possible to continuously deform the spectral function of the Mott Hubbard insulator to that of the Kondo insulator.

In order to answer these questions, we consider a Kondo lattice model with an additional local Coulomb repulsion U between the conduction electrons (*UKLM*) on a two-dimensional square lattice

$$\begin{aligned}
H = & \sum_{\mathbf{k},\sigma} \varepsilon(\mathbf{k}) c_{\mathbf{k},\sigma}^\dagger c_{\mathbf{k},\sigma} + J \sum_{\mathbf{i}} \vec{S}_{\mathbf{i}}^c \cdot \vec{S}_{\mathbf{i}}^f \\
& + U \sum_{\mathbf{i}} (n_{\mathbf{i},\uparrow}^c - 1/2) (n_{\mathbf{i},\downarrow}^c - 1/2). \tag{2.8}
\end{aligned}$$

The unit cell, \mathbf{i} , contains a localized orbital and an extended conduction band state. In the Kondo limit, charge fluctuations on the localized orbital are suppressed with only the spin degrees of freedom remaining, $\vec{S}_{\mathbf{i}}^f = \sum_{s,s'} f_{\mathbf{i}s}^\dagger \vec{\sigma}_{s,s'} f_{\mathbf{i}s'}/2$, where $\vec{\sigma}$ are Pauli spin-1/2 matrices and $f_{\mathbf{i}s}^\dagger$ are fermionic operators which satisfy the constraint $\sum_s f_{\mathbf{i}s}^\dagger f_{\mathbf{i}s} = 1$. Conduction band electrons of spin z -component σ are created by $c_{\mathbf{i},\sigma}^\dagger$ where $n_{\mathbf{i},\sigma} = c_{\mathbf{i},\sigma}^\dagger c_{\mathbf{i},\sigma}$ is the conduction band density for spin z -component σ . The extended orbitals overlap to form a band with a dispersion $\varepsilon(\mathbf{k}) = -2t(\cos(k_x) + \cos(k_y))$ assuming a nearest-neighbor (NN) hopping integral t . The Coulomb repulsion U is taken into account by the Hubbard interaction term. Geometry and interactions of the *UKLM* are visualized in Fig. 2.7.

At half-filling and for the particular conduction band structure chosen the *UKLM* is an insulator for all values of U and J [49, 103, 7, 18]. The phase diagram 2.8 summarizes what is known from strong coupling and previous work. Specifically, as $J = 0$ the *UKLM* maps onto the Hubbard model⁵. The latter is in a Mott insulating phase, which however

⁵Note however, that $U = 0$ is a singular point with complete degeneracy of the f -spins.

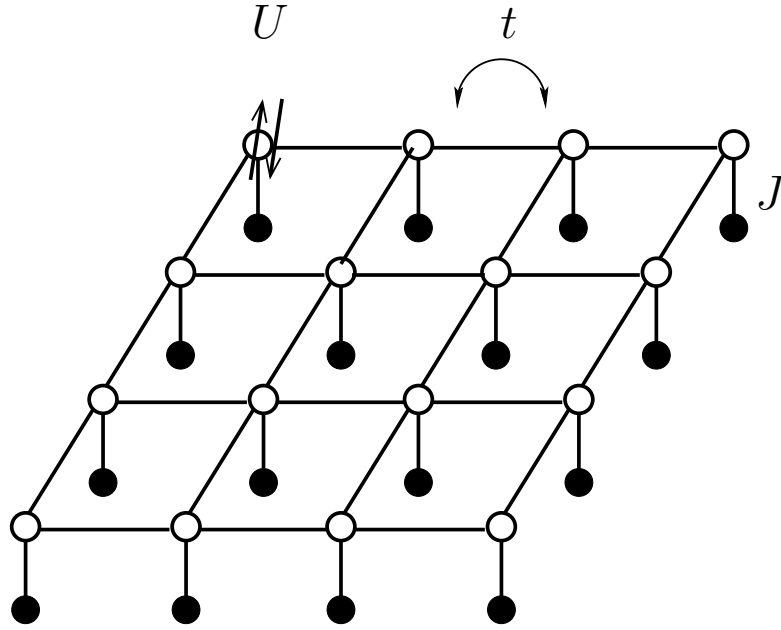


Figure 2.7: We consider a Kondo lattice problem on the square lattice. In addition to the Kondo interaction, conduction electrons experience a Coulomb repulsion U .

due to nesting on the square lattice is masked by an antiferromagnetic spin density wave with no spin gap. In the strong coupling limit a charge gap $\propto U$ opens, and the Hubbard model maps on the Heisenberg model.

For the KLM at $U = 0$ Assaad [7] finds a continuous transition between the ordered AF and disordered Kondo phase with a quantum critical point at $J_c = 1.45t$. The pure Kondo model in the strong coupling limit $J/t \gg 1$ has a ground state $|\Psi_K\rangle$ given by a product of Kondo singlets on the f - c bonds of the unit cell

$$|\Psi_K\rangle = \prod_{\mathbf{i}} \left(c_{\mathbf{i},\uparrow}^\dagger f_{\mathbf{i},\downarrow}^\dagger - c_{\mathbf{i},\downarrow}^\dagger f_{\mathbf{i},\uparrow}^\dagger \right) |0\rangle. \quad (2.9)$$

In lowest order the spin gap is due to a singlet-triplet excitation and $\Delta_s = J + O(t^2/J)$ [103]. A charge excitation is only possible by breaking two singlets with a charge gap $\Delta_c = 3/2J + O(t)$ (see Fig2.9). Therefore $\Delta_c > \Delta_s$ which is characteristic for Kondo insulators.

The limiting ground state for both lines $U \rightarrow \infty, J > 0$ and $J \rightarrow \infty, U \geq 0$ is again $|\Psi_K\rangle$: As $J/U \rightarrow \infty$ the Hubbard repulsion can be neglected relative to the exchange scattering and the model maps onto the pure Kondo lattice model. The whole line $U \rightarrow \infty, J > 0$ belongs also to the Kondo phase. Starting at $J = 0$ the effective Heisenberg

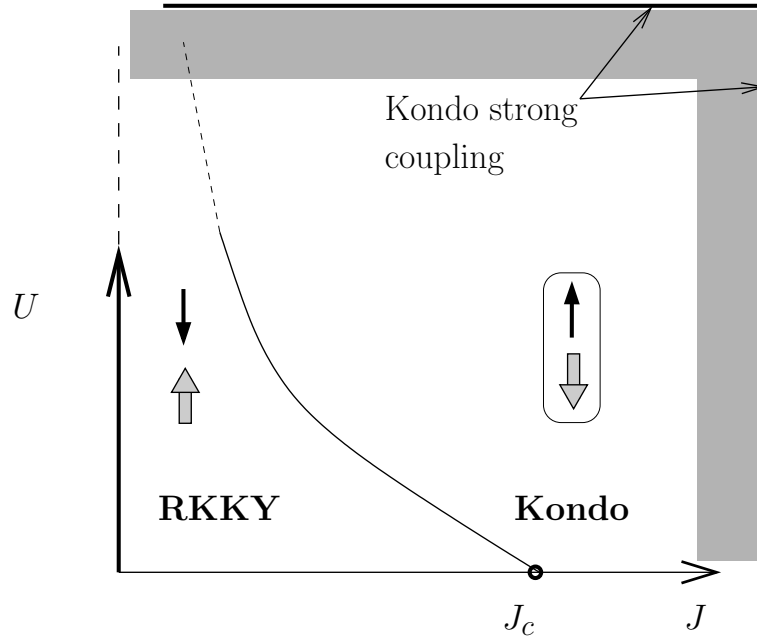


Figure 2.8: The phase diagram of the UKLM Kondo model. Along the line $J = 0$ the Hubbard model is responsible for charge dynamics. The groundstate for the two strong coupling lines is given by the Kondo singlet groundstate $|\Psi_K\rangle$ as in Eq. 2.9. In the shaded area the UKLM maps on an effective spin model. For $U = 0$ QMC calculations [7] indicate a critical value $J_c = 1.45t$. This point belongs to a critical line $J_c(U)$ that separates a magnetically ordered RKKY and disordered Kondo singlet phase.

coupling $J_{\text{Heis}} \propto 1/U$ and is irrelevant against any finite Kondo J . The only effect of U is to suppress any RKKY phase which needs itinerant electrons to mediate the magnetic interaction. Regions with a pure spin like ground state are shaded in Fig. 2.8.

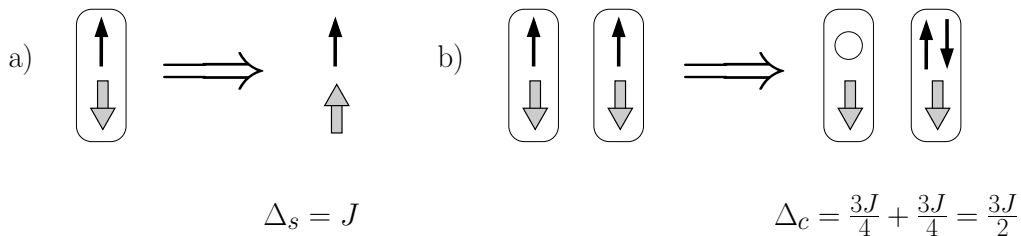


Figure 2.9: Panel a) the Kondo strong coupling groundstate is a product of local singlets. In lowest order the spin gap $\Delta_s = J$ the singlet-triplett excitation energy. Panel b) the charge gap $\Delta_c = 3/2J$ twice the singlet breaking.

In both of the aforementioned limiting cases, the single particle spectral function

displays very different behavior. For the Kondo ground state $|\Psi_K\rangle$, adding a hole into the conduction band will break a singlet. This leads to a hole dispersion relation

$$\tilde{\varepsilon}(\mathbf{k}) = 3J/4 + t(\cos(k_x) + \cos(k_y)) \quad (2.10)$$

in first order perturbation theory in t/J [103]. Hence the low energy hole dynamics is governed by the wave vectors $\mathbf{k} = (\pm\pi, \pm\pi) \equiv \pm\mathbf{Q}$. At present the precise form of the single particle spectral function for the Mott insulating state is still unknown. Yet, various numerical and analytical approaches confirm that the low energy hole dynamics is governed by \mathbf{k} -points on the boundary of the magnetic Brillouin zone, i.e., at $\mathbf{k} = (0, \pm\pi), (\pm\pi, 0)$ and $\mathbf{k} = (\pm\pi/2, \pm\pi/2)$. In order to shed light onto this situation we can fix U and, as a function of J/t , drive the system through a magnetic quantum phase transition at $J = J_c(U)$ from the Kondo insulator for $J/t \gg 1$ into the Mott insulating state for $J \rightarrow 0$. Along this path we compute the spectral function $A(\vec{k}, \omega)$, both, *exactly* by using quantum Monte Carlo methods and approximately using a bond-operator mean field theory. Based on our findings we argue that the low energy features of the spectral function are insensitive to the quantum phase transition. In other words, the low energy hole-states are found at $\vec{k} = (\pm\pi, \pm\pi)$ for *all* values of $J > 0$. It is only at $J = 0$ that the spectral weight of the low energy feature at $\vec{k} = (\pm\pi, \pm\pi)$ vanishes to produce the single-hole dispersion relation of the Hubbard model. Thus our main results are (i) that the local screening of the f -spins dominates the low energy features of the spectral function and (ii) that there is no continuous path from the Kondo to the Mott-Hubbard insulator with AFLRO in this specific model.

2.3 QMC

We have used the projector auxiliary field quantum Monte Carlo (PQMC) method to investigate the UKLM model. In order to find a suitable Hubbard-Stratonovich decoupling for the Kondo interaction we use the perfect square [7]

$$-\left(\sum_{\sigma} c_{\mathbf{i},\sigma}^{\dagger} f_{\mathbf{i},\sigma} + H.c.\right)^2 = 4\vec{S}_{\mathbf{i}}^c \vec{S}_{\mathbf{i}}^f - 2\left(\Delta_{\mathbf{i},c}^{\dagger} \Delta_{\mathbf{i},f} + H.c.\right) + n_{\mathbf{i}}^c n_{\mathbf{i}}^f - n_{\mathbf{i}}^c - n_{\mathbf{i}}^f, \quad (2.11)$$

with pair operators $\Delta_{\mathbf{i},c}^{\dagger} = c_{\mathbf{i},\uparrow}^{\dagger} c_{\mathbf{i},\downarrow}^{\dagger}$ ($\Delta_{\mathbf{i},f}^{\dagger} = f_{\mathbf{i},\uparrow}^{\dagger} f_{\mathbf{i},\downarrow}^{\dagger}$) and the total charge $n_{\mathbf{i}}^{\alpha} = n_{\mathbf{i},\uparrow}^{\alpha} + n_{\mathbf{i},\downarrow}^{\alpha}$. The general symmetries of the perfect square term (2.11) are discussed in detail in chapter

3.4. In order to use the term (2.11) for the simulation of the KLM we need to enforce a constraint of single occupancy on the f -electrons (which should only represent the Kondo spins)

$$(n_{\mathbf{i}}^f - 1)^2 = 0. \quad (2.12)$$

The pair-pair and charge-charge interactions in (2.11) give no contribution for the spin sector. We choose to enforce this constraint (2.12) with an additional Hubbard repulsion U_f for the f -electrons. The simulated Hamiltonian thus is

$$\begin{aligned} H_{\text{sim}} = & \sum_{\mathbf{k}, \sigma} \varepsilon(\mathbf{k}) c_{\mathbf{k}, \sigma}^\dagger c_{\mathbf{k}, \sigma} - \frac{J}{4} \sum_{\mathbf{i}} \left[\sum_{\sigma} c_{\mathbf{i}, \sigma}^\dagger f_{\mathbf{i}, \sigma} + H.c. \right]^2 \\ & + U \sum_{\mathbf{i}} (n_{\mathbf{i}, \uparrow}^c - 1/2) (n_{\mathbf{i}, \downarrow}^c - 1/2) + U_f \sum_{\mathbf{i}} (n_{\mathbf{i}, \uparrow}^c - 1/2) (n_{\mathbf{i}, \downarrow}^c - 1/2). \end{aligned} \quad (2.13)$$

The Hamiltonian H_{sim} has the property to conserve the total number of pairs and holes on the f -layer

$$\left[H_{\text{sim}}, \sum_{\mathbf{i}} (n_{\mathbf{i}}^f - 1)^2 \right] = 0. \quad (2.14)$$

Thus we might start a projection from a trial wave $|\Psi_T\rangle$ which contains the particle-hole symmetric Néel state for the f -spins and choose the real spin decoupling for the Hubbard terms. Due to the symmetry (2.14) the constraint (2.12) is always fulfilled and projection with U_f no longer necessary. Such an approach has the severe disadvantage [18] that we start with a trial wave $|\Psi_T\rangle$ which is not a singlet.

2.4 Mean-field approach

A variety of mean-field schemes [114, 51, 103] have been used for the KLM. In particular the approaches by [114, 51] provide order parameters for both the singlet formation and spin order. They give approximately the same value for J_c which agrees well with the QMC result.

Yu [114] uses a decoupling scheme with a hybridization strength V

$$V = \left\langle c_{\mathbf{i}, \uparrow}^\dagger f_{\mathbf{i}, \uparrow} + f_{\mathbf{i}, \downarrow}^\dagger c_{\mathbf{i}, \downarrow} \right\rangle \quad (2.15)$$

to describe screening and staggered moments m_f and m_c for the AF order

$$\langle f_{\mathbf{i},\uparrow}^\dagger f_{\mathbf{i},\uparrow} - f_{\mathbf{i},\downarrow}^\dagger f_{\mathbf{i},\downarrow} \rangle = m_f (-1)^{\mathbf{i}} \quad (2.16)$$

$$\langle c_{\mathbf{i},\uparrow}^\dagger c_{\mathbf{i},\uparrow} - c_{\mathbf{i},\downarrow}^\dagger c_{\mathbf{i},\downarrow} \rangle = -m_c (-1)^{\mathbf{i}}. \quad (2.17)$$

In the particle-hole symmetric KLM the *averaged* Kondo constraint $\langle f_{\mathbf{i},\uparrow}^\dagger f_{\mathbf{i},\uparrow} + f_{\mathbf{i},\downarrow}^\dagger f_{\mathbf{i},\downarrow} \rangle = 1$ is naturally satisfied. The ground state in the Kondo phase is obtained from hybridized bands which can not suppress charge fluctuations on the f -site but on the other hand ensure that the local moment is fully screened. The ordered ground state is a SDW state with f -spins aligned in a Néel state with full moment. Only in a narrow region close to the phase transition both V and $m_{c,f}$ are nonzero simultaneously. This describes a situation where the localized spins are partially screened and at the same time a remnant magnetic moment orders due to the RKKY interaction. In QMC calculations this coexistence extends to the whole RKKY phase.

For an approximate description of the UKLM we apply a mean field theory similar to the one proposed for the pure KLM in [51], where further details can be found. Essentially we construct a model of fermionic fluctuations on a mean field spin background. The description of the spin background can interpolate between two states: A Néel ordered state for the RKKY and Hubbard ground state and a Kondo singlet state for the Kondo phase.

We represent the local Hilbert space consisting of one f electron and additionally up to two itinerant electrons by applying the following operators onto the local vacuum $|0\rangle$

$$\begin{aligned} s^\dagger |0\rangle &= \frac{1}{\sqrt{2}}(c_\uparrow^\dagger f_\downarrow^\dagger + f_\uparrow^\dagger c_\downarrow^\dagger) |0\rangle \\ t_x^\dagger |0\rangle &= \frac{-1}{\sqrt{2}}(c_\uparrow^\dagger f_\uparrow^\dagger - c_\downarrow^\dagger f_\downarrow^\dagger) |0\rangle \\ t_y^\dagger |0\rangle &= \frac{i}{\sqrt{2}}(c_\uparrow^\dagger f_\uparrow^\dagger + c_\downarrow^\dagger f_\downarrow^\dagger) |0\rangle \\ t_z^\dagger |0\rangle &= \frac{1}{\sqrt{2}}(c_\uparrow^\dagger f_\downarrow^\dagger + c_\downarrow^\dagger f_\uparrow^\dagger) |0\rangle \\ a_\sigma^\dagger |0\rangle &= f_\sigma^\dagger |0\rangle \\ b_\sigma^\dagger |0\rangle &= c_\uparrow^\dagger c_\downarrow^\dagger f_\sigma^\dagger |0\rangle. \end{aligned} \quad (2.18)$$

The s and t operators are equivalent to the so-called bond operators of [89] and obey *bosonic* commutation relations. The *fermionic* operators a and b have been introduced

first in [23, 22] and label states with one or three electrons per site. In order to suppress unphysical states a constraint of no double occupancy

$$s_j^\dagger s_j + \sum_{\alpha} t_{\alpha,j}^\dagger t_{\alpha,j} + \sum_{\sigma} a_{\sigma,j}^\dagger a_{\sigma,j} + \sum_{\sigma} b_{\sigma,j}^\dagger b_{\sigma,j} = 1 \quad (2.19)$$

has to be fulfilled. The original Hamiltonian may be rewritten using the following identities for the conduction electron

$$\begin{aligned} c_{j,\sigma}^\dagger &\equiv p_{\sigma} \frac{1}{\sqrt{2}} \left[\left(s_j^\dagger + p_{\sigma} t_{z,j}^\dagger \right) a_{-\sigma,j} - \left(t_{x,j}^\dagger + p_{\sigma} i t_{y,j}^\dagger \right) a_{\sigma,j} \right] \\ &\quad - \frac{1}{\sqrt{2}} \left[b_{\sigma,j}^\dagger \left(s_j - p_{\sigma} t_{z,j} \right) - b_{-\sigma,j}^\dagger \left(t_{x,j} + p_{\sigma} i t_{y,j} \right) \right], \end{aligned} \quad (2.20)$$

for the Kondo term

$$\vec{S}_{i,c} \vec{S}_{i,f} \equiv -\frac{3}{4} s_i^\dagger s_i + \frac{1}{4} \sum_{\alpha} t_{\alpha i}^\dagger t_{\alpha i}, \quad (2.21)$$

and for the Hubbard term (at half filling)

$$(n_{i,\uparrow} - 1/2)(n_{i,\downarrow} - 1/2) = n_{i,\uparrow} n_{i,\downarrow} - 1/4 \quad (2.22)$$

$$\equiv \sum_{\sigma} b_{\sigma,j}^\dagger b_{\sigma,j} - \frac{1}{4} \quad (2.23)$$

$$= \frac{1}{4} - \frac{1}{2} \left(s_j^\dagger s_j + \sum_{\alpha} t_{\alpha,j}^\dagger t_{\alpha,j} \right). \quad (2.24)$$

Rewriting the UKLM in terms of (2.18) leads to a strongly correlated boson-fermion model. To proceed we use a mean-field approach for the bosons which encompasses two local states, namely the antiferromagnetic and the singlet state.

We want to trace out the boson states and find an effective Hamiltonian in terms of the a and b Fermions. In order to accomplish this, we first assume that the t_x, t_y bosons never occur.⁶ Second, the remaining s_i and $t_{z,i}$ bosons shall be completely uncorrelated. In addition bosons and fermions shall also be uncorrelated. Thus we propose a mean-field ground state of the form

$$|\Psi_{\text{MF}}\rangle = |\Psi_s\rangle \otimes |\Psi_{tz}\rangle \otimes |\Psi_{a,b}\rangle. \quad (2.25)$$

Furthermore we allow condensation of the bosons. This leads to the following simple decoupling scheme: in order to find the effective Hamiltonian, replace the remaining

⁶Disregarding the transverse t_x, t_y bosons, we neglect the whole spin dynamics around the ordered state.

Bose operators $s_{\mathbf{i}}$ and $t_{\mathbf{i},z}$ with c numbers

$$\begin{aligned} s_{\mathbf{i}} &\rightarrow s, \\ t_{\mathbf{i},z} &\rightarrow (-1)^{\mathbf{i}} m, \end{aligned} \quad (2.26)$$

where s^2 (m^2) is the probability to find site \mathbf{i} in state $|s_{\mathbf{i}}\rangle$, ($|t_{z,\mathbf{i}}\rangle$). The alternating sign for the triplet ensures that the magnetic order is staggered. Occupation of the effective fermionic Hamiltonian turns out to be small.

Inserting (2.18) into the UKLM and using the mean field approximation (2.26) we obtain

$$\begin{aligned} H = & -\frac{t}{2} \sum_{\{\mathbf{i},\mathbf{j}\},\sigma} (-sp_{\sigma} + m_{\mathbf{i}})(-sp_{\sigma} + m_{\mathbf{j}}) \times \\ & \times (a_{\sigma,\mathbf{i}} a_{\sigma,\mathbf{j}}^{\dagger} + b_{\sigma,\mathbf{i}}^{\dagger} b_{\sigma,\mathbf{j}}) + h.c. \\ & -\frac{t}{2} \sum_{\{\mathbf{i},\mathbf{j}\},\sigma} (-sp_{\sigma} + m_{\mathbf{i}})(sp_{\sigma} + m_{\mathbf{j}}) \times \\ & \times (-p_{\sigma} a_{\sigma,\mathbf{i}} b_{-\sigma,\mathbf{j}} + p_{\sigma} b_{\sigma,\mathbf{i}}^{\dagger} a_{-\sigma,\mathbf{j}}^{\dagger}) + h.c. \\ & -\frac{3}{4} J N s^2 + \frac{1}{4} J N m_{\mathbf{i}}^2 \\ & + \sum_{\mathbf{i},\sigma} \mu_{\mathbf{i}} (s^2 + m_{\mathbf{i}}^2 + a_{\sigma,\mathbf{i}}^{\dagger} a_{\mathbf{i},\sigma} + b_{\sigma,\mathbf{i}}^{\dagger} b_{\sigma,\mathbf{i}} - 1) \\ & + \lambda \sum_{\mathbf{i},\sigma} (b_{\sigma,\mathbf{i}}^{\dagger} b_{\sigma,\mathbf{i}} - a_{\sigma,\mathbf{i}}^{\dagger} a_{\sigma,\mathbf{i}}) \\ & + \frac{UN}{4} - \frac{UN}{2} (s^2 + m_{\mathbf{i}}^2) \end{aligned} \quad (2.27)$$

where $p_{\uparrow(\downarrow)} = 1(-1)$ and we have introduced a chemical potential λ to set the global particle density and a local Lagrange multiplier $\mu_{\mathbf{i}}$ in order to enforce the constraint (2.19). In the remainder of this work we assume $\mu_{\mathbf{i}}$ to be site independent, i.e. $\mu_{\mathbf{i}} = \mu$. The mean-field hopping terms describe the hybridization of a hole band a and a particle band b with renormalized hopping amplitude

$$-\frac{t}{2} (-sp_{\sigma} + m_{\mathbf{i}})(-sp_{\sigma} + m_{\mathbf{j}}) = -\frac{t}{2} (s^2 - m^2), \quad (2.28)$$

and the hybridization strength

$$-\frac{t}{2} (-sp_{\sigma} + m_{\mathbf{i}})(sp_{\sigma} + m_{\mathbf{j}}) = -\frac{t}{2} \left[2p_{\sigma} s m (-1)^{\mathbf{i}} - (s^2 + m^2) \right]. \quad (2.29)$$

where the alternating sign leads to couplings of type $a_{\mathbf{k}}b_{\mathbf{k}+\mathbf{Q}}$ across the Brillouin zone. This makes it necessary to diagonalize eight bands in the magnetic BZ instead of the original four bands a_{σ}, b_{σ} . The k -diagonal MF hamiltonian is

$$\begin{pmatrix} a_{\uparrow,\mathbf{k}} \\ a_{\uparrow,\mathbf{k}+\mathbf{Q}} \\ a_{\downarrow,\mathbf{k}} \\ a_{\downarrow,\mathbf{k}+\mathbf{Q}} \\ b_{\uparrow,\mathbf{k}}^{\dagger} \\ b_{\uparrow,\mathbf{k}+\mathbf{Q}}^{\dagger} \\ b_{\downarrow,\mathbf{k}}^{\dagger} \\ b_{\downarrow,\mathbf{k}+\mathbf{Q}}^{\dagger} \end{pmatrix} \begin{pmatrix} a_{\uparrow,\mathbf{k}}^{\dagger} & a_{\uparrow,\mathbf{k}+\mathbf{Q}}^{\dagger} & a_{\downarrow,\mathbf{k}}^{\dagger} & a_{\downarrow,\mathbf{k}+\mathbf{Q}}^{\dagger} & b_{\uparrow,\mathbf{k}} & b_{\uparrow,\mathbf{k}+\mathbf{Q}} & b_{\downarrow,\mathbf{k}} & b_{\downarrow,\mathbf{k}+\mathbf{Q}} \end{pmatrix} \begin{pmatrix} e_{\mathbf{k}} - \mu & 0 & 0 & 0 & 0 & 0 & -v_{\mathbf{k}} & -x_{\mathbf{k}} \\ 0 & -e_{\mathbf{k}} - \mu & 0 & 0 & 0 & 0 & x_{\mathbf{k}} & v_{\mathbf{k}} \\ 0 & 0 & e_{\mathbf{k}} - \mu & 0 & v_{\mathbf{k}} & x_{\mathbf{k}} & 0 & 0 \\ 0 & 0 & 0 & -e_{\mathbf{k}} - \mu & -x_{\mathbf{k}} & -v_{\mathbf{k}} & 0 & 0 \\ 0 & 0 & v_{\mathbf{k}} & -x_{\mathbf{k}} & e_{\mathbf{k}} + \mu & 0 & 0 & 0 \\ 0 & 0 & x_{\mathbf{k}} & -v_{\mathbf{k}} & 0 & -e_{\mathbf{k}} + \mu & 0 & 0 \\ -v_{\mathbf{k}} & x_{\mathbf{k}} & 0 & 0 & 0 & 0 & e_{\mathbf{k}} + \mu & 0 \\ -x_{\mathbf{k}} & v_{\mathbf{k}} & 0 & 0 & 0 & 0 & 0 & -e_{\mathbf{k}} + \mu \end{pmatrix} \quad (2.30)$$

where only non-zero components are shown. The band $e_{\mathbf{k}}$

$$e_{\mathbf{k}} = \frac{\varepsilon_{\mathbf{k}}}{2} (s^2 - m^2), \quad (2.31)$$

is the renormalized free $\varepsilon_{\mathbf{k}} = -2t \sum_{d=1}^D \cos k_d$ and mixing amplitudes are given by $x_{\mathbf{k}}$ and $v_{\mathbf{k}}$

$$x_{\mathbf{k}} = -\frac{\varepsilon_{\mathbf{k}}}{2} (s^2 + m^2), \quad (2.32)$$

$$v_{\mathbf{k}} = \varepsilon_{\mathbf{k}} p_{\sigma} s m. \quad (2.33)$$

The 8×8 matrix 2.30 has four doubly degenerate eigenvalues

$$\begin{aligned} E &= \pm \sqrt{e^2 + \Delta^2 \pm 2\sqrt{e^2 \Delta^2}} \\ &= \pm (e \pm \Delta), \end{aligned} \quad (2.34)$$

where $\Delta^2 = \mu^2 + x^2 + v^2$. The difference between (2.27) and the mean-field Hamiltonian for the pure KLM [51] resides in the last line of (2.27) which accounts for a suppression of doubly occupied conduction electron orbitals.

The four doubly degenerate bands in the magnetic BZ follow the dispersion $\omega_{1,2}(\mathbf{k}) = \lambda \pm E_1(\mathbf{k})$ and $\omega_{3,4}(\mathbf{k}) = \lambda \pm E_2(\mathbf{k})$

$$E_{2,\mathbf{k}} = \frac{1}{2} \left[\varepsilon_{\mathbf{k}} (m^2 - s^2) \mp \sqrt{\varepsilon_{\mathbf{k}}^2 (m^4 + 6m^2 s^2 + s^4) + 4\mu^2} \right] \quad (2.35)$$

Note, that the dispersions in (2.35) do depend on U , as the order parameters s , m and μ are functions of U . At half filling the lower(upper) two bands, i.e. $\omega_{2,4}$ ($\omega_{1,3}$), are completely filled(empty). The structure 2.35 follows the generic mean-field theories [103] for the KLM. In the Hubbard limit of a Néel spin background $s = m$ and the first term in the dispersion (2.35) vanishes.

Evaluating the ground state energy and using the stationarity conditions $\partial E/\partial s = 0$, $\partial E/\partial m = 0$, and $\partial E/\partial \mu = 0$ the mean-field equations in the magnetic phase ($m \neq 0$) read

$$\begin{aligned}
0 &= 2J + \frac{1}{2N} \sum_{\mathbf{k}} \frac{\epsilon_{\mathbf{k}}^2 \mu^2 (s^2 - m^2)}{W_{\mathbf{k}}} E_{\mathbf{k}}^- \\
0 &= s^2 + m^2 + 1 - \frac{1}{2N} \sum_{\mathbf{k}} \left[\mu E_{\mathbf{k}}^+ + \frac{\epsilon_{\mathbf{k}}^2 \mu (s^2 - m^2)^2}{4W_{\mathbf{k}}} E_{\mathbf{k}}^- \right] \\
0 &= -J + 4\mu - 2U \\
&\quad - \frac{1}{2N} \sum_{\mathbf{k}} \left[2\epsilon_{\mathbf{k}}^2 (m^2 + s^2) E_{\mathbf{k}}^+ + \frac{\epsilon_{\mathbf{k}}^4 (m^2 + s^2)^3}{2W_{\mathbf{k}}} E_{\mathbf{k}}^- \right]
\end{aligned} \tag{2.36}$$

where $E_{\mathbf{k}}^{\pm} = 2(E_{2,\mathbf{k}}^{-1} \pm E_{1,\mathbf{k}}^{-1})$. For the disordered Kondo-singlet phase ($m = 0$) we get

$$\begin{aligned}
0 &= -\frac{3}{2}J + 2\mu - U - \frac{1}{N} \sum_{\mathbf{k}} \frac{2\epsilon_{\mathbf{k}}^2 s^2}{\sqrt{4\mu^2 + \epsilon_{\mathbf{k}}^2 s^4}} \\
0 &= s^2 + 1 - \frac{1}{N} \sum_{\mathbf{k}} \frac{4\mu}{\sqrt{4\mu^2 + \epsilon_{\mathbf{k}}^2 s^4}}.
\end{aligned} \tag{2.37}$$

Fig. 2.10 shows numerical solutions of (2.36) and (2.37) as a function of J and U . In both cases we find a second order phase transition between the antiferromagnetically ordered and the Kondo phase. Fig. 1 also shows the staggered magnetizations [51] $m_{c(f)}^{\text{st}}$ of the $c(f)$ electron

$$\begin{aligned}
m_c^{\text{st}} &= \frac{2}{N} \sum_n (-1)^n \langle S_{z,n}^c \rangle = 2ms \\
m_f^{\text{st}} &= \frac{2}{N} \sum_n (-1)^n \langle S_{z,n}^f \rangle = \\
&= 2ms + \frac{1}{N} \sum_{\mathbf{k}} \frac{2\epsilon_{\mathbf{k}}^2 \mu m s (s^2 + m^2)}{E_{1,\mathbf{k}} E_{2,\mathbf{k}} (E_{1,\mathbf{k}} + E_{2,\mathbf{k}})}.
\end{aligned} \tag{2.38}$$

Using (2.18) we may express the spectral function $A_c(\mathbf{k}, \omega)$ of the conduction electron $c_{\mathbf{k}}$ via a multi-particle correlation function of the s , t , a and b operators. On the mean-field level however, this simplifies into a linear combination of one-particle propagators of

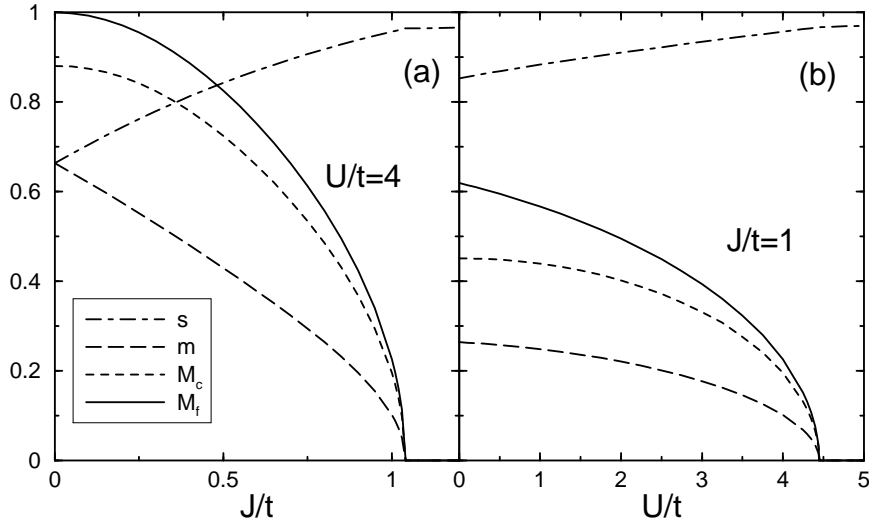


Figure 2.10: Mean-field order parameters s, m and the staggered magnetization M_c and M_f as function of (a) J/t for $U/t = 4$ and (b) U/t for $J/t = 1$.

the a and b fermions only, involving both, diagonal as well as off-diagonal contributions. After some algebra we get

$$A_c(\mathbf{k}, z) = -\frac{1}{\pi} \text{Im} \frac{(m^2 + s^2)(z^2 - \mu^2)z + \epsilon_{\mathbf{k}}(z^2(s^2 + m^2)^2 - 4m^2s^2\mu^2)}{\mu^4 + 4\epsilon_{\mathbf{k}}^2 m^2 \mu^2 s^2 - z^2(2\mu^2 + \epsilon_{\mathbf{k}}^2(s^2 + m^2)^2) + z^4}. \quad (2.39)$$

where $z = \omega + i\delta$.

It is a remarkable feature of this mean-field approach to be correct in the entire strong coupling region from a Hubbard-like dispersion to the Kondo behavior (2.10) where we use $\mu = 3J/4b$. Since the local spin background can also represent a mixed RKKY/Kondo phase a continuous phase transition is possible. Thus, the f -spins play a dual role in the RKKY phase. They are partially screened by conduction electrons. At the same time, the remnant magnetic moment orders due to RKKY. In this sense RKKY and screening coexist.

On the downside, this theory does not handle properly the weak coupling regime. The problem is that the phase space associated with singlets and triplets is reduced to a classical problem represented by the two numbers s and m . Since the kinetic energy of the conduction electrons is encoded in the phase factors a coherent hopping of spin states is impossible. The remaining electron motion of double occupied sites and holes is reduced, as seen from the renormalization factors (2.28) and (2.29). In addition, spin dynamics

are completely neglected in this mean field approach. One should also mention that the charge gap is overestimated which is a notorious shortcoming of mean field theories.

2.5 Magnetic Phase Diagram

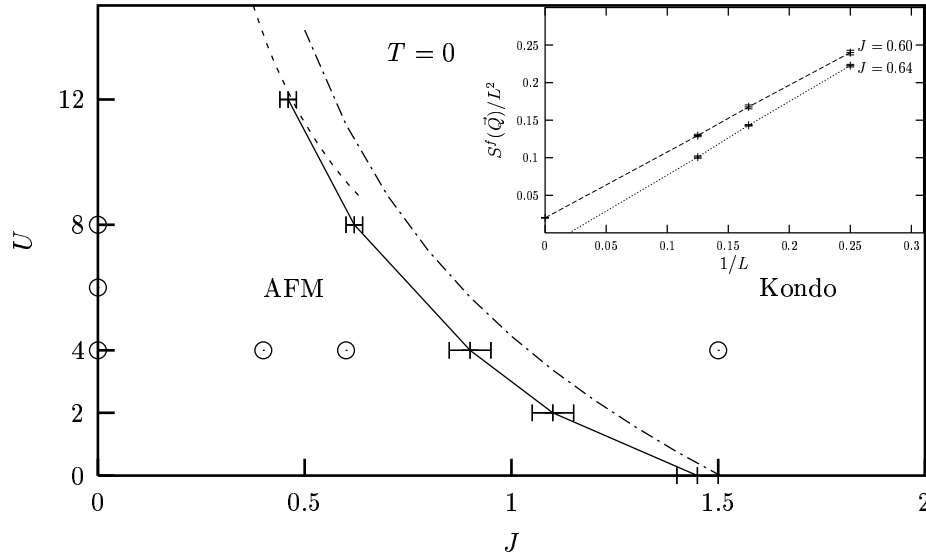


Figure 2.11: Phase diagram of the Kondo-Hubbard model. Solid line: QMC, dot-dashed line: MF, dashed line: Spin Hamiltonian H_{spin} Eq. (2.40). Circles show parameter values, where the spectral function has been evaluated. Long range magnetic order is detected by size scaling of $S^f(Q)/L^2$ (inset $U = 8$).

We start the discussion of our results with the magnetic phase diagram. At $U = 0$ the UKLM maps onto the KLM. In the latter, the competition between the RKKY interaction and the Kondo screening leads to a quantum phase transition between an ordered magnetic state and the disordered singlet phase at $J_c/t \sim 1.5$ [20, 7, 18]. For $U/t \rightarrow \infty$ double occupancy of the conduction electron sites is suppressed and the model maps onto a pure spin Hamiltonian of the form:

$$H_{spin} = J_{\parallel} \sum_{\langle \vec{i}, \vec{j} \rangle} \vec{S}_i^c \vec{S}_j^c + J \sum_{\vec{i}} \vec{S}_i^c \vec{S}_i^f \quad (2.40)$$

with $J_{\parallel} = 4t^2/U$. Hence in the limit $U \rightarrow \infty$, J_c vanishes and the ground state is a product of singlets on the f - c bonds.

We have determined J_c as a function of the Hubbard repulsion U both, on the mean-field (MF) level and with the QMC method. Within MF theory the staggered magnetization is given by Eq. (2.38), while from the QMC method it is determined using the static spin-spin correlation function

$$\begin{aligned} S^\alpha(\mathbf{j}) &= \langle \vec{S}_\mathbf{j}^\alpha \vec{S}_\mathbf{0}^\alpha \rangle \\ S^\alpha(\mathbf{q}) &= \sum_{\mathbf{j}} e^{i\mathbf{q}\mathbf{j}} S^\alpha(\mathbf{j}), \end{aligned} \quad (2.41)$$

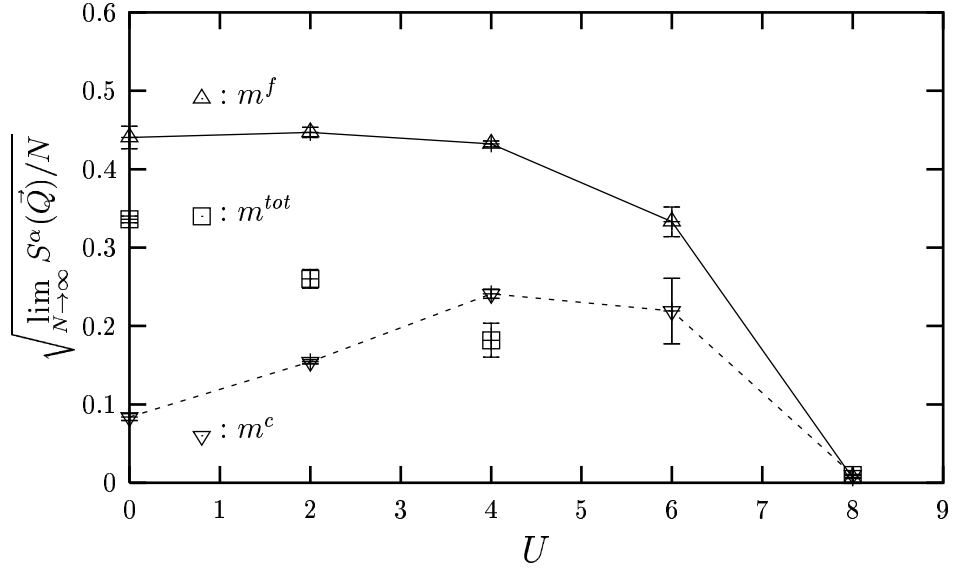
$\alpha = c(f)$ labels conduction (f) electron spins $S_j^{c(f)}$ and the total spin S_j^{tot} is given by $S_j^{tot} = S_j^c + S_j^f$. The staggered moment is extracted from finite size extrapolation

$$m^\alpha = \sqrt{\lim_{N \rightarrow \infty} S^\alpha(\mathbf{Q})/N}$$

where $\mathbf{Q} = (\pi, \pi)$ and N is the number of unit cells.

Fig. 2.11 depicts the phase diagram as a function of J/t for finite U/t . The solid line refers to QMC results, the dashed-dotted line shows the mean-field results. As anticipated already by the preceding discussion of the limiting points $U \rightarrow \infty$ and $U = 0$, the critical value J is a monotonically decreasing function of U . This can be understood as the Hubbard interaction tends to localize the conduction electrons leading to an effective reduction of the hopping amplitude. Hence, the formation of local singlets is favored. The above spin Hamiltonian (2.40) has been analyzed by Matsuhita and collaborators [72] who find a phase transition between a spin liquid and antiferromagnetically ordered phase at $(J_\parallel/J)_c = 0.71$. This leads to $U_c = \frac{4t^2}{0.71J}$, the dashed line in Fig. 2.11, in consistence with the results for the Kondo-Hubbard model in the *large* U/t limit.

Finally Fig. 2.12 plots the staggered magnetization from a QMC scan at fixed J . The broken symmetry ground state satisfies $m^{tot} = m^f - m^c$. In QMC m^{tot} was calculated independently and up to $U \leq 4$ the above relation is fulfilled within the error bars. With increasing U conduction electrons get more and more localized and their local moment grows until it reaches the maximum of $\langle (\vec{S}_j^c)^2 \rangle = 3/4$ in the strong coupling region $U > 8$. The staggered moments in the small $U \leq 4$ region are well understood within a Néel picture of almost fully ordered f -spins where the small local moment of a conduction electron is anti-parallel to the impurity spin. For larger values of U dimerization becomes important which suppresses both $m^{c,f}$.

Figure 2.12: Staggered magnetization for a fixed $J = 0.6$.

2.6 Single particle spectral function.

To study the single-hole dynamics we analyze the spectral function $A(\mathbf{k}, \omega)$, both using the MF expression (2.39) as well as results from the QMC. Within the QMC approach we first evaluate the imaginary time Green's function

$$G_{\mathbf{k}}(\tau) = \frac{\langle \Psi_0 | c_{\mathbf{k}}^\dagger(\tau) c_{\mathbf{k}} | \Psi_0 \rangle}{\langle \Psi_0 | \Psi_0 \rangle} = \frac{1}{\pi} \int_0^\infty d\omega e^{-\tau\omega} A(\mathbf{k}, -\omega). \quad (2.42)$$

from which $A(\mathbf{k}, \omega)$ is extracted using the maximum entropy (ME) method [50].

We begin with the pure Hubbard model. In Fig. 2.13 we plot $A(\mathbf{k}, \omega)$ as obtained from QMC as well as the MF dispersion as a function of U/t . While the comparison of the QMC with the MF dispersion is favorable one has to realize that the MF approach overestimates the quasiparticle gap. Therefore the MF band structure in these figures results from taking only s and m as obtained from the self-consistency equations (2.36) however adjusting μ such as to obtain the QMC gap at $\mathbf{k} = (\frac{\pi}{2}, \frac{\pi}{2})$. At weak coupling $U/t \ll 1$ we find that the overall form of the low-energy dispersion is well reproduced by a functional form $\pm\sqrt{\Delta^2 + \epsilon^2(\mathbf{k})}$ which is consistent with that in a spin density wave (SDW) state. Exactly this dispersion emerges also from the bond-operator MF theory at $J = 0$ where $E_{1,\mathbf{k}}$ reduces to the SDW dispersion and the spectral weight of excitations with the dispersion $E_{2,\mathbf{k}}$ vanishes. In the limit $J \rightarrow 0^+$ the condensate densities for the triplet and singlet are identical, i.e. $m = s$, which is equivalent to a Néel state of the

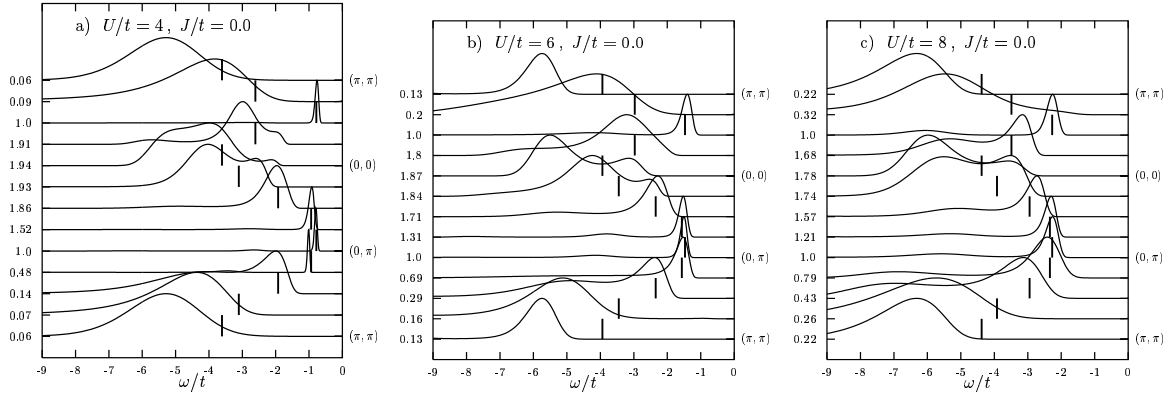


Figure 2.13: Single-particle spectral function for pure Hubbard model at $U = 4$, $U = 6$, and $U = 8$. For the QMC data (solid lines) we have normalized the maximum peak heights to unity. The numbers on the left-hand side of the figures correspond to the single-particle occupation number $\langle n_{\mathbf{k}} \rangle$. The integrated weight under each line shape is $\pi \langle n_{\mathbf{k}} \rangle$. The vertical bars show the MF dispersion relation.

f -spins.

At strong coupling $U/t \gg 1$ the Hubbard model maps approximately onto the t - J_{\parallel} model with $J_{\parallel} = 4t^2/U$. Monte Carlo results for the latter model at $J_{\parallel}/t < 1$ show the existence of a quasiparticle band of width $\sim J_{\parallel}$ [16]. This should be compared to an identical spectral feature which can be observed in our QMC data for the Hubbard model upon enhancing U/t in Fig. 2.13b,c) (see also [87]). Especially along the line from $\mathbf{k} = (0, \pi)$ to $\mathbf{k} = (0, 0)$, this narrow quasi particle band is clearly visible. In principle one should observe a similar band along $(0, \pi)$ – (π, π) , however, due to small spectral weight in this region, we are unable to resolve this feature. Of particular importance is, that for the parameters we have investigated, the momenta of the dominant lowest energy hole-states for the Hubbard model are found on the boundary of the magnetic Brillouin zone. For the calculations presented in this work we have been unable to resolve an energy difference between the $(\pi/2, \pi/2)$ and $(0, \pi)$ points.

Next we turn to the UKLM at finite J . In Fig. 2.14 we show a scan of QMC spectral functions and the MF dispersion ranging from the Kondo phase for $J/t = 1.5$ and $U/t = 4$ to the antiferromagnetic phase at $J/t = 0.4, 0.6$ and $U/t = 4$. As for the pure Hubbard model the QMC and MF results are reasonably consistent. From the perturbative argument for $J/t \gg 1$, given in section 2.2, we expect the momenta

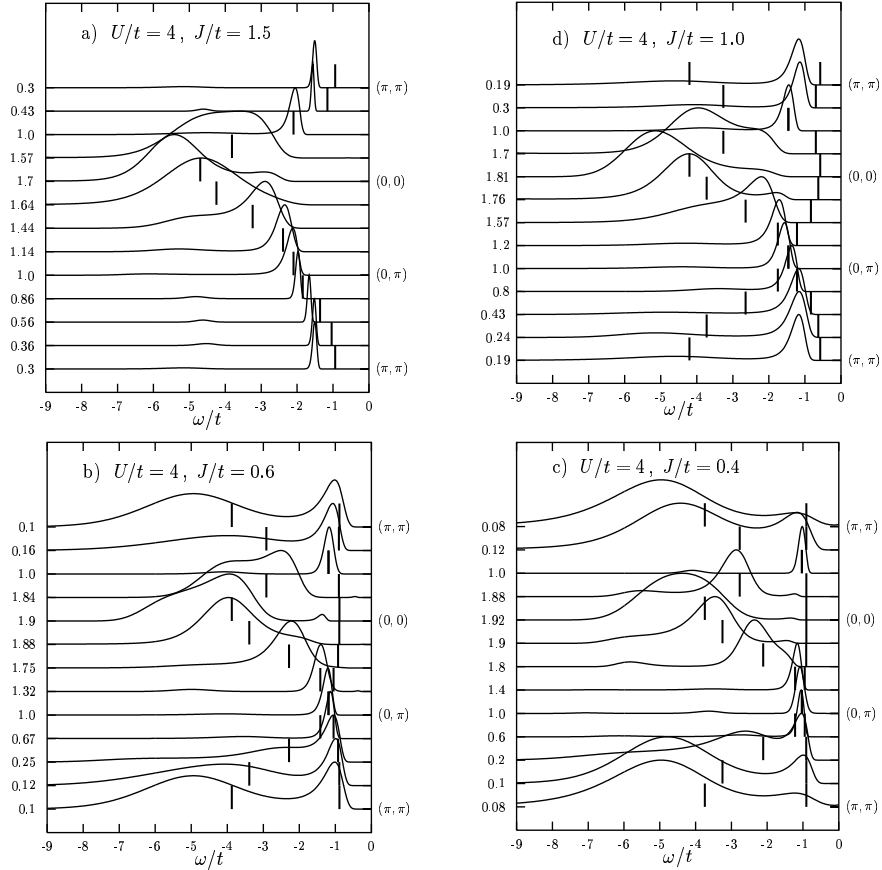


Figure 2.14: Single-particle spectra for the Kondo phase (a), at the transition (d) and in the antiferromagnetic phase (b) and (c). Vertical bars show the MF dispersion.

of the dominant lowest energy hole-states to occur at $\mathbf{k} = (\pm\pi, \pm\pi)$. As can be seen from Fig. 2.14a) this is consistent, both with the QMC as well as with the MF results. Moreover the QMC and MF dispersions agree very well.

Lowering J as in Figs. 2.14a)-c) reveals the evolution of the spectral density on going from the Kondo to the antiferromagnetically ordered phase. In fact, as J approaches zero *additional* bands with a dispersion similar to the pure Hubbard case, i.e. Fig. 2.13a), develop. Yet, in the antiferromagnetically ordered phase, but for a finite J the lowest energy hole-states are still Kondo-like, i.e. they occur at $\mathbf{k} = (\pm\pi, \pm\pi)$ as can be seen in Figs. 2.14b),c). However, the weight of this excitation decreases continuously with decreasing J and vanishes at $J = 0$. The weight of the Hubbard-like band at $\mathbf{k} = (\pi, \pi)$ increases from zero in the spin singlet phase to its maximum value at $J = 0$. Therefore we can interpret the change in the spectral function with decreasing J as a continuous transfer of weight from Kondo-like to Hubbard-like bands. This shift of spectral weight

renders the $J = 0$ point singular since there is a sudden change of the wave vector which dominates the low energy hole dynamics.

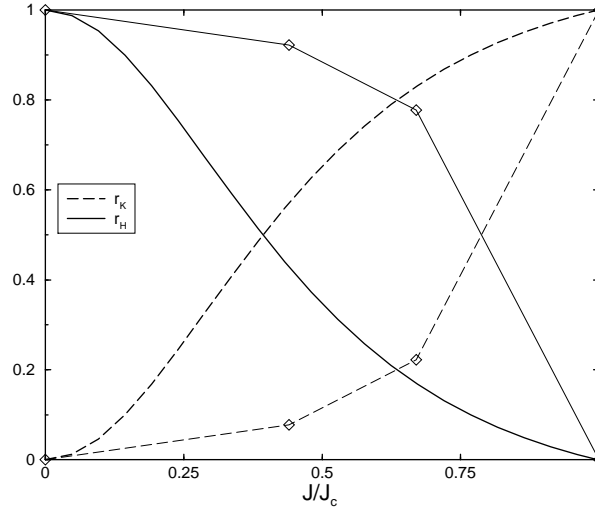


Figure 2.15: Relative spectral weight of Hubbard band vs. Kondo band. Thick lines: MF. Thin lines: QMC.

These findings are corroborated by our MF results. In Fig. 2.15 the relative weight $r_{H(K)} = Z_{H(K)}/(Z_H + Z_K)$ of the lower(upper) Hubbard(Kondo)-like band at momentum $\mathbf{k} = (\pi, \pi)$ as obtained from integrating $A_c(\mathbf{k}, \omega)$ is depicted. In the QMC approach Z_K results from fitting the long-time tail of the Greens function at $\mathbf{k} = (\pi, \pi)$ to the form $Z_K e^{-\Delta_{qp}\tau}$ where Δ_{qp} corresponds to the quasiparticle gap. In turn Z_H is obtained from the sum rule $Z_K + Z_H = \pi n(\mathbf{k})$ assuming a two-pole structure. Both, the QMC and the MF approximation display the same overall trend: at $J/t = 0$ the total weight is in the Hubbard-like band while with increasing J it becomes distributed into both bands. In the Kondo phase the Hubbard band disappears completely. In addition Fig. 2.15 shows, that the MF approximation underestimates the spectral weight in the Hubbard-like band. Nevertheless, this bond operator mean-field approximation captures the relevant physics of the model. This is not the case of other mean-field approximations which attempt to combine magnetism and local Kondo screening [114]. This latter approach yields a finite value of J below which the dispersion relation is pure Hubbard-like.

To compare the momentum dependence of the spectral weight as obtained from the MF theory with that of the QMC Fig. 2.16 depicts $A_c(\mathbf{k}, \omega)$ from (2.39) for $U/t = 4$ and $J/t = 0.4$. For visualization purpose, we have smeared the delta-function like MF-

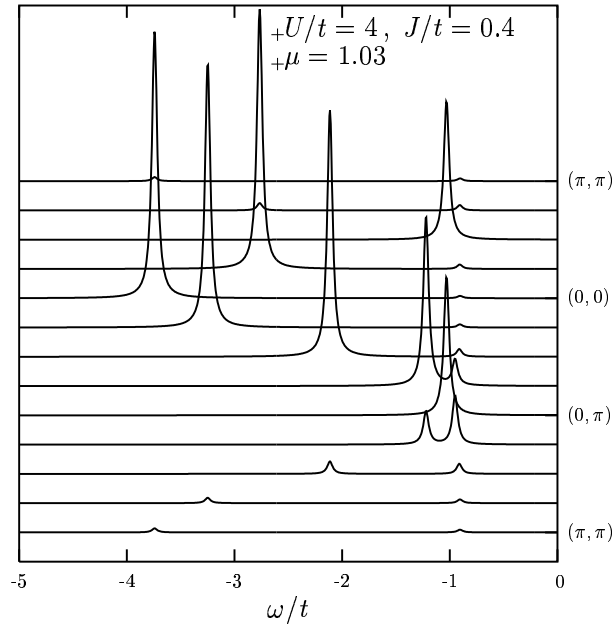


Figure 2.16: Mean-field spectral function Eq. (2.39) in the antiferromagnetic phase.

spectrum by a finite imaginary part $\delta = 0.03$. The weight of these delta-peaks strongly varies as a function of \mathbf{k} having its maximum around $(0, 0)$ and a very small value in the vicinity of (π, π) . Again, this is consistent with the QMC data of Fig. 2.14c). Obviously, since the imaginary part of the self energy vanishes in the MF approximation, the broadening of the QMC spectral function is not reproduced. Note however, that on the QMC side pinning down the details of the line shape is extremely challenging.

2.7 Conclusion

We have considered the single-hole dynamics in the Kondo-Hubbard model using both, QMC methods and a bond-operator mean-field approximation. Both approaches allow for similar conclusions. The UKLM shows a magnetic order-disorder transition. At $U = 0$ this transition is triggered by the competition between the RKKY interaction and the Kondo screening and occurs at $J_c/t \sim 1.5$. In the large U/t limit the model maps onto a bilayer spin-model and J_c scales to zero. Our results show that both limiting cases are linked continuously and that J_c is a monotonically decreasing function of U . Hence, as far as J_c is concerned the dominant effect of the Hubbard interaction U is to localize the conduction electrons which favors screening of the f -spins.

The single particle spectral function was shown to be insensitive to the magnetic phase transition. Irrespective of U and $J > 0$ the dominant low energy hole-states are found at the momenta $\mathbf{k} = (\pm\pi, \pm\pi)$. These excitations originate from the screening of the magnetic impurities and hence are local. In the ordered phase pronounced shadow features can be observed. As $J \rightarrow 0$, the spectral weight in the Kondo-like low energy band in the vicinity of $\mathbf{k} = (\pm\pi, \pm\pi)$ vanishes and is transferred to higher energy Hubbard-like bands. In the (U, J) -plane the Hubbard-line, i.e. $J = 0$, is singular since the localized spins decouple and lead to a macroscopically degenerate ground state. In turn, the evolution of the spectral function is discontinuous such that at $J = 0$ there is a sudden change of the wave vector which dominates the low energy hole dynamics. In this sense the model shows no continuous path from the Kondo insulator to the Mott insulator.

The singularity of the UKLM at $J = 0$ may be alleviated by including an antiferromagnetic coupling between the localized f -spins. In the large U/t limit this leads to a bilayer spin model which has been considered by Vojta and Becker [106]. The authors arrive at a similar conclusion namely that hole dynamics are governed by local spin environment.

Given our results it is very tempting to speculate on the effects of doping with a finite density of *holes* n_h away from half filling. In the limit $J/t \rightarrow \infty$ the Kondo lattice model can be mapped onto an effective Hubbard model with a Coulomb repulsion $U_{eff} \rightarrow \infty$ and a *particle* density n_h [58]. In this low-density limit single particle renormalizations [29] may be neglected which suggests that doping the UKLM can be understood approximately within a rigid-band picture. From this we would conclude that off half filling the UKLM displays a Fermi surface centered around $\mathbf{k} = (\pm\pi, \pm\pi)$ for all values of U and $J > 0$.

Chapter 3

Coexistence of *s*-wave SC and Antiferromagnetism

3.1 Introduction

3.2 Organic Superconductors

Let us start with an experimental motivation. The quasi-two-dimensional salts κ -(BEDT-TTF)₂X, with $X = \text{Cu} [\text{N}(\text{CN})_2] \text{Cl}$, $\text{Cu} [\text{N}(\text{CN})_2] \text{Br}$ and $\text{Cu} (\text{NCS})_2$, have a rich phase diagram. At low temperatures chemical or hydrostatic pressure drives a first order transition between an insulating antiferromagnetic phase and a superconducting phase. The generic phase diagram is shown in figure 3.1. Lefebvre et al. [61] report a phase diagram 3.2 for κ -Cl which changes from an AFI under ambient pressure to a superconductor at 300 bar. Comparing the two phase diagrams 3.1 and 3.2 we note that the pressure change of the latter is very small.

A review on the current status of organic superconductors is given by Lang and Müller. [60] In these compounds metallic behavior and chemical bonding is due to the π -hole on the donor BEDT-TTF molecule in contrast to van der Waals-bond organic molecules.

At temperatures of $T_c \sim 10 \text{ K}$ the superconducting phase undergoes a second order transition to a paramagnetic metal. Müller et al. [79] recently proposed a metallic state with a density wave on the one dimensional part of the Fermi surface.

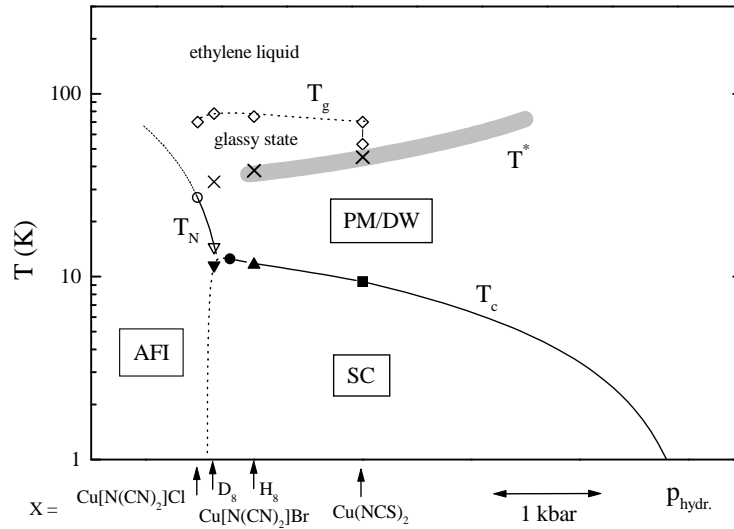


Figure 3.1: The generic phase diagram for the κ -(ET) $_2$ X compounds (from [79]). Chemical or hydrostatic pressure drives the phase transition between a magnetically ordered AF phase and the superconducting phase. Our interest is in this low temperature first order transition.

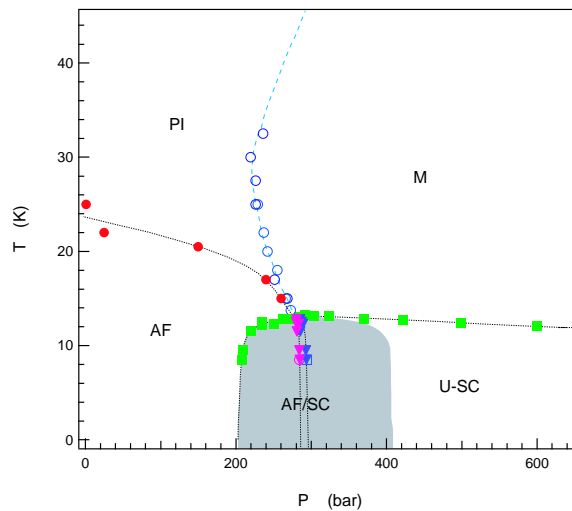


Figure 3.2: The phase diagram for κ -(BEDT-TTF) $_2$ Cu[N(CN) $_2$]Cl [61]. A first order transition separates AF and SC phases. Above the ordering temperature a Mott-Hubbard first order transition is found between an insulating (PI) and metallic (PM) phase.

The nature of the superconducting state, in particular the pairing mechanism and the symmetry of the superconducting order parameter remain a controversial issue. Many experimental studies are rather consistent with *s*-wave, phonon mediated superconduc-

tivity. In particular, Kini et al. could demonstrate a BCS-like mass isotope effect in κ -S. [53] They show that the relevant mass entity is the whole ET molecule which is a clear indication that electron-lattice phonon interaction is involved in the pairing. At the same time this rules out that intramolecular electron-phonon coupling is responsible for the electron attraction. The same material κ -S exhibits a strong superconductivity induced (acoustic) phonon renormalization. [85] Nodes in the pair order parameter are also incompatible with specific heat measurements. [78] Conversely Kanoda et al. [52] argue that the absence of a Hebel-Slichter peak in the $1/T_1$ NMR spin relaxation rate is consistent with an unconventional superconducting gap and nodal lines.

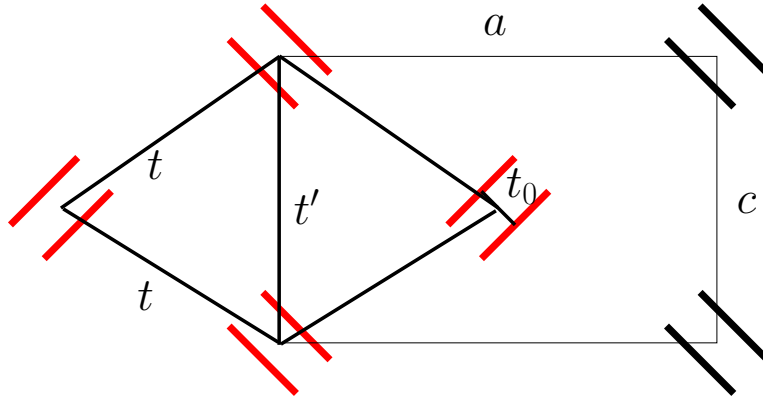
On the theoretical side electron-lattice phonon interaction has been studied as the dominant pairing mechanism. [36] The dimensionless Eliashberg parameter λ was determined both experimentally [82] and theoretically [36] around $\lambda \sim 1$. When the electron system is mapped to an effective lattice model the interaction between electrons and acoustic phonons is appropriately modeled with a Su-Schrieffer-Heeger interaction term. [98]

The κ -Cl and deuterated κ -Br compounds [75] are the only systems which show antiferromagnetism at ambient pressure. Resistivity remains activated to temperatures above 70 K in κ -Cl. [101] NMR studies by Miyagawa et al. suggest a commensurate antiferromagnetism with a large magnetic moment of $0.45 \mu_B$ /dimer below a Néel temperature $T_N \sim 27$ K. [76] [75]. Two interpretations exist for the nature of the AF state: (i) Antiferromagnetism results from a Mott-Hubbard transition to a regime with strong electron localization supported by the large magnetic moment and direct evidence of a metal-insulator transition in κ -Cl. [61] (ii) Tanatar et al. [101] argue that SDW antiferromagnetism linked to the good nesting properties of the 1d part of the Fermi surface could be responsible for the formation of a charge gap.

The normal-state is metallic due to the overlap of π -holes. De Haas-van Alphen [109] and Shubnikov-van Alphen [84] experiments reveal a closed hole-like Fermi-surface (FS) pocket and two FS sheets. After magnetic breakdown electrons may tunnel between the sheets and the closed FS resulting in a second large orbit. Experiments thus support a Fermi-liquid normal-state and the FS volume is that of half-filled conduction bands but cyclotron masses are strongly enhanced $m_c \sim 3.5$ and $6.9 m_e$ for the two orbits.

Band structure calculations are based on molecular orbits (MO) for the single ET

molecule. In a second step approximate tight-binding calculations are performed for a single MO per molecule. [54] [104] Figure 3.2 shows the unit cell of the κ -phase compounds which contains four ET molecules which are strongly dimerized. Intradimer hopping t_0 is strong and splits the four bands into a pair of bonding and antibonding bands with an approximate splitting $\Delta = 2t_0$. Neglecting the bonding bands one arrives at a half filled model with two bands. Kino and Fukuyama [54] introduced a further simplification, namely the dimer model: in this model one considers only the antibonding MO representing the dimer. In addition the two dimer sites are treated as equivalent sites, reducing the unit cell by half. Hopping t is between nearest-neighbor dimer orbitals and t' is the diagonal hopping (frustration).



The unit cell of κ -(ET)₂Cu[N(CN)₂]Cl contains 4 ET molecules grouped into 2 dimers. The intradimer hopping t_0 is almost twice as large then the hopping $t_{1,2}$. This results in a clear separation of the four orbitals into bonding and antibonding bands. In the dimer approximation we may drop the bonding bands and treat all hoppings as between dimers. In this approximation hoppings t_1 and t_2 are equal. This results in a further simplification to a 45° rotated unit cell containing only one dimer.

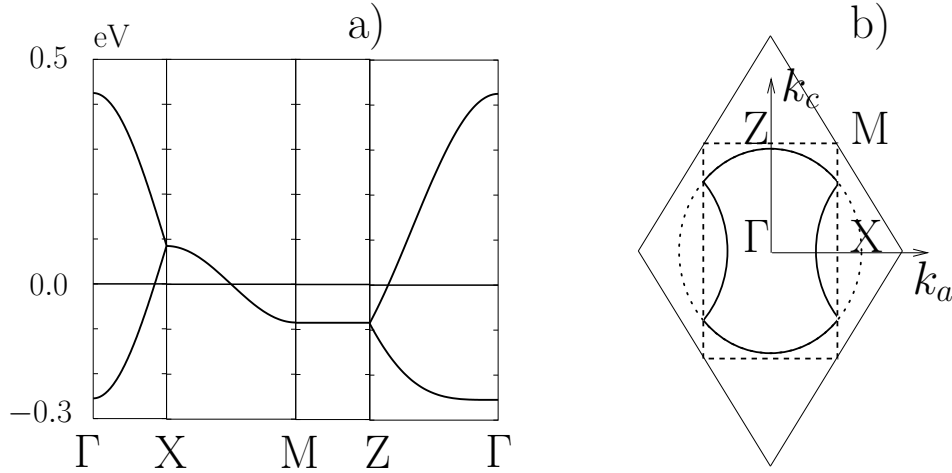
Approximate values for the parameters¹ from molecular *ab initio* calculations [104] [31] are

t_0	t	t'	U_{eff}	a	b	c
0.27 eV	0.17/2 eV	0.085/2 eV	0.4 eV	13 Å	30 Å	8.5 Å

which yields two bands in the original Brillouin zone (BZ)

$$\varepsilon(k) = 2t' \cos(k_c c) + 4t \cos \frac{k_c c}{2} \cos \frac{k_a a}{2}.$$

¹The one half accounts for taking effective hoppings from one pair to another pair of ET molecules $t = (p - q)/2$.



The bandwidth at the Γ point is $4t$ and the bandwidth from $X - M$ is given by $2t'$. Such a simplified one band model still gives an accurate FS (Fig. 3.2) only the gap between the 1D sheet and the closed orbit is missing.

Kino and Fukuyama [54] introduce an effective Hubbard repulsion per dimer $U_{\text{eff}} \sim 0.28 \text{ eV}$ and within mean-field calculation find a first order transition between a paramagnetic metal and an AF insulator. The transition is driven by a change in t'/t and t/U_{eff} both modified by the pressure change responsible for the observed transition. [45]

To summarize, experiment and theory is still controversially discussed for the κ -(ET) $_2X$ compounds. The proximity of AF and SC phases naturally leads to an interpretation where spin fluctuations mediate d -wave pairing and strongly correlated electrons are mainly responsible for the whole phase diagram. On the other hand it is not ruled out that superconductivity is ordinary phonon mediated BCS superconductivity with s -wave symmetry. Our interest here is to demonstrate that a first order transition between AF and s -wave superconductivity is possible.

3.3 Model

In order to model the scenario of a phase transition between an AFI and an s -wave SC on a half-filled two dimensional lattice we add to the standard Hubbard model a pair hopping term:

$$\begin{aligned}
H = & -t \sum_{\langle \mathbf{i}, \mathbf{j} \rangle, \sigma} \left(c_{\mathbf{i}, \sigma}^\dagger c_{\mathbf{j}, \sigma} + H.c. \right) + U \sum_{\mathbf{i}} (n_{\mathbf{i}, \uparrow} - 1/2) (n_{\mathbf{i}, \downarrow} - 1/2) \\
& - t_p \sum_{\langle \mathbf{i}, \mathbf{j} \rangle} \left(\sum_{\sigma} c_{\mathbf{i}, \sigma}^\dagger c_{\mathbf{j}, \sigma} + H.c. \right)^2 - 2V \sum_{\langle \mathbf{i}, \mathbf{j} \rangle} (n_{\mathbf{i}} - 1) (n_{\mathbf{j}} - 1)
\end{aligned} \tag{3.1}$$

where \mathbf{i} labels the sites of a square lattice and the sum $\langle \mathbf{i}, \mathbf{j} \rangle$ runs over nearest neighbor bonds. The pair hopping term arises exactly when we assume a Su-Schrieffer-Heeger (SSH) electron-phonon interaction [98] and integrate out the phonon in the antiadiabatic limit. For systems with well localized electrons the SSH mechanism describes the electron-lattice phonon coupling via a modulation of the electron hopping amplitude t

$$t \rightarrow t + \vec{\lambda} \left(\vec{Q}_{\mathbf{i}} - \vec{Q}_{\mathbf{j}} \right). \tag{3.2}$$

The full SSH hamiltonian is then given as [42] [9]

$$\begin{aligned}
H = & H_{el} + \sum_{\langle \mathbf{i}, \mathbf{j} \rangle, \sigma} \vec{\lambda}_{\mathbf{i}, \mathbf{j}} \left(\vec{Q}_{\mathbf{i}} - \vec{Q}_{\mathbf{j}} \right) \left(c_{\mathbf{i}, \sigma}^\dagger c_{\mathbf{j}, \sigma} + H.c. \right) \\
& + \sum_{\mathbf{i}} \frac{\vec{P}_{\mathbf{i}}^2}{2M} + \frac{1}{2} K \sum_{\langle \mathbf{i}, \mathbf{j} \rangle} \left(\vec{Q}_{\mathbf{i}} - \vec{Q}_{\mathbf{j}} \right)^2.
\end{aligned} \tag{3.3}$$

The effective electron-electron interaction may be considered instantaneous when $T_c < \omega_{\text{ph}}$. Formally this corresponds to the antiadiabatic limit with either $M \rightarrow 0$ or $\omega_{\text{ph}} \rightarrow \infty$ which allows to drop the phonon kinetic energy. Integrating out the phonons we find the pair hopping term

$$H_{t_p} = -t_p \sum_{\langle \mathbf{i}, \mathbf{j} \rangle} \left(\sum_{\sigma} c_{\mathbf{i}, \sigma}^\dagger c_{\mathbf{j}, \sigma} + H.c. \right)^2 \tag{3.4}$$

with an effective coupling t_p

$$t_p = \vec{\lambda} \frac{1}{K} \vec{\lambda}. \tag{3.5}$$

Such an effective term has already been discussed as a means to simulate the Kondo lattice [7] and Hirsch [42] studied exactly the Hamiltonian (3.1) away from half-filling in the context of high T_c superconductors.

The fermionic spin is given by $\vec{S}_{\mathbf{i}} = \frac{1}{2} \sum_{s,t} c_{\mathbf{i},s}^\dagger \vec{\sigma}_{s,t} c_{\mathbf{i},t}$ and $\vec{\sigma}$ denotes the Pauli matrices. The local pair creation operator is $\Delta_{\mathbf{i}}^\dagger = c_{\mathbf{i},\uparrow}^\dagger c_{\mathbf{i},\downarrow}^\dagger$ and the total charge $n_{\mathbf{i}} = n_{\mathbf{i},\uparrow} + n_{\mathbf{i},\downarrow}$. The

pair hopping term may be recast [18] [42] as

$$-\left(\sum_{\sigma} c_{i,\sigma}^{\dagger} c_{j,\sigma} + H.c.\right)^2 = 4\vec{S}_i \vec{S}_j - 2\left(\Delta_i^{\dagger} \Delta_j + H.c.\right) + n_i n_j - n_i - n_j. \quad (3.6)$$

Using spin language the minus sign in front of the pair hopping $\Delta_i^{\dagger} \Delta_j$ favors “ferromagnetic” in-plane order for the pairing and no frustration in the pair sector can be realized with the term (3.4). Spin and pair terms in Eq. (3.6) are obviously competing since a local energy gain on neighboring sites is only possible when *both* sites are either spin or pair/hole like. In addition the Fermion hopping will interfere with both spin and superconducting order.

3.4 Symmetries

We introduce a particle-hole transformation \mathcal{P} ² which transforms down electrons into down holes

$$\mathcal{P} c_{i,\downarrow}^{\dagger} \mathcal{P} = (-1)^i c_{i,\downarrow}, \quad (3.7)$$

leaves up electron invariant $\mathcal{P} c_{i,\uparrow} \mathcal{P} = c_{i,\uparrow}$, and has the property $\mathcal{P}^2 = \mathcal{P}$. The discrete symmetry group with elements $\{1, \mathcal{P}\}$ is denoted by $Z_{2,PH}$. It is convenient to introduce a set of eta-operators [111] as the particle hole transformed spin operators

$$\vec{\eta}_i \equiv \mathcal{P} \vec{S}_i \mathcal{P}, \quad (3.8)$$

$$\eta_i^{\dagger} = (-1)^i c_{i,\uparrow}^{\dagger} c_{i,\downarrow}^{\dagger}, \quad (3.9)$$

$$\eta_i^z = (n_{i,\uparrow} + n_{i,\downarrow} - 1)/2, \quad (3.10)$$

such that η_i^{\dagger} is the pair creation operator Δ_i^{\dagger} and η_i^z is the total charge.

The total spin operators

$$\vec{S} = \sum_{\mathbf{i}} \vec{S}_{\mathbf{i}} \quad (3.11)$$

are the generators of a spin $SU(2)$ group. Accordingly the η -operators

$$\vec{\eta} = \sum_{\mathbf{i}} \vec{\eta}_{\mathbf{i}} \quad (3.12)$$

²The same transformation was used to establish the sign free Hubbard-Stratonovich decoupling for the repulsive Hubbard model (see Eq. 1.48).

define a η - $SU(2)$ group. For the commutation between spin and eta consider

$$\vec{\eta}_i |\text{spin}\rangle = 0, \quad (3.13)$$

which implies that the product and commutators are zero

$$\eta_i^\alpha S_i^\beta = 0, \quad (3.14)$$

$$[\eta_i^\alpha, S_i^\beta] = 0. \quad (3.15)$$

Both the $SU(2) \times SU(2)$ product group and the $SO(4)$ group have such commutation relations but property (3.14) is incompatible with an irreducible $SO(4)$ representation.

Using spin and η operators we may rewrite the Hamiltonian (3.1) into a manifestly symmetric form

$$\begin{aligned} H = & -t \sum_{\langle i,j \rangle, \sigma} \left(c_{i,\sigma}^\dagger c_{j,\sigma} + H.c. \right) + \frac{U}{3} \sum_i \left[(\vec{\eta}_i)^2 - (\vec{S}_i)^2 \right] \\ & + 4t_p \sum_{\langle i,j \rangle} \left(\vec{S}_i \vec{S}_j + \vec{\eta}_i \vec{\eta}_j - \frac{1}{4} \right) - 8V \sum_{\langle i,j \rangle} \eta_i^z \eta_j^z. \end{aligned} \quad (3.16)$$

In order to analyze the symmetry we look at each term:

1. To see the spin and η invariance of the hopping term we use the spinor representation

$$H_t = -t \sum_{\langle i,j \rangle} \Psi_{i,\alpha}^\dagger h_{\alpha,\beta} \Psi_{j,\beta} + H.c. \quad (3.17)$$

with the spinor $\Psi_{i,\alpha}^\dagger = (c_{i,\uparrow}^\dagger, c_{i,\downarrow}^\dagger)$ and $h_{\alpha,\beta} = \delta_{\alpha,\beta}$. The infinitesimal spin rotation is given by

$$\left[S_i^i, \Psi_{i,\gamma}^\dagger \right] = \frac{1}{2} \Psi_{i,\beta}^\dagger \sigma_{\beta\gamma}^i, \quad (3.18)$$

which may verified using the anticommutator in

$$[AB, C] = A[B, C]_\pm - [C, A]_\pm B. \quad (3.19)$$

Thus the hopping term $\Psi_{i,\alpha}^\dagger h_{\alpha,\beta} \Psi_{j,\beta}$ is a scalar

$$\left[(S_i^i + S_j^i), \Psi_{i,\alpha}^\dagger h_{\alpha,\beta} \Psi_{j,\beta} \right] = \frac{1}{2} \Psi_{i,\alpha}^\dagger [\sigma, \mathbf{h}]_{\alpha,\beta} \Psi_{j,\beta} = 0, \quad (3.20)$$

and

$$\left[\vec{S}, H_t \right] = 0. \quad (3.21)$$

Hopping is also invariant under the particle-hole transformation \mathcal{P}

$$[\mathcal{P}, H_t] = 0. \quad (3.22)$$

The two commutators (3.22) and (3.22) imply the invariance under η -rotation

$$[\vec{\eta}, H_t] = [\mathcal{P}\vec{S}\mathcal{P}, H_t] = 0. \quad (3.23)$$

Thus the full $SU(2)_S \otimes SU(2)_\eta \otimes Z_{2,PH}$ symmetry has been established.³

2. The perfect square term in the form

$$H_{t_p} = 4t_p \sum_{\langle i,j \rangle} \left(\vec{S}_i \vec{S}_j + \vec{\eta}_i \vec{\eta}_j - \frac{1}{4} \right) \quad (3.24)$$

is clearly invariant under $SU(2)_S \otimes SU(2)_\eta \otimes Z_{2,PH}$.⁴

3. The Hubbard term can be rewritten into the manifestly $SU(2)_S \otimes SU(2)_\eta$ invariant form

$$H_U = \frac{U}{3} \sum_{\mathbf{i}} \left[(\vec{\eta}_{\mathbf{i}})^2 - (\vec{S}_{\mathbf{i}})^2 \right]. \quad (3.25)$$

Under \mathcal{P} -transformation the half-filled attractive Hubbard model maps onto the repulsive model

$$\mathcal{P}H_U\mathcal{P} = -H_U. \quad (3.26)$$

4. Finally the density-density interaction

$$H_{DD} = -8V \sum_{\langle i,j \rangle} \eta_i^z \eta_j^z \quad (3.27)$$

is spin symmetric and invariant under η^z rotation.

³In fact the simple perfect nesting H_t has an even higher $SO(6)$ symmetry. [70] [92]

⁴Although the pair hopping is simply the square of single particle hopping it does not have the full $SO(6)$ symmetry.

3.5 QMC

Due to the sign problem we can only simulate the Hamiltonian (3.1) for attractive (negative) U values. The Hubbard term is decoupled with the Hirsch discrete and real HS transformation (1.38). The pair hopping interaction is already in perfect square form and may be decoupled using a HS field with four discrete values (1.67). Finally the density-density interaction is implemented via the perfect square

$$- \left| \tilde{V} \right| \sum_{\langle i,j \rangle} ((n_i - 1) + p (n_j - 1))^2 = -2 \left| \tilde{V} \right| N - 2V \sum_{\langle i,j \rangle} (n_i - 1) (n_j - 1) \quad (3.28)$$

$$- 8 \left| \tilde{V} \right| \sum_{\mathbf{i}} (n_{\mathbf{i},\uparrow} - 1/2) (n_{\mathbf{i},\downarrow} - 1/2) \quad (3.29)$$

where $p = \pm 1$ and $V = p \left| \tilde{V} \right|$. This includes the term H_{DD} we want to represent. But it also includes an additional attractive Hubbard term which restricts the effective U to values

$$U \leq -8|V|. \quad (3.30)$$

This is the shaded region in Fig. 3.3. Using particle-hole symmetry the region of repulsive

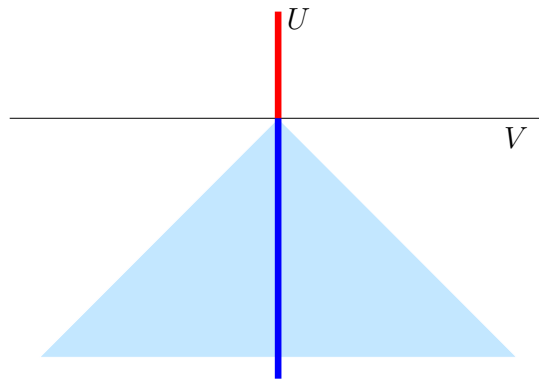


Figure 3.3: The shaded region is accessible to sign free QMC simulation. Simulation of the density-density interaction implicitly includes additional attractive terms which results in the constraint $U < -8|V|$. Using particle-hole symmetry the repulsive U at $V = 0$ is also accessible.

U at $V = 0$ is also accessible. The chemical potential is kept at $\mu = 0$.

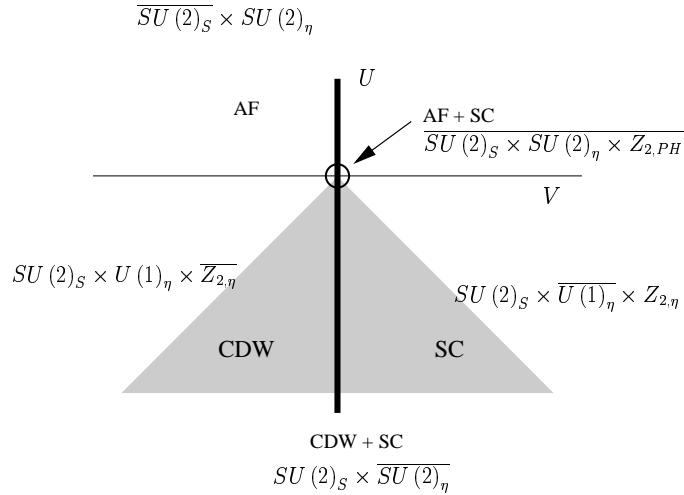


Figure 3.4: For every region in the phase diagram the full symmetry of the Hamiltonian is indicated. Broken symmetries are marked by bars.

3.6 Results

In Fig. 3.4 the various symmetries for different parameter regions are displayed. Bars denote symmetries which we numerically find to be spontaneously broken in the thermodynamic limit. The point $U = V = 0$ has the full symmetry: $SU(2)_S \otimes SU(2)_\eta \otimes Z_{2,PH}$. Here two scenarios are possible: i) Long range order (LRO) for *both* AF and SC correlations since one implies the other through $Z_{2,PH}$ symmetry or ii) The competition between the two broken symmetry states leads to a disordered state. We find that the system realizes the first possibility of coexistence of *s*-wave SC and AF and spontaneous breaking of all the symmetries. Switching on U breaks the particle-hole symmetry and only $SU(2)_\eta$ symmetry is broken for $U < 0$ and $V = 0$. A finite V reduces the $SU(2)_\eta \rightarrow U(1) \otimes Z_{2,\eta}$ and for positive (negative) V we find a SC (CDW) phase. Finally in the region of repulsive U and $V = 0$ the $SU(2)_S$ symmetry is broken.

In the following, we will first discuss numerical results for the point of high symmetry at $U = V = 0$ (Fig a), continue with the phase transition as U (Fig. b) and finally consider the transition varying $V \rightarrow \pm 0$ (Fig c).

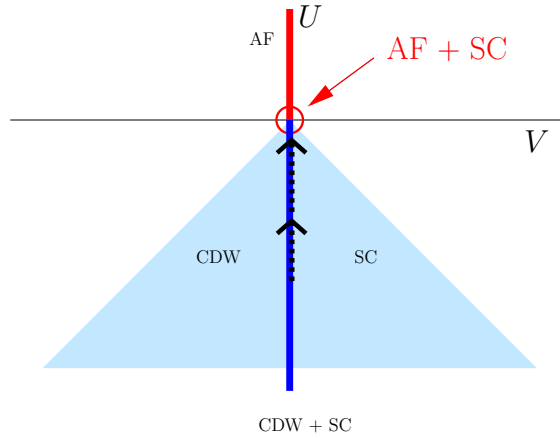


Figure 3.5: We concentrate our attention on three regions in the phase diagram: (a) The point of high symmetry. (b) The phase transition as $U \rightarrow 0$ and (c) The transition upon varying V .

Coexistence

Precisely at $U = 0$ particle-hole symmetry implies that boson correlation functions are equal to their spin counterparts

$$\langle S_{\mathbf{k}}^{\alpha} S_{-\mathbf{k}}^{\alpha} \rangle = \langle \eta_{\mathbf{k}}^{\alpha} \eta_{-\mathbf{k}}^{\alpha} \rangle. \quad (3.31)$$

Thus the existence of LRO for spin implies LRO for the pairs and vice-versa. Both orders are competing in phase space and reduced by single particle hopping. For strong coupling in the pair hopping $t_p/t \rightarrow \infty$ the remaining Hamiltonian (3.24) has a degenerate ground state which is the solution of the spin or the η Heisenberg model. Thus we expect LRO for large values of t_p/t with a staggered moment $m_s = m_{\text{Heisb}}/\sqrt{2}$. The staggered moment of the Heisenberg model m_{Heisb} is reduced because the simulated ground state is

$$|\Psi\rangle = \frac{1}{\sqrt{2}} (|\Psi_S^{\text{Heisb}}\rangle + |\Psi_{\eta}^{\text{Heisb}}\rangle). \quad (3.32)$$

After finite size extrapolation the results of Fig. 3.6 are consistent with a finite value of the magnetization m_s up to weak coupling ($t_p/t \ll 1$). However hopping strongly suppresses the order parameter. At the same time the superconducting order parameter Δ is also nonzero and the measured value $\Delta = \sqrt{2}m_s$ agrees with Eq. 3.31. The weak coupling situation deserves closer attention. Assuming a superconducting BCS ground state particle-hole excitations will be gapped. But this is in contradiction with the

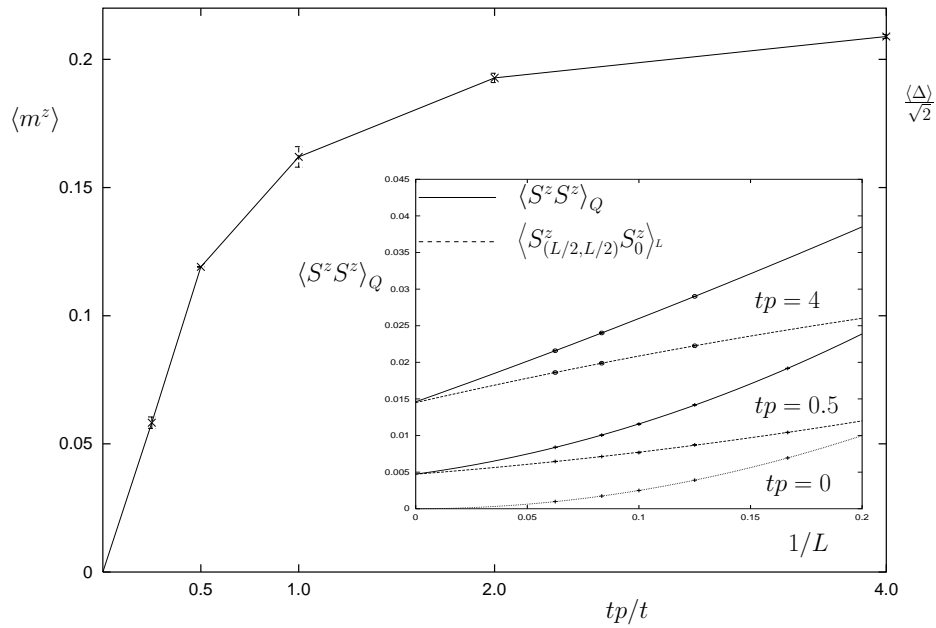


Figure 3.6: The staggered moment m_s which coexists with the superconducting order parameter $\Delta = m_s \sqrt{2}$ plotted as a function of t_p ($U/t = V/t = 0$). The inset shows finite size extrapolation for $t_p = 4$ and $t_p = 0.5$.

observed spin LRO. Thus the question arises how the observed coexistence can be realized:

- i) Coexistence of orders can be the result of a continuous symmetry we missed to identify in section 3.4.⁵ In particular we searched for a $SO(5)$ symmetry which rotates AF order into extended s -wave SC. We found no sign of extended pair condensation or softening of the associated π -modes.
- ii) The system gains energy via phase separation into one patch with ordered spins and another patch with pair order. In case of phase separation the long wave-length correlations between spin and η occupation should diverge with the volume

$$PS = \lim_{\mathbf{q} \rightarrow 0} \left\langle (2S_{\mathbf{q}}^z)^2 (2\eta_{\mathbf{q}}^z)^2 \right\rangle \propto N. \quad (3.33)$$

Figure 3.7 plots PS for $t_p = 0.5$. A weak long wavelength divergence is visible but finite size scaling reveals that it does not grow with system size. A similar plot for $t_p = 0.25$ shows no divergence at all. The probability to find two η -sites at random separation

$$P_{\eta\eta} = \frac{1}{N} \sum_{\mathbf{i}, \mathbf{j}} \left\langle (2\eta_{\mathbf{i}}^z)^2 (2\eta_{\mathbf{j}}^z)^2 \right\rangle \quad (3.34)$$

⁵This is exactly what happens in transition (c).

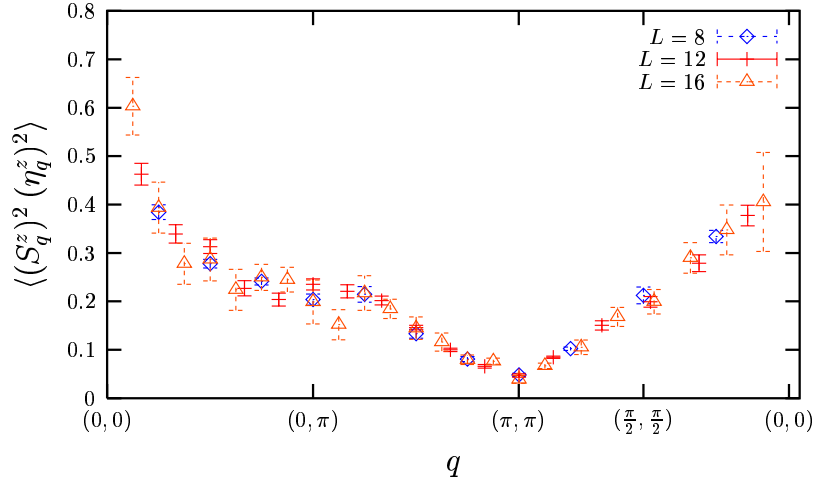


Figure 3.7: Phase separation would be signalled by strong divergence of $PS = \lim_{q \rightarrow 0} \langle (2S_q^z)^2 (2\eta_q^z)^2 \rangle \propto N$.

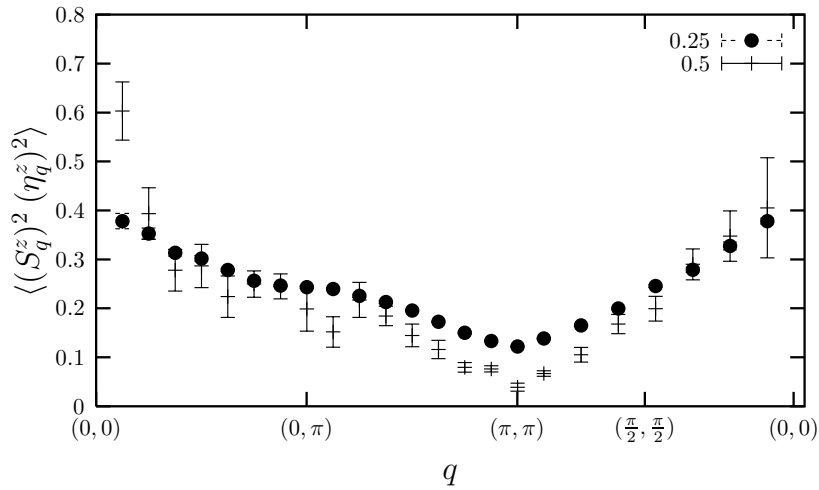


Figure 3.8: For $t_p = 0.25$ we find no divergence at all.

is plotted in Fig. 3.9

iii) Similar to the strong coupling situation (Eq. 3.32) the ground state remains a coherent superposition of two ordered states only with suppressed order parameters. In the next section we find that transition (a) is of first order. This supports the idea that at $U = 0$ the ground-state is formed as the superposition of the two crossing eigenstates.

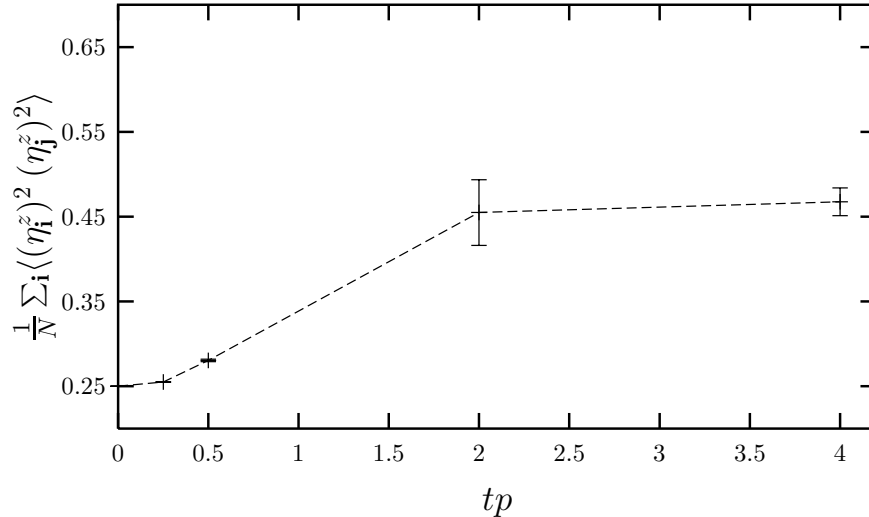


Figure 3.9: For large t_p/t the probability to find two η -sites approaches 0.5. In weak coupling $P_{\eta\eta}$ approaches 0.25 the uncorrelated value for the non-interacting system.

A first order transition

It proved difficult in the above section to characterize the observed coexistence of LRO's in the simulated ground state. We find that a simple picture emerges when we study the phase transition across the $U = 0$ point.

Following the $V = 0$ line as $U \rightarrow 0$ we find η LRO decreasing only slightly with a finite limit at $U = 0^+$. This is shown in Fig. 3.10 where the pair-pair correlation at maximum distance is plotted. Fig. 3.12.c) plots the quasi particle gap Δ_{qp} . Electrons remain gapped due to LRO even for small U . Crossing the $U = 0$ point we encounter a phase transition which is linked to a higher symmetry: the discrete particle-hole symmetry. In Fig. 3.10 the η order parameter jumps by a factor two from the extrapolated $U \rightarrow 0$ value to the coexistence value at $U = 0$. This is well explained when we assume a ground state $|\Psi_\eta(U \rightarrow 0^-)\rangle$ which jumps to a particle-hole symmetrized form

$$|\Psi\rangle = \frac{1}{\sqrt{2}} (|\Psi_\eta\rangle + |\Psi_S\rangle). \quad (3.35)$$

Thus we propose that the transition is a first order level crossing transition. This poses severe constraints on the behavior of all correlation functions across the transition. Most important it excludes continuous behavior with a diverging correlation length and in particular precludes the existence of a hidden continuous symmetry. The additional Goldstone modes which exist at $U = 0$ disappear immediately for a finite value of U .

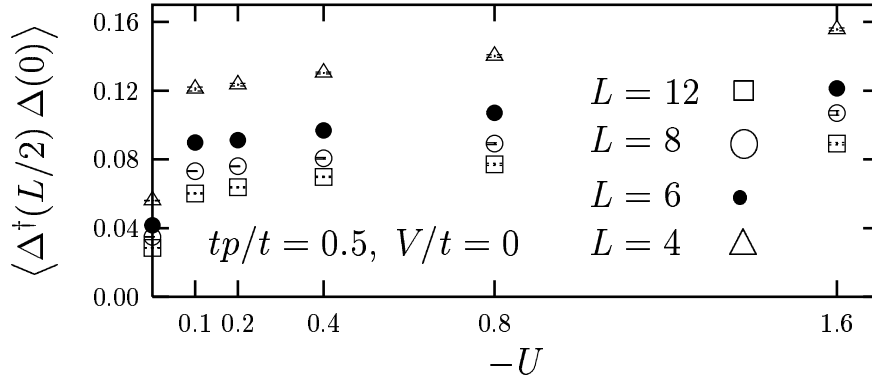


Figure 3.10: (the plot is really for $nn = 2\Delta^\dagger\Delta$.) The pair-pair correlation function $1/N \langle \Delta^\dagger(L/2) \Delta(0) \rangle$ at maximum separation $(L/2, L/2)$. The correlation function jumps by a factor two once a finite Hubbard U term breaks the $Z_{2,PH}$ symmetry.

In Fig. 3.11 we compute the equal time correlation $\langle S_{\mathbf{Q}}^z S_{-\mathbf{Q}}^z \rangle$ and the uniform spin susceptibility $\text{Re } \chi_{S^z S^z}(\omega = 0, \mathbf{k} = \mathbf{Q})$ where $\mathbf{Q} = (\pi, \pi)$ and

$$S_{\mathbf{Q}}^z = (1/\sqrt{N}) \sum_{\mathbf{r}} e^{i\mathbf{Q}\mathbf{r}} n_{\mathbf{r}}. \quad (3.36)$$

The susceptibility is obtained from integration of the time displaced correlation function

$$\chi'_{S^z S^z}(\omega = 0, \mathbf{k} = \mathbf{Q}) = \int_0^\infty \langle S_{\mathbf{Q}}^z(\tau) S_{-\mathbf{Q}}^z(0) \rangle d\tau. \quad (3.37)$$

We assume that close to the transition the correlation function has the form

$$S(\mathbf{r}, t) = \langle S_{\mathbf{r}}^z(\tau) S_0^z(0) \rangle \sim e^{-\frac{|\mathbf{r}|}{\xi}} e^{-\frac{\tau}{\xi_\tau}} \quad (3.38)$$

and U only changes the correlation lengths. Then by a simple change of variables in the integration the structure factor and the susceptibility are proportional to the correlation length

$$\langle S_{\mathbf{Q}}^z S_{-\mathbf{Q}}^z \rangle \sim \xi^2 \quad (3.39)$$

$$\chi'_{S^z S^z}(0, \mathbf{Q}) \sim \xi^2 \xi_\tau. \quad (3.40)$$

Fig. 3.11 shows no sign of a diverging correlation length at the phase transition. Note that $\chi'_{S^z S^z}(0, \mathbf{Q})$ appears to be further suppressed by the integration of an exponentially decaying time correlation controlled by a finite gap $\Delta_S \sim 1/\xi_\tau$.

It is also interesting to look at the free energy $F(U)$ which is the proper thermodynamic potential for this transition. At zero temperature the free energy reduces to the

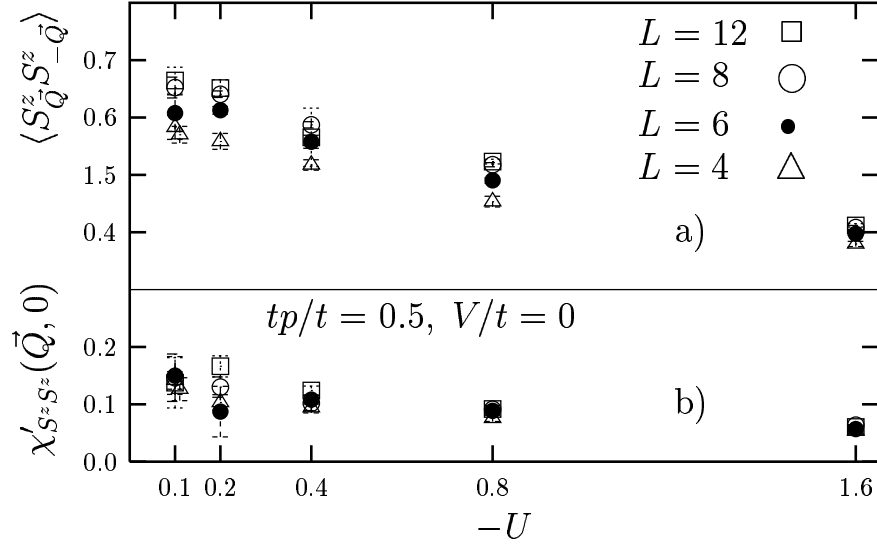


Figure 3.11: Values for the uniform susceptibility $\chi'_{S^z, S^z}(\vec{k} = \vec{Q}, \omega = 0) \propto \xi^2 \xi_\tau$ (lower curve) are well below the correlation function $\langle S_{\vec{k}}^z S_{-\vec{k}}^z \rangle(\vec{k} = \vec{Q}) \propto \xi^2$

ground state energy

$$F(U) = -kT \ln \text{Tr} \exp -\beta \left[H_0 + U/4 \sum_{\mathbf{i}} \mathcal{D}_{\mathbf{i}} \right], \quad (3.41)$$

$$\stackrel{T \rightarrow 0}{=} \frac{\langle \Psi_0 | H_0 + U/4 \sum_{\mathbf{i}} \mathcal{D}_{\mathbf{i}} | \Psi_0 \rangle}{\langle \Psi_0 | \Psi_0 \rangle}, \quad (3.42)$$

where H_0 contains hopping and pair hopping

$$H_0 = H_t + H_{t_p}, \quad (3.43)$$

and the Hubbard interaction is normalized to ± 1

$$\mathcal{D}_{\mathbf{i}} = 4(n_{\mathbf{i}, \uparrow} - 1/2)(n_{\mathbf{i}, \downarrow} - 1/2). \quad (3.44)$$

It is a general principle in statistical mechanics that a free energy as in Eq. (3.41) is a convex down function in an *arbitrary* intensive parameter (here the Hubbard U). The proof is given in appendix D. This allows to apply the usual concepts of thermodynamics to quantum phase transitions driven by an interaction parameter. Here the relevant pair of conjugate variables is the Hubbard U (intensive) and double occupancy \mathcal{D} (extensive). The ground state energy $E(U)$ in Fig. 3.12 has a kink and the derivative with respect to U

$$\frac{\partial E}{\partial U} = \frac{N}{4} \langle \mathcal{D}_{\mathbf{i}} \rangle = N \left(\langle n_{\mathbf{i}, \uparrow} n_{\mathbf{i}, \downarrow} \rangle - \frac{1}{4} \right) \quad (3.45)$$

is discontinuous. Our initial identification of the phase transition as first order is thus verified. Performing a Legendre transform to a new free energy $\tilde{F}(\langle n_{i,\uparrow} n_{i,\downarrow} \rangle)$

$$\tilde{F}(\langle n_{i,\uparrow} n_{i,\downarrow} \rangle) = E(U) - N U \langle n_{i,\uparrow} n_{i,\downarrow} \rangle, \quad (3.46)$$

a plateau marks the region of phase coexistence (Fig. 3.13). The two states at the endpoints of the plateau ($\langle n_{i,\uparrow} n_{i,\downarrow} \rangle = 0.15, 0.35$) correspond to states for $U \rightarrow 0^+, 0^-$. Intermediate values of the double occupancy somewhere on the plateau can only be realized by a mixture of the phases. Such states will have a higher energy due to the domain wall and will not be realized on small lattice sizes. Thus the particle-hole symmetric simulation at $U = 0$ must be a superposition of the two extremal states.

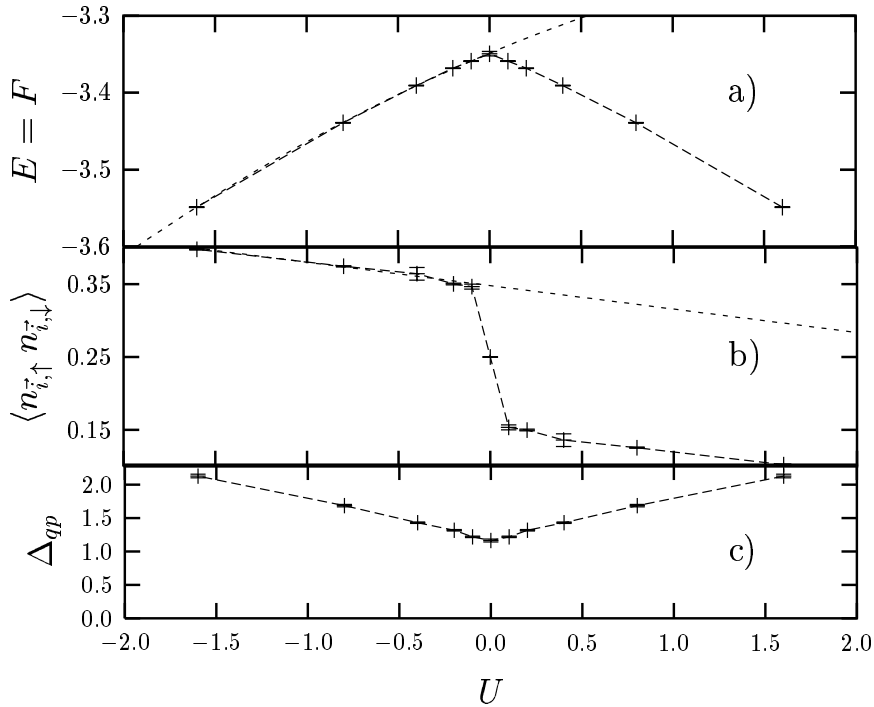


Figure 3.12: a) The free energy $E(U)$ shows a kink at $U = 0$. b) The "Hubbard" correlation $\langle n_{\uparrow} n_{\downarrow} \rangle = 1/N(\partial F/\partial U)$ has a jump at the transition point $U = 0$. The first order transition is signaled by a discontinuity of the first derivative of the free energy. The dashed line is the numerical derivative of the energy $E(U)$ c) The quasi-particle gap Δ_{qp} .

In order to understand how the $SU(2)_S \otimes SU(2)_\eta$ symmetries are spontaneously broken at $U = 0$ we also need to discuss whether the discrete particle-hole symmetry is

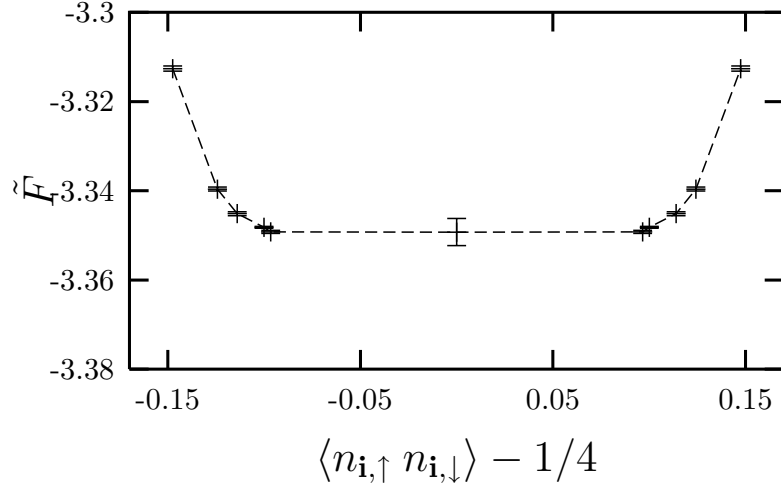


Figure 3.13: Legendre transformation to $\tilde{F}(\langle n_{i,\uparrow} n_{i,\downarrow} \rangle)$ reveals a plateau which marks the region of phase coexistence..

broken and how this affects the spontaneous breaking of the continuous symmetries. We introduce the double occupancy \mathcal{D} as a pseudo-spin order parameter

$$\mathcal{D}_i = ((2S_i^z)^2 - (2\eta_i^z)^2) \begin{cases} +1 : |\uparrow\rangle, |\downarrow\rangle \\ -1 : |\uparrow\downarrow\rangle, |0\rangle \end{cases}, \quad (3.47)$$

$$\langle \mathcal{D} \rangle = \langle \mathcal{P} \mathcal{D} \mathcal{P} \rangle = -\langle \mathcal{D} \rangle \quad (3.48)$$

which has to be zero as long as the $Z_{2,PH}$ symmetry is not broken as assumed in Eq. (3.48). A positive (negative) value for $\langle \mathcal{D} \rangle$ indicates a majority of spins (pairs) in the system. Using particle-hole symmetry the double occupancy correlation functions simplifies to

$$\langle \mathcal{D}_i \mathcal{D}_j \rangle_{\mathcal{P}} = 4 \langle (2S_i^z)^2 (2S_j^z)^2 \rangle - 1. \quad (3.49)$$

Plotting the uniform correlations $1/N \langle \mathcal{D}_{\mathbf{k}} \mathcal{D}_{\mathbf{k}} \rangle$ ($\mathbf{k} = 0$) as a function of temperature, one sees in Fig. 3.14 that below a temperature $T_c \sim 1.8t$ particle-hole symmetry is indeed broken ($t_p = 2t$). Hence below T_c and in the thermodynamic limit the $Z_{2,PH}$ particle-hole symmetry is broken and depending on the orientation of the pseudo-spin, $\mathcal{D}_{\vec{i}}$, the SC or AF ground state will be chosen.

A continuous transition

In the following, we will discuss the phase transition at constant negative $U = 1.6t$ and $tp = 0.5t$ as a function of V . For $V = 0$ the system has a higher $SU(2)$ symmetry and

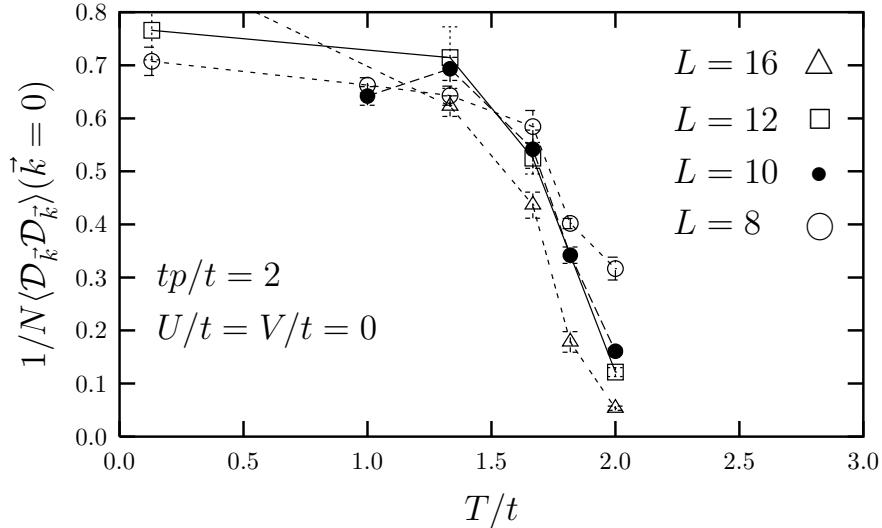


Figure 3.14: The $1/N \langle \mathcal{D}_{\mathbf{k}} \mathcal{D}_{-\mathbf{k}} \rangle (\mathbf{k} = 0)$ correlations show that at least up to $T \leq 1.8t$ particle-hole symmetry is broken ($t_p = 2t$).

we already know that η LRO exists. A finite V lowers the symmetry and some Goldstone modes at $V = 0$ must acquire a gap proportional to V . Thus we can expect to find a continuous transition.

In the $U \rightarrow -\infty$ limit the model is equivalent to hard-core bosons with repulsive nearest neighbor interactions. In this strong coupling limit the Hamiltonian (3.16) reduces to those terms which involve only η operators and the hard-core boson operators are

$$b_{\mathbf{i}}^{\dagger} = \eta_{\mathbf{i}}^{+} \quad (3.50)$$

$$b_{\mathbf{i}}^{\dagger} b_{\mathbf{i}} = \eta_{\mathbf{i}}^{+} \eta_{\mathbf{i}} = \eta_{\mathbf{i}}^z + \frac{1}{2} = \frac{1}{2} (n_{\mathbf{i},\uparrow} + n_{\mathbf{i},\downarrow}). \quad (3.51)$$

At half-filling this system experiences a transition from SC to charge-density wave states (CDW) going across $V = 0$. [40] [90] The transition point is marked by the higher symmetry $SU(2)_{\eta}$ and broken symmetry states may be labeled according to the direction of the magnetization. Therefore it is possible to find broken symmetry states which show a coexistence of CDW and SC order parameters. One can view this as a consequence of merging the Ising and the $U(1)$ symmetries into a continuous group. The finite temperature behavior is also dictated by symmetries. [40] The CDW has a finite Néel temperature T_N and the two-dimensional $U(1)$ breaking SC phase is characterized by a Kosterlitz-Thouless transition with a finite temperature T_{KT} . But at the $SU(2)$ symmetric point LRO at finite temperature is forbidden by the Mermin-Wagner theorem. Thus

the ordering temperatures T_{KT} and T_N drop to zero in the vicinity of the symmetric point.

The same behavior is still present for finite attractive U . In particular our simulations show (see Figs. 3.12c) and 3.16c) that single particle excitations are always gapped so we can argue that the system still renormalizes to the bosonic model. As we will see, crossing the $V = 0$ line at $T = 0$, we observe a divergence of the correlation length (Fig. 3.15) which points to a second order phase transition. Furthermore, we find no sign of a discontinuity in the first derivative of the free energy $(1/N)\partial F/\partial V = -2\langle n_i n_{i+x} \rangle$ (see Fig. 3.16b). At the same time we observe a jump for the CDW and SC order parameters at $V = 0$. To understand this transition, we split it up into three parts: a) $V \rightarrow 0^-$, b) $V = 0^- \rightarrow 0^+$ and c) $V \rightarrow 0^+$. Part b) is responsible for the jump in the order parameters. Let us introduce the two limiting ground states via

$$\Psi_{\text{Ising}} = \lim_{V \rightarrow 0^-} \lim_{N \rightarrow \infty} \Psi(V) \quad (3.52)$$

$$\Psi_{\text{XY}} = \lim_{V \rightarrow 0^+} \lim_{N \rightarrow \infty} \Psi(V). \quad (3.53)$$

The ground state in the Ising regime Ψ_{Ising} has CDW order and the SC order parameter is zero. Jumping to positive V and Ψ_{XY} the situation reverses. Thus the observed jump in the order parameters is the simple consequence of forcing the transition from one broken symmetry state to the other: $\Psi_{\text{Ising}} \rightarrow \Psi_{\text{XY}}$. Next we look at the critical behavior as we approach the phase transition from either side. Linear spin wave theory (LSWT) predicts for both transitions a) and c) the same square root divergence for the respective transverse correlation function. Dispersion relation and structure factors for the purely bosonic case are worked out in Appendix E. In case c) the equal time transverse correlation function is $\langle n_{\mathbf{Q}} n_{-\mathbf{Q}} \rangle$ where $n_{\mathbf{Q}} = (1/\sqrt{N}) \sum_{\mathbf{r}} e^{i\mathbf{Q}\mathbf{r}} n_{\mathbf{r}}$, $n_{\mathbf{r}} = n_{\mathbf{r},\uparrow} + n_{\mathbf{r},\downarrow}$ and $\mathbf{Q} = (\pi, \pi)$. According to LSWT this density-density correlation diverges like $\langle n_{\mathbf{Q}} n_{-\mathbf{Q}} \rangle = 8S/\sqrt{V/t_p}$ as $V \rightarrow 0^+$. The real part of the uniform susceptibility

$$\chi'_{n,n}(\mathbf{k} = \mathbf{Q}, \omega = 0) = \int_0^\infty d\tau \langle n_{\mathbf{Q}} n_{-\mathbf{Q}} \rangle(\tau) \quad (3.54)$$

picks up the inverse of the gap $\Delta = 8\sqrt{2Vt_p}$ and in LSWT diverges like $\chi'_{n,n}(\mathbf{Q}, 0) = \sqrt{1/2}S/V$. Asymptotically the correlation function $\langle n_i n_0 \rangle(\tau)$ decays exponentially in space and time thus the integrated correlation functions are proportional to the correla-

tion length and gap

$$\langle n_{\mathbf{Q}} n_{-\mathbf{Q}} \rangle \propto \xi^2 \quad (3.55)$$

$$\chi'_{n,n}(\mathbf{k} = \mathbf{Q}, \omega = 0) \propto \xi^2 \Delta^{-1}. \quad (3.56)$$

Data for both $\chi'_{n,n}(\mathbf{Q}, 0)$ and $\langle n_{\mathbf{Q}}^z n_{-\mathbf{Q}}^z \rangle(\tau = 0)$ are shown in Fig. 3.15 where the dotted line plots the LSWT result multiplied with a single constant to account for the reduced moment.

The ordered state in the XY regime has one Goldstone mode and the transverse correlations $\langle n_{\mathbf{Q}} n_{-\mathbf{Q}} \rangle$ are gapped. Approaching the critical point the gap closes and the $\langle n_{\mathbf{Q}} n_{-\mathbf{Q}} \rangle$ correlation length diverges. Thus critical behavior reflects the softening of the observed mode which turns into a Goldstone mode at the point with higher symmetry. Ultimately it is the softening of the transverse mode which is responsible for the observed critical behavior.

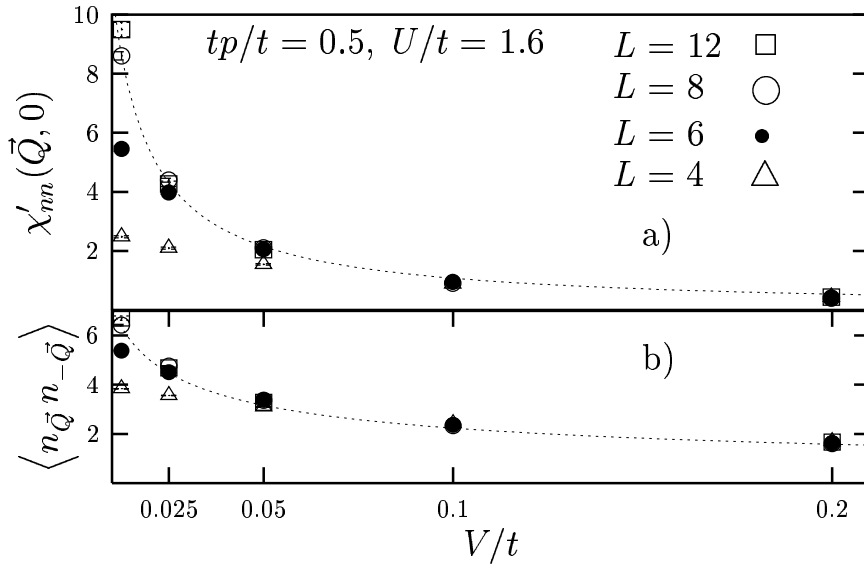


Figure 3.15: a) Uniform susceptibility $\chi'_{n,n}(\mathbf{Q}, 0) \propto \xi^2 \Delta^{-1}$ b) $\langle n_{\mathbf{Q}} n_{-\mathbf{Q}} \rangle \propto \xi^2$. The dotted line is proportional to results from LSWT.

The critical behavior is also apparent from the mode dispersions. Figures 3.6, 3.6 and 3.6 plot the spectral functions $\langle n_{\mathbf{k}} n_{-\mathbf{k}} \rangle(\omega)$ and $\langle \Delta_{\mathbf{k}}^\dagger \Delta_{\mathbf{k}} \rangle(\omega)$.

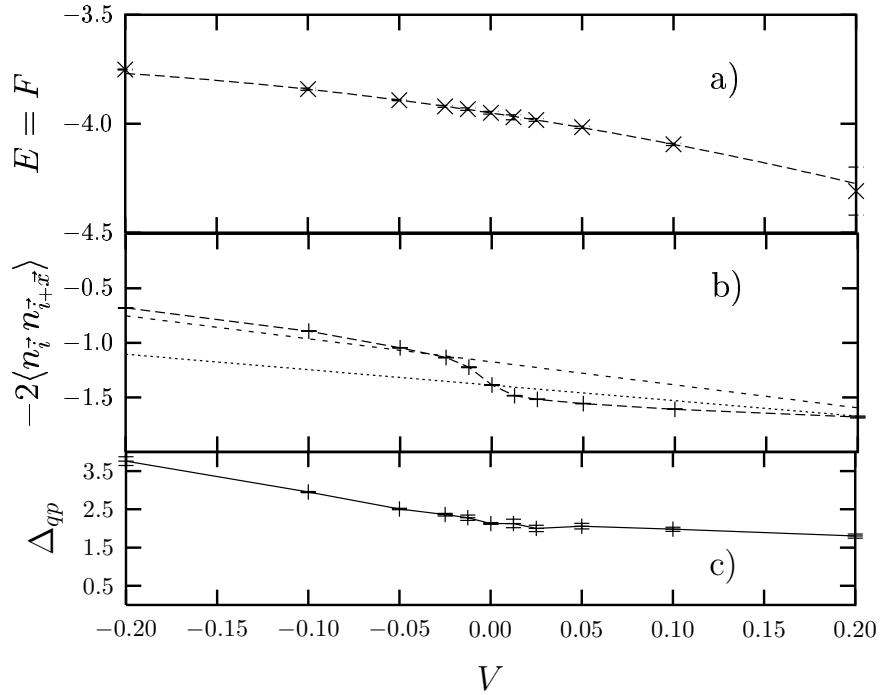
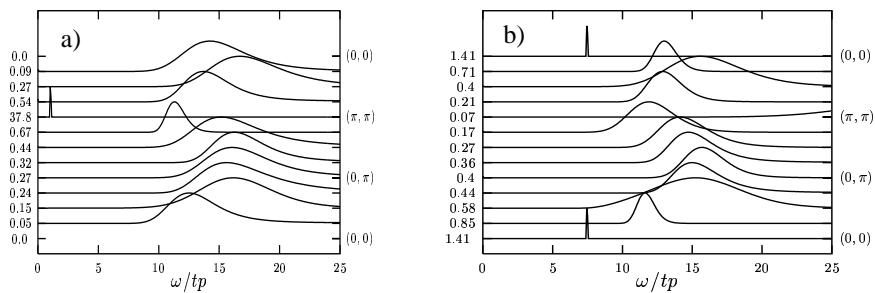
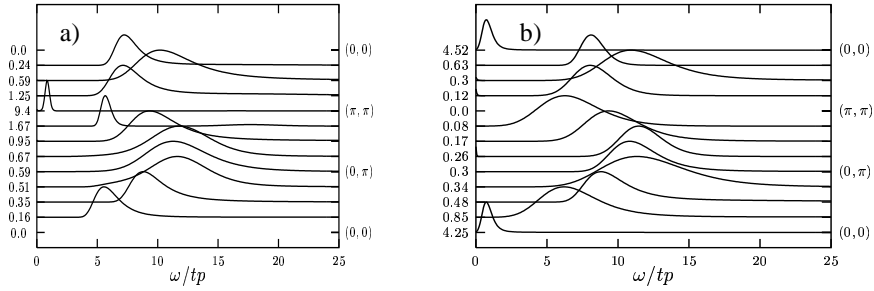


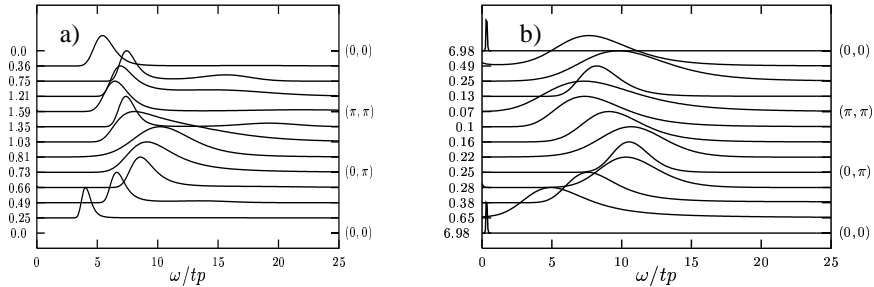
Figure 3.16: a) The energy $E(V)$. The dashed line is a fit which is used to take numerical derivatives on both sides of the transition. b) Density-density correlations $2\langle n_{\mathbf{i}} n_{\mathbf{i}+\mathbf{x}} \rangle = -1/N(\partial F/\partial V)$ where $n_{\mathbf{i}} = n_{\mathbf{i},\uparrow} + n_{\mathbf{i},\downarrow}$. The derivative of the free energy is continuous. Dashed and dotted lines indicate the numerical derivative c) The quasi-particle gap Δ_{qp} was obtained by fitting the tail of the imaginary time correlation function $G(\tau)$.



CDW phase at $V = -0.2t$: a) the density-density mode condenses at momentum $\mathbf{Q} = (\pi, \pi)$. At momentum $\mathbf{k} = 0$ density is conserved but the mode has zero weight. b) the transverse pair-pair excitations are always gapped.



$SU(2)$ symmetric phase at $V = 0$: a) the density-density mode condenses (Goldstone) at $\mathbf{k} = \mathbf{Q}$. The dispersion approaches zero continuously. Particle number is conserved but the density mode at $\mathbf{k} = 0$ is weightless b) Pairs condense at $\mathbf{k} = 0$ and due to symmetry the pair mode has zero weight at $\mathbf{k} = \mathbf{Q}$.



SC phase: a) the density-density mode opens a gap at $\mathbf{k} = \mathbf{Q}$. Particle number conservation leads to a gapless branch at $\mathbf{k} = 0$ but with vanishing weight. b) the pair mode condenses at $\mathbf{k} = 0$ but opens a gap at $\mathbf{k} = \mathbf{Q}$.

3.7 Conclusion

Organic superconductors have a rich phase diagram. In particular we are interested in the ordered superconducting and antiferromagnetic low temperature phases. Upon pressure a first order transition is observed. The nature of the superconducting order parameter remains controversial but we show that a transition between AF and *s*-wave superconducting states can be represented by a simple toy model. We argue that the pair hopping term which is responsible for the ordering may arise from electron-phonon interaction via a Su-Schrieffer-Heeger term.

Conclusion

We will first make some general statements on Quantum Monte Carlo as applied to fermionic lattice problems and then summarize the research subjects carried out in this thesis. Apart from exactly solvable models in one dimension, Quantum Monte Carlo is one of the few methods which give exact results for interacting many body systems. But when applied to Fermions, there are also severe limitations:

- The method scales like $N^3\beta$, which makes only small systems of up to 500 sites accessible. This restriction of small system sizes is especially problematic in the study of critical behavior which is characterized by a diverging length scale.
- The notorious sign problem limits the applicability of determinant QMC either to the study of high temperature behavior or a special set of known Hamiltonian which can be decoupled in a sign free way. The class of sign-free Hamiltonians is restricted to some systems with attractive interaction and a few equivalent systems such as the repulsive Hubbard model at half filling. A common feature of all sign free simulations is a gapped single particle spectrum. This is maybe less dramatic then it appears at first sight, as the “normal” Fermi liquid state is also unstable towards some ordered low temperature phase.
- A big advantage of determinantal QMC is that almost any time displaced correlation function can be measured. For example, this is not at all trivial in the so called cluster algorithms such as stochastic series expansion. But charge and spin dynamics are initially obtained for imaginary times. The analytic continuation to real frequencies still poses a mayor challenge. As the QMC results for a time displaced correlation is always blurred by statistical error the inverse Laplace transformation is ill defined and a statistical procedure known as Maximum Entropy method has to be used.

- Non-equilibrium thermodynamics as found in a quantum dot with persistent current, can not be studied. In fact the path integral for such a problem is afflicted again by a sign problem.

Typically, one has to resort to some approximation, when studying many-body problems. A minimal requirement to cope with the uncontrolled nature of these approximations, is a check against well established results. Here, QMC provides benchmark results, albeit for special points in the phase diagram. In this thesis we provide such results for two canonical models in the field of strongly correlated electron systems, namely the Hubbard and the Kondo model.

Now we would like to discuss in more detail the main results of this thesis:

Auxiliary field Quantum Monte Carlo

In the first chapter we give a detailed account of determinantal quantum Monte Carlo and the BSS algorithm [14]. A number of models which allow sign free simulations is reviewed. In principle the method is well suited to calculate imaginary-time-displaced correlations functions but a straight forward evaluation of the time-displaced Green's function suffers from numerical instabilities. So far, numerically stable methods to compute the zero temperature Green's function were based on a stabilization scheme developed for the finite temperature algorithm [8]. Although precise, this method is expensive in CPU time. We developed an alternative approach [28] for the zero temperature algorithm, based on the observation that for a given auxiliary field the equal-time Green's function matrix G is a projector $G^2 = G$. The new method is easy to implement and an order of magnitude faster than the previously used stabilization. We made extensive use of this method when we calculated the single hole dynamics in the Kondo-Hubbard model. We also discuss the Dyson equation of the full lattice Green's function that allows a conceptual unification of the Hirsch-Fye impurity algorithm and the BSS algorithm.

Kondo-Hubbard model

The second chapter introduces the Kondo lattice model, which was only recently studied with determinantal QMC after a sign free formulation was found [7]. The low energy

charge excitations in this Kondo model behave very differently from the Hubbard case. Due to the constraint of achieving a sign free simulation, we can only investigate the insulating phase at half filling. But we can identify the k -points of the charge gap, i.e. the minimum of the hole dispersion. For the Hubbard model this minimum is observed at $(\pi/2, \pi/2)$ but pronounced shadow features due to the antiferromagnetism are found out to the corner of the Brillouin zone. On the other hand in the Kondo model the minimum is at (π, π) which originates from the screening of the magnetic impurities. Apparently, these two behaviors can not be easily reconciled when we study a combined model with both a Kondo interaction and an additional Hubbard interaction for the conduction electrons (*UKLM*). In such a *UKLM* we find, that the position of the charge gap is always dictated by the Kondo behavior (i.e. $k = (\pi, \pi)$), even when the Kondo coupling is weak compared to the Hubbard interaction. As $J \rightarrow 0$, the spectral weight in the Kondo-like low-energy band in the vicinity of $k = (\pi, \pi)$ vanishes and is transferred to higher energy Hubbard like bands. In the (U, J) plane the Hubbard line, i.e. $J = 0$, is singular since the localized spins decouple and the ground state is macroscopically degenerate. The evolution of the spectral function at $J = 0$ is discontinuous regarding the wave vector that dominates the low energy hole dynamics which jumps from (π, π) to $(\pi/2, \pi/2)$. In this sense the model shows no continuous path from the Kondo insulator to the Mott insulator. Given our results, it is very tempting to speculate on the effects of doping with a finite density of holes. Assuming a rigid band picture we would conclude that off half filling the *UKLM* displays a Fermi surface centered around (π, π) for all values of U and $J > 0$. In addition the Kondo lattice model shows a quantum critical point, arising from a competition of the magnetic phases. For small J the RKKY interaction leads to a antiferromagnetic ordered state whereas at large J the formation of local Kondo singlets is favored. The magnetic phase diagram of the *UKLM* has then been determined.

Coexistence of *s*-wave SC and Antiferromagnetism

Finally, in the third chapter we study a complicated Hubbard model on a square lattice. The simple Hubbard model with a local interaction U was augmented by nearest neighbor spin-spin and charge-charge interaction terms. Both spin and charge nearest neighbor interactions arise simultaneously from a pair hopping term (coupling t_p) in the form of

a squared kinetic energy on single bonds. In addition we consider a density-density coupling V , in order to break the $SU(2)$ η -symmetry in the charge sector. We study the phase diagram at half filling for attractive U . For $V = 0$, particle hole symmetry makes the repulsive U sector also accessible. In the regions we could study the phase diagram is found to be completely determined by the various symmetries. Two points are of special interest. First the line of attractive U and $V = 0$ which separates a superfluid phase for $V > 0$ and a charge-density-wave phase for $V < 0$. We demonstrate that the phase transition $V \rightarrow 0$ is a continuous phase transition. Second, the point $U = V = 0$ separates a superconducting phase at $U < 0$ from an antiferromagnetic phase at $U > 0$. This transition is observed to be of first order. The simulation at the symmetric point $U = V = 0$ displays coexistence of superconducting and antiferromagnetic correlations. Recently, such a first order transition between antiferromagnetism and superconductivity has been observed in the organic layered superconductor κ -(BEDT-TTF)-Cl [61]. We speculate, that our model describes these low temperature phases while the nearest neighbor spin and charge interactions are generated by a Su-Schrieffer-Heeger [98] electron-phonon interaction.

Appendix A

QMC: Proofs

A.1 Scalar Product

Let us show in more detail the matrix implementation of the scalar product

$$\langle L|R\rangle = \det \mathbf{L}^\dagger \mathbf{R}. \quad (\text{A.1})$$

We insert the definition (1.70)

$$|R\rangle = \prod_{i=1}^{N_e} \left(\sum_x c_x^\dagger R_{x,i} \right) |0\rangle = \sum_{x_1 \dots x_{N_e}} c_{x_1}^\dagger c_{x_2}^\dagger \dots c_{x_{N_e}}^\dagger |0\rangle R_{x_1,1} \dots R_{x_{N_e},N_e} \quad (\text{A.2})$$

and obtain

$$\langle L|R\rangle = \sum_{\substack{x_1 \dots x_{N_e} \\ y_1 \dots y_{N_e}}} \langle 0| c_{y_{N_e}} \dots c_{y_1} c_{x_1}^\dagger \dots c_{x_{N_e}}^\dagger |0\rangle \bar{L}_{N_e, y_{N_e}} \dots \bar{L}_{1, y_1} R_{x_1,1} \dots R_{x_{N_e},N_e}. \quad (\text{A.3})$$

The expectation value of $\langle 0| c_{y_{N_e}} \dots c_{y_1} c_{x_1}^\dagger \dots c_{x_{N_e}}^\dagger |0\rangle$ can only be nonzero iff a permutation π transforms the set of numbers $(x_1 \dots x_{N_e})$ into $(y_1 \dots y_{N_e})$ and all entries in $(x_1 \dots x_{N_e})$ are mutually different. Then the expectation value is equal to the sign of the permutation

$$\langle 0| c_{y_{N_e}} \dots c_{y_1} c_{x_1}^\dagger \dots c_{x_{N_e}}^\dagger |0\rangle = \langle 0| c_{x_{\pi(N_e)}} \dots c_{x_{\pi(1)}} c_{x_1}^\dagger \dots c_{x_{N_e}}^\dagger |0\rangle = (-1)^\pi. \quad (\text{A.4})$$

We now have

$$\langle L|R\rangle = \sum'_{\substack{x_1 \dots x_{N_e} \\ \pi}} (-1)^\pi \bar{L}_{N_e, x_{\pi(N_e)}} \dots \bar{L}_{1, x_{\pi(1)}} R_{x_1,1} \dots R_{x_{N_e},N_e}, \quad (\text{A.5})$$

where the sum \sum' is restricted to mutually different $(x_1 \dots x_{N_e})$. In fact this restriction is not necessary. Summing instead over the unrestricted sum

$$\langle L|R\rangle = \sum_{\substack{x_1 \dots x_{N_e} \\ \pi}} (-1)^\pi \bar{L}_{N_e, x_{\pi(N_e)}} \dots \bar{L}_{1, x_{\pi(1)}} R_{x_1,1} \dots R_{x_{N_e},N_e} \quad (\text{A.6})$$

we encounter for instance a term $x_1 = x_2$. But there is also a transposition π_0 that exchanges

$$\begin{aligned}\pi_0\pi(x_1) &= \pi(x_2), \\ \pi_0\pi(x_2) &= \pi(x_1),\end{aligned}\tag{A.7}$$

and has always a negative sign $(-1)^{\pi_0} = -1$. Finally we pair rows of L and columns of R

$$\langle L|R \rangle = \sum_{\substack{x_1 \dots x_{N_e} \\ \pi}} (-1)^\pi \bar{L}_{\pi^{-1}(1), x_1} R_{x_1, 1} \dots \bar{L}_{\pi^{-1}(N_e), x_{N_e}} R_{x_{N_e}, N_e}\tag{A.8}$$

$$= \det \mathbf{L}^\dagger \mathbf{R},\tag{A.9}$$

which completes the proof.

A.2 Grand canonical Trace

A formal proof of Eq. (1.83) follows the simple example for a two particle system. We want to show

$$\text{Tr} e^{-\mathbf{c}^\dagger \mathbf{H}_m \mathbf{c}} \dots e^{-\mathbf{c}^\dagger \mathbf{H}_1 \mathbf{c}} = \det(1 + \mathbf{B}).\tag{A.10}$$

First we define a basis in Fock space

$$|\mathbf{P}(x_1, \dots, x_{N_e})\rangle : \mathbf{P}(x_1, \dots, x_{N_e}) = \mathbf{e}_{x_1} \oplus \mathbf{e}_{x_2} \oplus \dots \oplus \mathbf{e}_{x_{N_e}}\tag{A.11}$$

where the particle number N_e runs from 0 to N , and the sequence of x_1 through x_{N_e} satisfies

$$x_1 < x_2 < \dots < x_{N_e}.\tag{A.12}$$

Vectors \mathbf{e}_x are unit vectors

$$e_{x,i} = \delta_{x,i}.\tag{A.13}$$

We use the Fock basis (A.11) to evaluate the trace

$$\begin{aligned}\text{Tr} e^{-\mathbf{c}^\dagger \mathbf{H}_m \mathbf{c}} \dots e^{-\mathbf{c}^\dagger \mathbf{H}_1 \mathbf{c}} &= \sum_{N_e=1}^N \sum_{x_1 < \dots < x_{N_e}} \langle \mathbf{P}(x_1, \dots, x_{N_e}) | e^{-\mathbf{c}^\dagger \mathbf{H}_m \mathbf{c}} \dots e^{-\mathbf{c}^\dagger \mathbf{H}_1 \mathbf{c}} | \mathbf{P}(x_1, \dots, x_{N_e}) \rangle \\ &= \sum_{N_e=1}^N \sum_{x_1 < \dots < x_{N_e}} \det \mathbf{P}^\dagger(x_1, \dots, x_{N_e}) \mathbf{B} \mathbf{P}(x_1, \dots, x_{N_e}) \\ &= \sum_{N_e=1}^N \sum_{x_1 < \dots < x_{N_e}} \det \mathbf{B}(x_1, \dots, x_{N_e}).\end{aligned}\tag{A.14}$$

Multiplying \mathbf{B} from the right and left side with the rectangular matrix $\mathbf{P}(x_1, \dots, x_{N_e})$ results in a matrix of size $N_e \times N_e$

$$\mathbf{B}(x_1, \dots, x_{N_e}) = \mathbf{P}^\dagger(x_1, \dots, x_{N_e})\mathbf{B}\mathbf{P}(x_1, \dots, x_{N_e}). \quad (\text{A.15})$$

Note that $\mathbf{B}(x_1, \dots, x_{N_e})$ is the submatrix of \mathbf{B} obtained by keeping rows and columns running through the diagonal elements indexed by (x_1, \dots, x_{N_e}) . We realize that the sum used in Eq. (A.14) generates all possible submatrices of the above type which alternatively may be generated from the row (or column) expansion of $\det(1 + \mathbf{B})$ using the multilinear property of the determinant.

A.3 $\det(1 + AB) = \det(1 + BA)$

Let \mathbf{A} be $N \times M$ and \mathbf{B} be $M \times N$ matrices. Then the different size determinants satisfy

$$\det(\mathbf{1}_N + \mathbf{A}\mathbf{B}) = \det(\mathbf{1}_M + \mathbf{B}\mathbf{A}).$$

This may be verified using a formal power series expansion of $\ln \det(\mathbf{1}_N + \lambda\mathbf{A}\mathbf{B})$

$$\begin{aligned} \ln \det(\mathbf{1}_N + \lambda\mathbf{A}\mathbf{B}) &= \text{Tr} \ln(\mathbf{1}_N + \lambda\mathbf{A}\mathbf{B}) = \text{Tr} \sum_{n=1}^{\infty} \frac{(-\lambda\mathbf{A}\mathbf{B})^n}{n} \\ &\stackrel{!}{=} \text{Tr} \sum_{n=1}^{\infty} \frac{(-\lambda\mathbf{B}\mathbf{A})^n}{n} = \ln \det(\mathbf{1}_M + \lambda\mathbf{B}\mathbf{A}), \end{aligned}$$

where we used

$$\ln \det = \text{Tr} \ln. \quad (\text{A.16})$$

Appendix B

QMC vs. Diagrams

We already mentioned that the Trotter decomposition is a valuable tool to introduce path integrals. [81] Once we have the path integral we can always attempt a formal expansion in the interaction coupling and obtain a diagrammatic representation for the coefficients in the Taylor series. For a system

$$H = H_0 + \lambda H_I, \tag{B.1}$$

we obtain the following series for the partition sum $Z(\lambda)$

$$Z(\lambda) = \sum_{i=0}^{\infty} d_i \lambda^i. \tag{B.2a}$$

All connected and disconnected diagrams of order i are collected in the coefficient d_i . This expansion will necessarily break down at a finite convergence radius r , since $Z(\lambda)$ is never an entire function (i.e. analytic for all $\lambda \in \mathbb{C}$).

This should be compared to the Trotter formula, where we may safely approximate (see Eq. 1.32)

$$e^{-\Delta\tau H_I} \sim 1 - \Delta\tau \lambda H_I, \tag{B.3}$$

when $\Delta\tau$ is small enough. Then we obtain an approximant for $Z(\lambda)$

$$Z^m(\lambda) = \sum_{i=0}^m c_i^m \lambda^i, \tag{B.4}$$

and the Trotter product formula guarantees

$$\lim_{m \rightarrow \infty} Z^m(\lambda) = Z(\lambda) \tag{B.5}$$

for all $\lambda \in \mathbb{R}$ so that approximants $Z^m(\lambda)$ are not limited by the convergence radius r of the Taylor series (B.2a). The c_i^m are a reasonable approximations for the d_i (although converging slowly)

$$\lim_{m \rightarrow \infty} c_i^m = d_i \quad (\text{B.6})$$

and the approximant $Z^m(\lambda)$ converges term by term to the Taylor series. For $\lambda \leq r$ we are allowed to rearrange limits¹

$$\lim_{m \rightarrow \infty} \sum_{i=0}^m c_i^m \lambda^i = \lim_{m \rightarrow \infty} \sum_{i=0}^m \left(\lim_{n \rightarrow \infty} c_i^n \right) \lambda^i = \sum_{i=0}^{\infty} d_i \lambda^i. \quad (\text{B.7})$$

For $\lambda \geq r$ the right hand side diverges but the approximants still converge!

In any case, the convergence of the Trotter approximant for the partition function is not very good, but the corresponding rational function approximant for the energy

$$E(\lambda) = \frac{\sum_{i=0}^m e_i^m \lambda^i}{\sum_{i=0}^m c_i^m \lambda^i} \quad (\text{B.8})$$

is very stable.

Finally we should briefly discuss the analytic behavior we expect for finite systems at finite temperature, which after all are the systems amenable to lattice QMC. All thermodynamic quantities are analytic for $\lambda \in \mathbb{R}$ but for complex λ one must encounter branchpoints. This is most easily seen for the eigenvalues $E_i(\lambda)$ which have branchpoints. For a 2×2 matrix this is just the square root branchpoint $V = |E_2 - E_1|/2$

$$\begin{pmatrix} E_1 & V \\ V & E_2 \end{pmatrix} \implies E_{1,2}(\lambda) = \frac{1}{2} (E_2 + E_1) \pm \frac{1}{2} \sqrt{(E_2 - E_1)^2 + 4V^2}. \quad (\text{B.9})$$

Thermodynamic functions at finite temperature inherit these branchpoints since the energy enters the Boltzmann weight. Hence a Taylor expansion of these functions will converge only until this point.

¹The rearrangement of limits is best understood when visualizing the coefficients c_i^m (where $i \leq m$) in a triangular diagram.

Appendix C

Path integrals to Green's function

We used the Hubbard-Stratonovich decoupling to reduce the interacting many body problem to a sum of non interacting single particle problems (i.e. Hamiltonians are quadratic in fermion operators) in an external potential that varies with time. We proceed to solve a single such problem exactly which amounts to ‘integrate out’ the fermionic degrees of freedom. A very complete derivation of the final formulas using standard operator formalism may be found in [64]. The following proofs use the alternative coherent state basis with the main advantage that one obtains a closed formula for the generating functional

$$Z[x^*, y] = \left\langle \mathcal{T} \hat{U}_1 e^{x^* c_i} \hat{U}_2 e^{y c_i^\dagger} \hat{U}_3 \right\rangle \quad (\text{C.1})$$

where x^*, y are Grassmann variables.

C.1 Grassmann variables

Let us first introduce Grassmann variables (see [10] appendix C, [80]). We introduce conjugated pairs of Grassmann variables

$$\mathbf{z} = (z_1, \dots, z_N), \quad \mathbf{z}^* = (z_1^*, \dots, z_N^*). \quad (\text{C.2})$$

These variables are *operators* which can be added and multiplied. They commute with any scalar x , but *anticommute* with each other:

$$\begin{aligned} xz &= zx, \\ z_i z_j &= -z_j z_i, \\ z_i z_j^* &= -z_j^* z_i, \end{aligned} \quad (\text{C.3})$$

which implies

$$z_i^2 = 0. \quad (\text{C.4})$$

The ‘Grassmann integration’ is a counting operation which acts on a polynomial of Grassmann variables as follows:

$$\int dz_1 \prod_{i=1}^N z_i^{n_i} \prod_{j=1}^N (z_j^*)^{m_j} = n_1 \prod_{i=2}^N z_i^{n_i} \prod_{j=1}^N (z_j^*)^{m_j}, \quad (\text{C.5})$$

where $n_i = 0, 1$. (Note: the Grassmann algebra is defined over complex numbers, but the above ‘integration’ does *not* involve complex integration!) Since z_i, z_i^* are treated as independent variables we define the integration over d^2z as

$$\int d^2z \mathcal{O}(z^*, z) = \int dz^* \left(\int dz \mathcal{O}(z^*, z) \right). \quad (\text{C.6})$$

Now it is easy to verify that

$$\int d^2z \exp(-z^* z) z^m (z^*)^n = \delta_{n,m}, \quad n, m = 0, 1. \quad (\text{C.7})$$

With these definitions it is possible to prove the following identity for multidimensional Grassmann Gaussian integrals

$$\int d^2\mathbf{z} \exp(-\mathbf{z}^* \mathbf{G}^{-1} \mathbf{z} + \mathbf{z}_a^* \mathbf{z} + \mathbf{z}^* \mathbf{z}_b) = \det \mathbf{G}^{-1} \exp(\mathbf{z}_a^* \mathbf{G} \mathbf{z}_b). \quad (\text{C.8})$$

Applied to any Grassmann polynomial we may verify the anticommutation relation

$$\left\{ \frac{\partial}{\partial z_i^*}, z_j^* \right\} = \delta_{i,j}. \quad (\text{C.9})$$

Above we have introduced Grassmann variables and further established that Grassmann integrals are an alternative way to handle determinants. Next we need to make contact with the fermionic Fock space. To this end we define a generalized Fock space over the Grassmann algebra instead of simple c numbers. It is further necessary to require anticommutation between Grassmann generators and fermi operators

$$\{c, z\} = 0, \quad (\text{C.10})$$

and to define a conjugate of the following form

$$(zc)^\dagger = c^\dagger z^*.$$

Using these definitions it is possible to introduce the fermion *coherent* state with the usual coherent state properties

$$\begin{aligned}
|\mathbf{z}\rangle &= \exp(-\mathbf{z}\mathbf{c}^\dagger) |0\rangle, \\
c_i |\mathbf{z}\rangle &= z_i |\mathbf{z}\rangle, \\
c_i^\dagger |\mathbf{z}\rangle &= -\frac{\partial}{\partial z_i} |\mathbf{z}\rangle, \\
\langle \mathbf{z} | c_i^\dagger &= \langle \mathbf{z} | z_i^*, \\
\langle \mathbf{z} | \mathbf{z}' \rangle &= e^{\mathbf{z}^* \mathbf{z}'}, \\
z_i |0\rangle &= |0\rangle z_i.
\end{aligned} \tag{C.11}$$

With the help of equation (C.7) we may define a completeness relation using Grassmann integration

$$\int d^2 z e^{-\mathbf{z}^* \mathbf{z}} |\mathbf{z}\rangle \langle \mathbf{z}| = I. \tag{C.12}$$

The trace of an operator \mathcal{A} may also be stated in coherent state basis

$$\begin{aligned}
\text{Tr } \mathcal{A} &= \sum_x \langle x | \mathcal{A} | x \rangle = \sum_x \int d^2 z e^{-z^* z} \langle x | z \rangle \langle z | \mathcal{A} | x \rangle \\
&= \sum_x \int d^2 z e^{-z^* z} \langle z | \mathcal{A} | x \rangle \langle x | -z \rangle \\
&= \int d^2 z e^{-z^* z} \langle z | \mathcal{A} | -z \rangle = \int d^2 z e^{-z^* z} \langle -z | \mathcal{A} | z \rangle,
\end{aligned} \tag{C.13}$$

where the minus arises from commuting two Grassmann polynomials in \mathbf{z}^* and \mathbf{z} .

Finally we need matrix elements of an arbitrary operator between coherent states: let us assume that the operator may be written as a normal ordered polynomial in a^\dagger, a

$$\mathcal{O}[\mathbf{a}^\dagger, \mathbf{a}] = \sum_{\{n_i, m_i\}} O_{\{n_i, m_i\}} \left[(a_1^\dagger)^{n_1} \dots (a_N^\dagger)^{n_N} a_1^{m_1} \dots a_N^{m_N} \right], \tag{C.14}$$

where $n_i, m_i = 0, 1$. Using (C.11), the matrix elements are

$$\langle \mathbf{z} | \mathcal{O}[\mathbf{a}^\dagger, \mathbf{a}] | \mathbf{z}' \rangle = O(\mathbf{z}^*, \mathbf{z}') e^{\mathbf{z}^* \mathbf{z}'}, \tag{C.15}$$

where

$$O(\mathbf{z}^*, \mathbf{z}') = \sum_{\{n_i, m_i\}} O_{\{n_i, m_i\}} \left[(z_1^*)^{n_1} \dots (z_N^*)^{n_N} (z'_1)^{m_1} \dots (z'_N)^{m_N} \right]. \tag{C.16}$$

We will also need coherent state matrix elements for the single particle evolution

$$\begin{aligned}
\langle \mathbf{z} | e^{\mathbf{c}^\dagger \mathbf{H} \mathbf{c}} | \mathbf{z}' \rangle &= e^{\mathbf{z}^* e^{\mathbf{H}} \mathbf{z}'}, \\
\langle \mathbf{z} | e^{\mathbf{c}^\dagger \mathbf{H} \mathbf{c}} e^{\mathbf{y}^* \mathbf{c}} | \mathbf{z}' \rangle &= e^{\mathbf{z}^* e^{\mathbf{H}} \mathbf{z}' + \mathbf{y}^* \mathbf{c}}, \\
\langle \mathbf{z} | e^{\mathbf{c}^\dagger \mathbf{x}} e^{\mathbf{c}^\dagger \mathbf{H} \mathbf{c}} | \mathbf{z}' \rangle &= e^{\mathbf{z}^* \mathbf{x} + \mathbf{z}^* e^{\mathbf{H}} \mathbf{z}'},
\end{aligned} \tag{C.17}$$

where \mathbf{x}, \mathbf{y}^* are Grassmann variables. From this we obtain a very useful result for a sequence of two single particle propagations

$$\begin{aligned}
\langle \mathbf{z}_3 | e^{-\Delta\tau \mathbf{c}^\dagger \mathbf{h}_2 \mathbf{c}} e^{-\Delta\tau \mathbf{c}^\dagger \mathbf{h}_1 \mathbf{c}} | \mathbf{z}_1 \rangle &= \int d^2 z \langle \mathbf{z}_3 | e^{-\Delta\tau \mathbf{c}^\dagger \mathbf{h}_2 \mathbf{c}} | \mathbf{z}_2 \rangle e^{-\mathbf{z}_2^* \mathbf{z}_2} \langle \mathbf{z}_2 | e^{-\Delta\tau \mathbf{c}^\dagger \mathbf{h}_1 \mathbf{c}} | \mathbf{z}_1 \rangle \\
&= \int d^2 z e^{-\mathbf{z}_2^* \mathbf{z}_2 + \mathbf{z}_3^\dagger \mathbf{B}_2 \mathbf{z}_2 + \mathbf{z}_2^\dagger \mathbf{B}_1 \mathbf{z}_1} \\
&= e^{\mathbf{z}_3^\dagger \mathbf{B}_2 \mathbf{B}_1 \mathbf{z}_1}
\end{aligned} \tag{C.18}$$

with

$$B_i = e^{-\Delta\tau \mathbf{h}_i}. \tag{C.19}$$

Of course this generalizes to an arbitrary sequence of propagations.

C.2 Finite temperature

We want the partition function and the generating functional for a given Hubbard-Stratonovich field.

$$\begin{aligned}
Z &= \sum_i \langle i | e^{-\mathbf{c}^\dagger \mathbf{h}_m \mathbf{c}} \dots e^{-\mathbf{c}^\dagger \mathbf{h}_1 \mathbf{c}} | i \rangle \\
Z[\mathbf{x}^*, \mathbf{x}] &= \sum_i \langle i | e^{\mathbf{x}_m^* \mathbf{c}} e^{\mathbf{c}^\dagger \mathbf{x}_m} e^{-\mathbf{c}^\dagger \mathbf{h}_m \mathbf{c}} \dots e^{-\mathbf{c}^\dagger \mathbf{h}_{\tau+1} \mathbf{c}} e^{\mathbf{x}_\tau^* \mathbf{c}} e^{\mathbf{c}^\dagger \mathbf{x}_\tau} e^{-\mathbf{c}^\dagger \mathbf{h}_\tau \mathbf{c}} \dots e^{-\mathbf{c}^\dagger \mathbf{h}_1 \mathbf{c}} | i \rangle,
\end{aligned} \tag{C.20}$$

where we introduced a $\mathcal{N} = m \times L$ dimensional space-time vector of Grassmann variables $\mathbf{x} = x_{i,\tau}$ and \mathbf{x}_τ is the vector of spatial coordinates at a given time τ . As usual a logarithmic derivative of the generating functional yields the Green's function in $\mathcal{N} \times \mathcal{N}$ matrix form

$$\left. \frac{\partial^2 \ln Z[\mathbf{x}^*, \mathbf{x}]}{\partial \mathbf{x} \partial \mathbf{x}^*} \right|_{\mathbf{x}^* = \mathbf{x} = 0} = G((i^*, \tau^*), (i, \tau)) = \frac{\langle \mathcal{T} c_{i^*, \tau^*}^\dagger c_{i, \tau} \rangle}{Z}. \tag{C.21}$$

Time ordering is natural in the path integral approach because it only says that creation and annihilation operators are embedded in a strictly directed time evolution. The

fermionic sign associated with the symbol \mathcal{T} may be traced back to the anticommutation relation of the Grassmann derivatives

$$\frac{\partial^2}{\partial y \partial x^*} = -\frac{\partial^2}{\partial x^* \partial y}. \quad (\text{C.22})$$

We emphasize that an equal time derivative $\tau = \tau'$ results in

$$\left. \frac{\partial^2 \ln Z[\mathbf{x}^*, \mathbf{x}]}{\partial \mathbf{x} \partial \mathbf{x}^*} \right|_{\mathbf{x}^* = \mathbf{x} = 0} = \frac{\langle c_{i^*, \tau^*}^\dagger c_{i, \tau} \rangle}{Z} \quad (\text{C.23})$$

and there is no freedom to choose the other operator ordering because in (C.20) we can not revert the order of $e^{\mathbf{z}_\tau^* \mathbf{c}} e^{\mathbf{c}^\dagger \mathbf{z}_\tau}$ when we plan to insert $m + 1$ coherent state identities in the following way:

$$\begin{aligned} Z[\mathbf{x}^*, \mathbf{x}] &= \int d^2 z \int d^2 z_0 e^{-\mathbf{z}_0^* \mathbf{z}_0} \langle \mathbf{z}_0 | e^{\mathbf{x}_m^* \mathbf{c}} | \mathbf{z}_m \rangle e^{-\mathbf{z}_m^* \mathbf{z}_m} \times \\ &\quad \times \langle \mathbf{z}_m | e^{\mathbf{c}^\dagger \mathbf{x}_m} e^{-\mathbf{c}^\dagger \mathbf{h}_m \mathbf{c}} \dots e^{-\mathbf{c}^\dagger \mathbf{h}_{\tau+1} \mathbf{c}} e^{\mathbf{x}_\tau^* \mathbf{c}} | \mathbf{z}_\tau \rangle e^{-\mathbf{z}_\tau^* \mathbf{z}_\tau} \langle \mathbf{z}_\tau | e^{\mathbf{c}^\dagger \mathbf{x}_\tau} e^{-\mathbf{c}^\dagger \mathbf{h}_\tau \mathbf{c}} \dots e^{-\mathbf{c}^\dagger \mathbf{h}_1 \mathbf{c}} | -\mathbf{z}_0 \rangle. \end{aligned} \quad (\text{C.24})$$

It was useful to insert an additional basis for the trace operation. After integrating out \mathbf{z}_0 we do not have to keep track of the minus sign in $|-\mathbf{z}_0\rangle$ and find a \mathcal{N} fold Gaussian Grassmann integral that defines the Green's function

$$\begin{aligned} Z[\mathbf{x}^*, \mathbf{x}] &= \int d^2 z e^{-\mathbf{z}^* \mathbf{G}^{-1} \mathbf{z} + \mathbf{x}^* \mathbf{z} + \mathbf{z}^* \mathbf{x}} \\ &= \det \mathbf{G}^{-1} e^{\mathbf{x}^* \mathbf{G} \mathbf{x}}. \end{aligned} \quad (\text{C.25})$$

The matrix G^{-1} is a $\mathcal{N} \times \mathcal{N}$ space-time matrix where for the moment we show only the time indices explicitly

$$\mathbf{G}^{-1} = \begin{pmatrix} I & 0 & 0 & \dots & \mathbf{B}_1 \\ -\mathbf{B}_2 & I & 0 & \dots & 0 \\ 0 & -\mathbf{B}_3 & I & 0 & \vdots \\ \vdots & \ddots & & \ddots & 0 \\ 0 & \dots & 0 & -\mathbf{B}_m & I \end{pmatrix}. \quad (\text{C.26})$$

The inverse is most easily stated in the general form

$$\begin{aligned} \tau^* \geq \tau : \quad \mathbf{G}_{\tau^*, \tau} &= \langle U(\beta, \tau^*) c_{\tau^*} U(\tau^*, \tau) c_\tau^\dagger U(\tau, 0) \rangle / Z \\ &= (\mathbf{B}^{-1}(\tau^*, \tau) + \mathbf{B}(\tau, 0) \mathbf{B}(\beta, \tau^*))^{-1} \end{aligned} \quad (\text{C.27})$$

$$\begin{aligned} \tau^* < \tau : \quad \mathbf{G}_{\tau^*, \tau} &= -\langle U(\beta, \tau) c_\tau^\dagger U(\tau, \tau^*) c_{\tau^*} U(\tau^*, 0) \rangle / Z \\ &= -([\mathbf{B}(\tau^*, 0) \mathbf{B}(\beta, \tau)]^{-1} + \mathbf{B}(\tau, \tau^*))^{-1}, \end{aligned} \quad (\text{C.28})$$

which may be shown by direct multiplication $\mathbf{G}^{-1}\mathbf{G} = \mathbf{G}\mathbf{G}^{-1} = I$.

The easiest way to obtain the partition function Z , given by $Z = \det \mathbf{G}^{-1}$, is to successively integrate out coherent states using Eq. (C.18) until there is only the trace operation left

$$Z = \int d^2 z_0 e^{-z_0^*(1+\mathbf{B}_m \dots \mathbf{B}_1)z_0} = \det (1 + \mathbf{B}_m \dots \mathbf{B}_1). \quad (\text{C.29})$$

summarize

$$Z[\mathbf{x}^*, \mathbf{x}] = \det \mathbf{G}^{-1} e^{\mathbf{x}^* \mathbf{G} \mathbf{x}} \quad (\text{C.30})$$

$$\mathbf{G}_{\tau^*, \tau} = (\mathbf{B}^{-1}(\tau^*, \tau) + \mathbf{B}(\tau, \tau^*))^{-1} \times \begin{cases} +1 : \tau^* \geq \tau \\ -1 : \tau^* < \tau. \end{cases} \quad (\text{C.31})$$

C.3 Zero temperature limit

For the projector QMC version we want to restrict the trace to a single projector $|P_R\rangle \langle P_L|$ where $|P_R\rangle$ and $|P_L\rangle$ denote Slater determinants of N_e electrons used as trial wave functions as in (1.70). Thus we are interested in the partition function and Green's function

$$Z = \langle P_L | \hat{U} | P_R \rangle \quad (\text{C.32})$$

$$G = \langle P_L | \mathcal{T} \hat{U}_1 c_t \hat{U}_2 c_t^\dagger \hat{U}_3 | P_R \rangle / Z \quad (\text{C.33})$$

$$G_{t,t'} = \begin{cases} \langle P_L | \hat{U}_1 c_t \hat{U}_2 c_{t'}^\dagger \hat{U}_3 | P_R \rangle / Z & t \geq t' \\ -\langle P_L | \hat{U}_1 c_{t'}^\dagger \hat{U}_2 c_t \hat{U}_3 | P_R \rangle / Z & t < t' \end{cases}. \quad (\text{C.34})$$

Unfortunately coherent states are not well suited to describe states with a fixed particle number. To introduce Slater determinants of a fixed number of fermions into the coherent state formalism, we need to represent them in an exponential form and find a suitable limiting process that projects on the desired N -particle subspace. To this end let us introduce some notation. Formally we will need to enlarge the projectors (rectangular matrices) $\mathbf{P}_L, \mathbf{P}_R$ to matrices $\mathbf{U}_L, \mathbf{U}_R$ with nonzero determinants

$$\mathbf{U}_L^\dagger = \begin{pmatrix} \mathbf{P}_L^\dagger \\ \mathbf{Q}_L^\dagger \end{pmatrix}, \quad \mathbf{U}_R = (\mathbf{P}_R, \mathbf{Q}_R). \quad (\text{C.35})$$

Without loss of generality we assume from now on that \mathbf{U}_L and \mathbf{U}_R have been chosen as unitary matrices. Next we need the exponential operator which represents the projector

$|R\rangle \langle L|$

$$|R\rangle \langle L| = \lim_{E \rightarrow \infty} e^{-NeE} \exp [i\mathbf{c}^\dagger \mathbf{X} \mathbf{c}] \exp \left[-\mathbf{c}^\dagger \mathbf{U}_L \mathbf{h} \mathbf{U}_L^\dagger \mathbf{c} \right] \quad (\text{C.36})$$

$$e^{i\mathbf{X}} \mathbf{U}_L = \mathbf{U}_R \implies e^{i\mathbf{X}} \mathbf{P}_L = \mathbf{P}_R \quad (\text{C.37})$$

$$\mathbf{h} = \begin{pmatrix} -E & 0 \\ 0 & E \end{pmatrix}. \quad (\text{C.38})$$

The idea behind this is to define a Hamiltonian with ground state $|L\rangle$ and a gap E to the first excited state. Finally we rotate $|L\rangle \rightarrow |R\rangle$ with the use of a unitary operator in exponential form $\exp [i\mathbf{c}^\dagger \mathbf{X} \mathbf{c}]$ where \mathbf{X} exists and is uniquely defined through $e^{i\mathbf{X}} \mathbf{U}_L = \mathbf{U}_R$.

Observe that by series expansion we may obtain

$$\exp \left[-\mathbf{U}_L \mathbf{h} \mathbf{U}_L^\dagger \right] = \mathbf{U}_L e^{-\mathbf{h}} \mathbf{U}_L^\dagger. \quad (\text{C.39})$$

We may use these results to compute again the partition function $Z = \langle L | \hat{U} | R \rangle$ to illustrate that the above limiting process indeed gives the correct result

$$\begin{aligned} Z &= \text{Tr} |R\rangle \langle L| \hat{U} = \lim_{E \rightarrow \infty} e^{-NeE} \text{Tr} \exp [i\bar{\mathbf{c}}^\dagger \mathbf{X} \bar{\mathbf{c}}] \exp \left[-\bar{\mathbf{c}}^\dagger \mathbf{U}_L \mathbf{h} \mathbf{U}_L^\dagger \bar{\mathbf{c}} \right] \hat{U} \\ &= \lim_{E \rightarrow \infty} e^{-NeE} \det \left[\mathbf{1} + e^{i\mathbf{X}} \mathbf{U}_L e^{-\mathbf{h}} \mathbf{U}_L^\dagger \mathbf{B} \right] \\ &= \lim_{E \rightarrow \infty} e^{-NeE} \det \left[\mathbf{1} + \mathbf{U}_R e^{-\mathbf{h}} \mathbf{U}_L^\dagger \mathbf{B} \right] \\ &= \lim_{E \rightarrow \infty} \det \left[\begin{pmatrix} e^{-E} & 0 \\ 0 & 1 \end{pmatrix} + \begin{pmatrix} \mathbf{1} & 0 \\ 0 & e^{-E} \end{pmatrix} \mathbf{U}_L^\dagger \mathbf{B} \mathbf{U}_R \right] \\ &= \lim_{E \rightarrow \infty} \det \left[\begin{pmatrix} \mathbf{P}_L^\dagger \mathbf{B} \mathbf{P}_R + e^{-E} \mathbf{1} & \mathbf{P}_L^\dagger \mathbf{B} \mathbf{Q}_R \\ e^{-E} \mathbf{Q}_L^\dagger \mathbf{B} \mathbf{P}_R & e^{-E} \mathbf{Q}_L^\dagger \mathbf{B} \mathbf{Q}_R + 1 \end{pmatrix} \right] \\ &= \det \left[\begin{pmatrix} \mathbf{P}_L^\dagger \mathbf{B} \mathbf{P}_R & \mathbf{P}_L^\dagger \mathbf{B} \mathbf{Q}_R \\ 0 & 1 \end{pmatrix} \right] = \det \left(\mathbf{P}_L^\dagger \mathbf{B} \mathbf{P}_R \right). \end{aligned} \quad (\text{C.40})$$

C.4 Generating functional at zero temperature

Next we use the same procedure for the generating functional

$$\begin{aligned} Z(\mathbf{x}^*, \mathbf{x}) &= \lim_{E \rightarrow \infty} e^{-NE} \text{Tr} \exp [i\mathbf{c}^\dagger \mathbf{X} \mathbf{c}] \exp \left[-\mathbf{c}^\dagger \mathbf{U}_L \mathbf{h} \mathbf{U}_L^\dagger \mathbf{c} \right] \hat{U} \times \lim_{\beta \rightarrow \infty} \exp [\mathbf{x}^* \mathbf{G} \mathbf{x}] \\ &= \det \left(\mathbf{P}_L^\dagger \mathbf{B} \mathbf{P}_R \right) \lim_{E \rightarrow \infty} \exp [\mathbf{x}^* \mathbf{G} \mathbf{x}] \end{aligned} \quad (\text{C.41})$$

and the Green's function is given by the limit

$$\mathbf{G}_{\tau^*,\tau}^0 = \lim_{E \rightarrow \infty} \mathbf{G}_{\tau^*,\tau} = \lim_{E \rightarrow \infty} \pm (\mathbf{B}^{-1}(\tau^*, \tau) + \mathbf{B}(\tau, \tau^*))^{-1} \quad (\text{C.42})$$

where we note that the limit

$$\lim_{E \rightarrow \infty} (\mathbf{B}^{-1}(\tau^*, \tau) + \mathbf{B}(\tau, \tau^*)) \quad (\text{C.43})$$

is not defined. The zero temperature limit is now calculated for $\tau^* \geq \tau$. Results for time displaced Green's functions are found in the same way. First we rearrange the finite temperature result to a suitable form

$$\begin{aligned} \mathbf{G}_{\tau^*,\tau} &= \left(\mathbf{B}^{-1}(\tau^*, \tau) + \mathbf{B}(\tau, 0) \mathbf{U}_R e^{-\mathbf{h}} \mathbf{U}_L^\dagger \mathbf{B}(\beta, \tau^*) \right)^{-1} \\ &= \mathbf{B}(\tau^*, \tau) - \mathbf{B}(\tau^*, 0) \mathbf{U}_R \left(e^{\mathbf{h}} \mathbf{1} + \mathbf{U}_L^\dagger \mathbf{B}(\beta, 0) \mathbf{U}_R \right)^{-1} \mathbf{U}_L^\dagger \mathbf{B}(\beta, \tau). \end{aligned} \quad (\text{C.44})$$

Using the limiting formula

$$\lim_{x \rightarrow \infty} \left[\begin{pmatrix} x^{-1} \mathbf{1} & 0 \\ 0 & x \mathbf{1} \end{pmatrix} + \begin{pmatrix} a & b \\ c & d \end{pmatrix} \right]^{-1} = \begin{pmatrix} a^{-1} & 0 \\ 0 & 0 \end{pmatrix}. \quad (\text{C.45})$$

we calculate the limit

$$\lim_{E \rightarrow \infty} \left(e^{\mathbf{h}} \mathbf{1} + \mathbf{U}_L^\dagger \mathbf{B} \mathbf{U}_R \right)^{-1} = \begin{pmatrix} \left(\mathbf{P}_L^\dagger \mathbf{B} \mathbf{P}_R \right)^{-1} & 0 \\ 0 & 0 \end{pmatrix} \quad (\text{C.46})$$

in this way giving the final result

$$\mathbf{G}_{\tau^*,\tau} = \mathbf{B}(\tau^*, \tau) - \mathbf{B}(\tau^*, 0) \mathbf{P}_R \frac{1}{\mathbf{P}_L^\dagger \mathbf{B}(\beta, 0) \mathbf{P}_R} \mathbf{P}_L^\dagger \mathbf{B}(\beta, \tau). \quad (\text{C.47})$$

Green's functions for $\tau^* < \tau$ may be computed in a similar way

$$\mathbf{G}_{\tau^*,\tau} = -\mathbf{B}(\tau^*, 0) \mathbf{P}_R \frac{1}{\mathbf{P}_L^\dagger \mathbf{B}(\beta, 0) \mathbf{P}_R} \mathbf{P}_L^\dagger \mathbf{B}(\beta, \tau). \quad (\text{C.48})$$

C.5 Wick theorem

Within the coherent state formalism the proof of Wick's theorem is very elegant (see for instance Negele, Orland [80]).

Obviously all multi-point Green's functions are derivatives of the generating functional $Z[x^*, x]$. Evaluating these derivatives must yield the familiar Wick theorem. We illustrate this with two examples. First the Green's function $\mathbf{G}_{\tau_2^*, \tau_1}$ itself is

$$\frac{\partial^2}{\partial x_1 \partial x_2^*} \frac{Z[x^*, x]}{Z} \Big|_{x_1=x_2^*=0} = \frac{\partial^2}{\partial x_1 \partial x_2^*} e^{x^* G x} \Big|_{x_1=x_2^*=0} = \mathbf{G}_{\tau_2^*, \tau_1}. \quad (\text{C.49})$$

Second the four point function is

$$\langle \mathcal{T} c^\dagger(4) c(3) c^\dagger(2) c(1) \rangle = \frac{\partial^4}{\partial x_1 \partial x_2^* \partial x_3 \partial x_4^*} \frac{Z[x^*, x]}{Z} \quad (\text{C.50})$$

$$= \frac{\partial^3}{\partial x_1 \partial x_2^* \partial x_3} G_{x_4^*, i} x_i e^{x^* G x} \quad (\text{C.51})$$

$$= \frac{\partial^2}{\partial x_1 \partial x_2^*} (G_{x_4^*, x_3} - G_{x_4^*, i} x_i x_j^* G_{j, x_3}) e^{x^* G x} \quad (\text{C.52})$$

$$= G_{x_4^*, x_3} G_{x_2^*, x_1} - G_{x_4^*, x_1} G_{x_2^*, x_3}. \quad (\text{C.53})$$

The sum over all contractions is generated by the simple chain rule. The fermionic sign follows from the commutation of Grassmann variables.

Appendix D

Thermodynamics

D.1 Introduction

In this thesis we consider several “quantum phase transitions”. These transitions are controlled by some intensive thermodynamic parameter other than the temperature which is fixed to $T = 0$. An example for such a parameter is the Hubbard U with double occupancy D as the conjugate extensive variable as in Eq. (3.1). We thus want to consider the function $F(T, V, N, U)$

$$F(T, V, N, U) = -kT \ln \text{Tr} e^{-\beta(H_0 + UD)} \quad (\text{D.1})$$

with a double occupancy $D = \sum_i n_{i,\uparrow} n_{i,\downarrow}$ as a free energy potential. Such an interpretation of U and D transfers the interaction energy $H_I = UD$ from the internal energy to a work energy against the ‘external’ field U . Hence $F(T, V, N, U)$ must be a Legendre transform of the first free energy $\tilde{F}(T, V, N, D)$

$$F = \tilde{F} + UD, \quad (\text{D.2})$$

and it should be possible to construct an ensemble with fixed double occupancy to directly compute \tilde{F} . But how do we know that $F(T, V, N, U)$ really behaves like a thermodynamic potential? In particular does it obey the second law?

In the *phenomenological* theory of thermodynamics there are many equivalent ways [97] to phrase the second law: i) the entropy $S(\vec{X})$ (X_i are the extensive variables $E, V, N \dots$) can only grow in any thermodynamic process. In particular the entropy

grows when two subsystems are joined $\vec{X}_1 + \vec{X}_2 \rightarrow \vec{X}$

$$S(\vec{X}) \geq S(\vec{X}_1) + S(\vec{X}_2). \quad (\text{D.3})$$

ii) the function $S(\vec{X})$ is convex up in all the X_i variables

$$S(t\vec{X}_1 + (1-t)\vec{X}_2) \geq tS(\vec{X}_1) + (1-t)S(\vec{X}_2). \quad (\text{D.4})$$

iii) the entropy obeys a maximum principle when a constraint is removed that had split the system in subsystems \vec{X}_1, \vec{X}_2

$$S(\vec{X}) = \sup_{\vec{X}=\vec{X}_1+\vec{X}_2} \left\{ S(\vec{X}_1) + S(\vec{X}_2) \right\}. \quad (\text{D.5})$$

In *classical* statistical mechanics it is possible to proof convexity of $F(T, V, N, H)$ in intensive parameters using only the Hölder inequality (see Goldenfeld [37]p.39). In this proof $\partial^2 F / \partial H^2$ need not be calculated!

The more conventional approach is to proof Gibbs' inequality

$$\sum_i P_i \ln P_i \geq \sum_i P_i \ln P'_i \quad (\text{D.6})$$

for arbitrary probability distributions P and P' .

What does all this imply for our candidate thermodynamic potential $F(T, V, N, U)$? It turns out that it is sufficient to proof that the free energy in Eq. (D.1) is convex down in U . We will show this for finite β, N only. But the limit of convex functions is again convex so $F(T \rightarrow 0, V, N \rightarrow \infty, U)$ must also be convex.

Our aim here is to give a *direct* proof for the following statement: Let H_0 and H_1 be hermitian matrices. The free energy

$$F(\alpha) = -kT \ln \text{Tr} e^{-\frac{1}{kT}(H_0 + \alpha H_1)} \quad (\text{D.7})$$

is then a convex down function for all $T \geq 0$.

D.2 Convexity of a General Free Energy

The free energy $F(\alpha)$ (D.7) is analytic in α and the convex property may be tested by taking a second derivative

$$\frac{\partial^2}{\partial \alpha^2} \ln \text{Tr} e^{-\beta(H_0 + \alpha H_1)} \geq 0. \quad (\text{D.8})$$

Singularities which indicate phase transitions show up only in the zero temperature or in the thermodynamic limit.

In order to proof inequality (D.8) we establish two corollaries. First we introduce a special version of the Cauchy-Schwarz inequality: Let us define a suitable scalar product for matrices A, B using the statistical operator as a measure

$$(A, B) = \frac{\text{Tr } \rho A^* B}{Z} = \frac{\text{Tr } e^{-\beta H_0} A^* B}{\text{Tr } e^{-\beta H_0}}. \quad (\text{D.9})$$

We use the Cauchy-Schwarz inequality with $A = 1$ and $B = H_1$

$$\left(\frac{\text{Tr } \rho H_1}{Z} \right)^2 \leq \frac{\text{Tr } \rho H_1^* H_1}{Z}, \quad (\text{D.10})$$

in other terms the variance of H_1 is always positive. Then we generalize the inequality to the desired form

$$\left(\frac{\text{Tr } \rho H_1}{Z} \right)^2 \leq \frac{\text{Tr } e^{-(\beta-\Delta)H_0} H_1^* e^{-\Delta H_0} H_1}{Z} \quad (\text{D.11})$$

which is obtained from Eq. (D.10) through redefinition $H_1 \rightarrow e^{-\frac{\Delta}{2}H_0} H_1 e^{\frac{\Delta}{2}H_0}$ and making use of the cyclical property of the trace. Second we will need to take derivatives of the type

$$\frac{\partial}{\partial \alpha} e^{-\beta(H_0 + \alpha H_1)}. \quad (\text{D.12})$$

The noncommutativity of H_0 and H_1 is resolved by the usual Trotter decomposition

$$\begin{aligned} \frac{\partial}{\partial \alpha} e^{-\beta(H_0 + \alpha H_1)} &= \frac{\partial}{\partial \alpha} \prod_1^m e^{-\frac{\beta}{m} H_0} e^{-\frac{\beta \alpha}{m} H_1} \\ &= \sum_{i=1}^m \prod_{k=1}^m \left(e^{-\frac{\beta}{m} H_0} e^{-\frac{\beta \alpha}{m} H_1} \right) \left[1 + \delta_{i,k} \frac{\beta}{m} (H_1 - 1) \right]. \end{aligned} \quad (\text{D.13})$$

The continuous version reads

$$\frac{\partial}{\partial \alpha} e^{-\beta(H_0 + \alpha H_1)} = - \int_0^\beta e^{-(\beta-t)(H_0 + \alpha H_1)} H_1 e^{-t(H_0 + \alpha H_1)} dt \quad (\text{D.14})$$

and is related to the Kubo identity.

Now we have the prerequisites to demonstrate the positivity of the second derivative

$$\frac{\partial^2}{\partial \alpha^2} \ln Z(\alpha) \Big|_{\alpha=0} = \frac{Z''}{Z} - \left(\frac{Z'}{Z} \right)^2, \quad (\text{D.15})$$

where the restriction to $\alpha = 0$ is possible without loss of generality. Performing cyclical shifts under the trace the derivative $Z'(\alpha)$ simplifies to

$$Z'(\alpha) = -\beta \text{Tr} e^{-\beta(H_0 + \alpha H_1)} H_1. \quad (\text{D.16})$$

Yet the second derivative takes the form of a time displaced correlation function

$$Z''(0) = \beta \int_0^\beta dt \text{Tr} e^{-(\beta-t)H_0} H_1 e^{-tH_0} H_1. \quad (\text{D.17})$$

Finally we use inequality (D.11) to proof the positivity

$$0 \leq \frac{\partial^2}{\partial \alpha^2} \ln Z(\alpha) \Big|_{\alpha=0} = \beta \int_0^\beta dt \left[\frac{\text{Tr} e^{-(\beta-t)H_0} H_1 e^{-tH_0} H_1}{Z} - \left(\frac{\text{Tr} e^{-\beta H_0} H_1}{Z} \right)^2 \right]. \quad (\text{D.18})$$

At finite temperature a phase transition is only possible in the thermodynamic limit where the system size $L \rightarrow \infty$. The free energy is thus the limit of convex functions

$$F_\infty(\alpha) = \lim_{L \rightarrow \infty} F_L(\alpha) \quad (\text{D.19})$$

and therefore also convex.

D.3 Comments

Remark 1. In order to see that $F(T, V, N, D)$ is convex down as a function of temperature we look at the second derivate

$$\frac{\partial^2 F(T)}{\partial T^2} = -\frac{1}{T^3} [\langle H^2 \rangle - \langle H \rangle^2] \leq 0. \quad (\text{D.20})$$

In this way we proof the full convexity of the grand partition function $\Omega(T, V, N) = -PV = V\Omega(T, 1, \mu)$ since we know it already for $\Omega(T, 1, \mu)$.

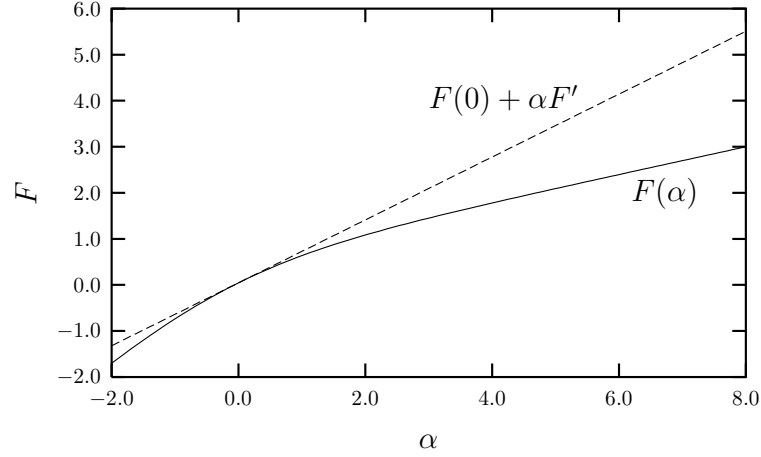
Remark 2. Let us insert our results into an expansion of $F(\alpha)$

$$F(\alpha) = F(0) + \alpha F'(0) + \frac{\alpha^2}{2} F''(0) + O(\alpha^3) \quad (\text{D.21})$$

$$F(\alpha) \leq F(0) + \alpha \langle H_1 \rangle_{H_0} \quad (\text{D.22})$$

$$\langle A \rangle_{H_0} \equiv \frac{\text{Tr} e^{-\beta H_0} A}{\text{Tr} e^{-\beta H_0}}. \quad (\text{D.23})$$

The inequality holds for all α which is illustrated in Fig. 2.



A convex down function like $F(\alpha)$ is always smaller than the tangent function

$$F(0) + \alpha F'.$$

Another proof of inequality (D.22) is given by Feynman. [30]

Remark 3. Inequality (D.22) is equivalent to Gibbs' inequality

$$\text{Tr } \rho(0) \ln \rho(0) \geq \text{Tr } \rho(0) \ln \rho(\alpha), \quad (\text{D.24})$$

where $\rho(0)$ and $\rho(\alpha)$ are arbitrary density matrices. For convenience we represent $\rho(\alpha)$ in the form

$$\rho(\alpha) = \frac{e^{-\beta(H_0 + \alpha H_1)}}{\text{Tr } e^{-\beta(H_0 + \alpha H_1)}}. \quad (\text{D.25})$$

We find

$$kT \text{Tr } \rho(0) \ln \rho(0) = F(0) - \langle H_0 \rangle_{H_0} \quad (\text{D.26})$$

$$kT \text{Tr } \rho(0) \ln \rho(\alpha) = F(\alpha) - \langle H_0 \rangle_{H_0} - \alpha \langle H_1 \rangle_{H_0} \quad (\text{D.27})$$

which establishes the equivalence of the two inequalities (D.22) and (D.24).

Remark 4. Convexity is equivalent to another important statement about the energy functional F

$$F[\rho] \equiv \text{Tr } \rho \left(H + \frac{1}{\beta} \ln \rho \right) \quad (\text{D.28})$$

which assigns a free energy to a system H which is in state ρ . Then a variational principle states that $F[\rho]$ is minimized by $\rho^* = \exp(-\beta H) / \text{Tr } \exp(-\beta H)$ or

$$F[\rho^*] \leq F[\rho] \quad : \quad \forall \rho \quad (\text{D.29})$$

This is the finite temperature version for the ground state variational principle

$$\frac{\langle \Psi | H | \Psi \rangle}{\langle \Psi | \Psi \rangle} \geq E_0. \quad (\text{D.30})$$

Among many other applications this variational principle is the starting point for finite temperature density functional theory. [74] In order to proof Eq. (D.29) we introduce the system Hamiltonian H , the suggested minimum ρ^* and an arbitrary ρ represented by H_0

$$\rho = \frac{e^{-\beta H_0}}{\text{Tr } e^{-\beta H_0}}, \quad (\text{D.31})$$

$$H_1 \equiv H - H_0. \quad (\text{D.32})$$

We insert

$$F[\rho^*] = -kT \ln \text{Tr } e^{-\beta H}, \quad (\text{D.33})$$

$$F[\rho] = \langle H_1 \rangle_{H_0} - kT \ln \text{Tr } e^{-\beta H_0} \quad (\text{D.34})$$

into

$$F[\rho^*] \leq F[\rho] \quad (\text{D.35})$$

$$-kT \ln \text{Tr } e^{-\beta(H_0+H_1)} \leq -kT \ln \text{Tr } e^{-\beta H_0} + \langle H_1 \rangle_{H_0} \quad (\text{D.36})$$

and the equivalence to Eq. (D.22) is obvious.

Remark 5. The inequality (D.11) is an interesting result by itself because it demonstrates the positivity of correlation functions of the type

$$0 \leq \left| \left(\frac{\text{Tr } \rho A}{Z} \right) \right|^2 \leq \frac{\text{Tr } e^{-(\beta-\Delta)H_0} A^* e^{-\Delta H_0} A}{Z}. \quad (\text{D.37})$$

Remark 6. We are able to demonstrate that the partition function is convex. Bessis, Moussa and Villani (BMV) [12] conjecture that *all* derivatives $Z^{[n]}(\alpha)$ are again convex. More precisely they propose the following

$$Z(\alpha) = \text{Tr } \exp[-\beta(H_0 + \alpha H_1)] = \int \exp(-\alpha \tau) d\mu(\tau), \quad (\text{D.38})$$

where $d\mu(\tau)$ is a *positive measure* with a support between the inf and the sup of the spectrum $\sigma(H_1)$. For $\inf \{\sigma(H_1)\} \geq 0$ this is equivalent to the convex property for all derivatives

$$Z^{[n]}(\alpha) (-1)^n \geq 0. \quad (\text{D.39})$$

The conjecture is automatically true for all those problems which can be attacked with a worldline QMC algorithm with positive weight. From the positive QMC weight the positive measure in the conjecture (D.38) is constructed. For the auxiliary field QMC such a construction of positive $d\mu(\tau)$ is not possible even when the QMC weight is positive everywhere. Equivalent formulations to the BMV conjecture are given by Lieb. [63]

Remark 7. Thermodynamic potentials for finite systems at finite temperatures are always analytic functions. Phase transitions i.e non-analytic behaviour may only happen at zero temperature or in the thermodynamic limit.

In the introduction we considered nonanalytic behaviour in the zero temperature function $F(T=0, N, V, U)$. We asked whether F is a meaningful thermodynamic potential and conclude that a free energy like $F(0, N, V, U)$ fits naturally into the framework of thermodynamics because it will always be a convex function. The buildup of singular behaviour at zero temperature also happens in much the same way as in the finite temperature situation. The *only* novel point about zero temperature transitions is the possibility that an additional correlation length (i.e correlations in time) diverges. The term *quantum phase transition* is usually reserved for this situation. [88]

Appendix E

Spin-Wave Theory

When approaching the $SU(2)$ symmetric Heisenberg point from either the SC or the CDW phase we find critical behaviour in the “transverse” correlation functions. It is interesting to compare our results for the complex fermionic Hamiltonian 3.1 with a spin wave calculation for the bosonic limit $U \rightarrow -\infty$. Let us first write down the purely bosonic Hamiltonian

$$H = \sum_{\langle i,j \rangle} J_x \frac{\eta_i^\dagger \eta_j + \eta_i \eta_j^\dagger}{2} + J_z \eta_i^z \eta_j^z, \quad (\text{E.1})$$

with $J_x = 4t_p$ and $J_z = 4(t_p - 2V)$. In linear spin-wave theory (LSWT) we need to distinguish “easy axis” CDW with $J_z > J_x$ and “easy plane” SC with $J_z < J_x$.

E.1 Easy axis

We introduce linear spin-wave theory for the CDW phase [17, 105] via

$$\eta_{A,\mathbf{k}}^+ = \left(u_{\mathbf{k}} \alpha_{\mathbf{k}} - v_{\mathbf{k}} \beta_{\mathbf{k}}^\dagger \right), \quad (\text{E.2})$$

$$\eta_{B,\mathbf{k}}^+ = \left(u_{\mathbf{k}} \beta_{\mathbf{k}}^\dagger - v_{\mathbf{k}} \alpha_{\mathbf{k}} \right) \quad (\text{E.3})$$

where A, B are sublattice labels and $\alpha_{\mathbf{k}}$ and $\beta_{\mathbf{k}}$ are the Bogoliubov transforms of the original bosons. The Bogoliubov factors are

$$u_{\mathbf{k}} = \sqrt{\frac{J_z + \varepsilon_{\mathbf{k}}}{2\varepsilon_{\mathbf{k}}}}, \quad (\text{E.4})$$

$$v_{\mathbf{k}} = \sqrt{\frac{J_z - \varepsilon_{\mathbf{k}}}{2\varepsilon_{\mathbf{k}}}} \quad (\text{E.5})$$

where we introduced the dispersion $\varepsilon_{\mathbf{k}}$

$$\varepsilon_{\mathbf{k}} = \sqrt{J_z^2 - J_x^2 \gamma_{\mathbf{k}}^2} \quad (\text{E.6})$$

with $\gamma_{\mathbf{k}} = -1/2(\cos k_x + \cos k_y)$.

In the CDW phase the η correlation function became critical, therefore we need

$$\langle \eta_{\mathbf{k}}^\dagger \eta_{\mathbf{k}} \rangle (\mathbf{Q}, \omega) = \langle (\eta_{A,\mathbf{k}}^\dagger + \eta_{B,\mathbf{k}}^\dagger) (\eta_{A,\mathbf{k}} + \eta_{B,\mathbf{k}}) \rangle (\mathbf{Q}, \omega) \quad (\text{E.7})$$

$$= (u_{\mathbf{k}} - v_{\mathbf{k}})^2 \langle \alpha_{\mathbf{k}} \alpha_{\mathbf{k}}^\dagger + \beta_{\mathbf{k}}^\dagger \beta_{\mathbf{k}} \rangle (\mathbf{Q}, \omega) \quad (\text{E.8})$$

$$= \sqrt{\frac{J_z + J_x}{J_z - J_x}} 2\delta(\omega), \quad (\text{E.9})$$

where we dropped terms $\langle \alpha_{\mathbf{k}}^\dagger \alpha_{\mathbf{k}}^\dagger \rangle$ and used $\gamma_{\mathbf{Q}} = -1$ and $\varepsilon_{\mathbf{Q}} = 0$. For the equal time correlations (in CDW $V < 0$)

$$\langle \Delta_{\mathbf{k}}^\dagger \Delta_{\mathbf{k}} \rangle (0) = \int_0^\infty \langle \eta_{\mathbf{k}}^\dagger \eta_{\mathbf{k}} \rangle (\mathbf{Q}, \omega) d\omega = 2\sqrt{\frac{t_p + (-V)}{(-V)}} \sim \sqrt{\frac{t_p}{|V|}} \quad (\text{E.10})$$

we obtain a square root divergence as we approach the phase transition. The integrated correlation function is equal to the uniform susceptibility

$$\text{Re } \chi_{\Delta^\dagger \Delta}^{+-} (0, \omega = 0) = \int_0^\infty \langle \Delta_{\mathbf{k}}^\dagger(\tau) \Delta_{\mathbf{k}} \rangle d\tau \propto \Delta^{-1} \langle \Delta_{\mathbf{k}}^\dagger \Delta_{\mathbf{k}} \rangle (0) \quad (\text{E.11})$$

and picks up the inverse gap $\Delta_{\mathbf{k}}^{-1}$ of the $\langle \eta_{\mathbf{k}}^+ \eta_{\mathbf{k}}^- \rangle$ transverse mode. The gap of the LSW dispersion $\varepsilon_{\mathbf{k}}$ at $\mathbf{k} = 0$ is

$$\Delta = \sqrt{(4t_p - 8V)^2 - 16t_p^2} \sim 8\sqrt{|V|t_p}. \quad (\text{E.12})$$

Thus the transverse susceptibility (E.11) diverges as

$$\text{Re } \chi^{+-} (0, \omega = 0) \propto \frac{1}{V}. \quad (\text{E.13})$$

E.2 Easy Plane

The analogous spin wave calculation [105] for the SC phase ($J_z < J_x$) gives a dispersion with two branches, $\varepsilon_{\mathbf{k}}^+$ for the in-plane fluctuations $\langle \eta_{\mathbf{k}}^\dagger \eta_{\mathbf{k}} \rangle$ and $\varepsilon_{\mathbf{k}}^-$ for the out-of-plane fluctuations $\langle \eta_{\mathbf{k}}^z \eta_{-\mathbf{k}}^z \rangle$

$$\varepsilon_{\mathbf{k}}^\pm = \sqrt{(J_x \pm J_x \gamma_{\mathbf{k}})(J_x \mp J_z \gamma_{\mathbf{k}})}. \quad (\text{E.14})$$

Now the out-of-plane fluctuations close their gap at $\mathbf{k} = \mathbf{Q}$ and diverge as we approach the transition.

For the spin-wave calculation we choose LRO into y -direction. For convenience we rotate the system such that ordered state lies again in z -direction and the new coupling j_α are

$$J_x \rightarrow j_z \quad (\text{E.15})$$

$$J_y \rightarrow j_x \quad (\text{E.16})$$

$$J_z \rightarrow j_y \quad (\text{E.17})$$

and the easy plane condition is $j_z = j_x > j_y$.

Notice that in the Hamiltonian \mathbf{k} now couples to $-\mathbf{k}$ and the sum is over half the Brioullin zone (BZ/2) because of sublattice A, B

$$\begin{aligned} H = \sum_{\text{BZ}/2} j_z \left(a_{\mathbf{k}}^\dagger a_{\mathbf{k}} + b_{\mathbf{k}}^\dagger b_{\mathbf{k}} + a_{-\mathbf{k}}^\dagger a_{-\mathbf{k}} + b_{-\mathbf{k}}^\dagger b_{-\mathbf{k}} \right) + \frac{\gamma_{\mathbf{k}}(j_x + j_y)}{2} (a_{\mathbf{k}} b_{\mathbf{k}} + b_{-\mathbf{k}} a_{-\mathbf{k}} + H.c.) \\ + \frac{\gamma_{\mathbf{k}}(j_x - j_y)}{2} (a_{\mathbf{k}} b_{-\mathbf{k}}^\dagger + b_{\mathbf{k}} a_{-\mathbf{k}}^\dagger + H.c.). \end{aligned} \quad (\text{E.18})$$

The easy axis calculation was easier because the last term was missing. We proceed by first diagonalizing the first and the third term with the unitary base change

$$\begin{pmatrix} a_{\mathbf{k}} \\ b_{\mathbf{k}} \\ a_{-\mathbf{k}} \\ b_{-\mathbf{k}} \end{pmatrix} =: \frac{1}{\sqrt{2}} \begin{pmatrix} A_{\mathbf{k}} - B_{-\mathbf{k}} \\ B_{\mathbf{k}} - A_{-\mathbf{k}} \\ B_{\mathbf{k}} + A_{-\mathbf{k}} \\ A_{\mathbf{k}} + B_{-\mathbf{k}} \end{pmatrix}. \quad (\text{E.19})$$

The Hamiltonian (E.18) becomes

$$\begin{aligned} H = \sum_{\text{BZ}/2} \left(j_z + \frac{\gamma_{\mathbf{k}}(j_x - j_y)}{2} \right) (A_{\mathbf{k}}^\dagger A_{\mathbf{k}} + B_{\mathbf{k}}^\dagger B_{\mathbf{k}}) \\ + \left(j_z - \frac{\gamma_{\mathbf{k}}(j_x - j_y)}{2} \right) (A_{-\mathbf{k}}^\dagger A_{-\mathbf{k}} + B_{-\mathbf{k}}^\dagger B_{-\mathbf{k}}) \\ + \frac{\gamma_{\mathbf{k}}(j_x + j_y)}{2} (A_{\mathbf{k}} B_{\mathbf{k}} + A_{\mathbf{k}}^\dagger B_{\mathbf{k}}^\dagger + A_{-\mathbf{k}} B_{-\mathbf{k}} + A_{-\mathbf{k}}^\dagger B_{-\mathbf{k}}^\dagger). \end{aligned} \quad (\text{E.20})$$

This also decoupled \mathbf{k} and $-\mathbf{k}$ and we can use a Bogoliubov transformations (here for \mathbf{k})

$$A_{\mathbf{k}} = \left(u_{\mathbf{k}} \alpha_{\mathbf{k}} - v_{\mathbf{k}} \beta_{\mathbf{k}}^\dagger \right), \quad (\text{E.21})$$

$$B_{\mathbf{k}} = \left(u_{\mathbf{k}} \beta_{\mathbf{k}}^\dagger - v_{\mathbf{k}} \alpha_{\mathbf{k}} \right) \quad (\text{E.22})$$

to solve for the spectrum

$$\begin{aligned}\varepsilon_{\pm\mathbf{k}} &= \sqrt{\left(j_z \pm \frac{\gamma_{\mathbf{k}}(j_z - j_y)}{2}\right)^2 - \frac{\gamma_{\mathbf{k}}^2(j_z + j_y)^2}{4}} \\ &= \sqrt{(j_z \pm j_z\gamma_{\mathbf{k}})(j_z \mp j_y\gamma_{\mathbf{k}})}.\end{aligned}\tag{E.23}$$

After rotating back to a LRO in y -direction we recover the result (E.14). In-plane and out-of-plane fluctuations do not mix. The respective spectral functions are thus again

$$A^{\pm}(\mathbf{k},\omega) = (u_{\mathbf{k}}^{\pm} - v_{\mathbf{k}}^{\pm})^2 2\delta(\omega)\tag{E.24}$$

with Bogoliubov factors

$$u_{\mathbf{k}}^{\pm} = \sqrt{\frac{J_x + \varepsilon_{\mathbf{k}}^{\pm}}{2\varepsilon_{\mathbf{k}}^{\pm}}},\tag{E.25}$$

$$v_{\mathbf{k}}^{\pm} = \sqrt{\frac{J_x - \varepsilon_{\mathbf{k}}^{\pm}}{2\varepsilon_{\mathbf{k}}^{\pm}}}.\tag{E.26}$$

For the gapped density-density mode this implies a divergence as $V \rightarrow 0$

$$\langle n_{\mathbf{Q}}n_{-\mathbf{Q}} \rangle \sim \frac{1}{\sqrt{V}}\tag{E.27}$$

and

$$\text{Re } \chi_{nn}(\mathbf{Q},0) \sim \frac{1}{V}.\tag{E.28}$$

This is the same behaviour as in the CDW phase.

Bibliography

- [1] G. Aeppli and Z. Fisk. *Comm. Cond. Mat. Phys.*, 16:155, 1992. Kondo insulators. [51](#)
- [2] S. Allen and A.-M. S. Tremblay. Non-Perturbative Approach to the Attractive Hubbard Model. *Phys. Rev. B*, 64:75115, 2001. [X](#), [4](#)
- [3] P. W. Anderson. A Poor Man’s Derivation of Scaling Laws for the Kondo Problem. *J. Phys. C*, 3:2436–41, 1970. [47](#)
- [4] V. I. Anisimov, A. I. Poteryaev, M. A. Korotin, A. O. Anokhin, and G. Kotliar. First-Principles Calculations of the Electronic Structure and Spectra of Strongly Correlated Systems: Dynamical Mean-Field Theory. *J. Phys.: Condens. Matter*, 9:7359, 1997. [X](#), [4](#)
- [5] V. I. Anisimov, J. Zaanen, and O. K. Andersen. Band theory and mott insulators: Hubbard u instead of stoner i . *Phys. Rev. B*, 44:943, 1991. [X](#), [4](#)
- [6] F. Assaad. Quantum, Monte Carlo Methods on Lattices: The Determinantal Approach. In J. Grotendorst, D. Marx, and A. Muramatsu, editors, *Quantum Simulations of Complex Many-Body Systems: From Theory to Algorithms*, page 99, Jülich, 2002. NIC. [13](#), [15](#), [17](#), [24](#), [32](#), [40](#)
- [7] F. F. Assaad. Quantum Monte Carlo Simulations of the Half-Filled Two-Dimensional Kondo Lattice. *Phys. Rev. Lett.*, 83:796, 1999. [XIII](#), [7](#), [52](#), [54](#), [55](#), [56](#), [57](#), [65](#), [78](#), [98](#)
- [8] F. F. Assaad and M. Imada. Stable Quantum Monte Carlo Algorithm for $T = 0$ Calculation of Imaginary Time Green Function. *J. Phys. Soc. Jpn.*, 65(1):189–194, 1996. [IV](#), [XIII](#), [43](#), [98](#)

- [9] F. F. Assaad, M. Imada, and D. J. Scalapino. Charge and Spin Structures of a $d_{x^2-y^2}$ Superconductor in the Proximity of an Antiferromagnetic Mott Insulator. *Phys. Rev. B*, 56:15001, 1997. [23](#), [78](#)
- [10] A. Auerbach. *Interacting Electrons and Quantum Magnetism*. Springer, Berlin, 1994. [24](#), [107](#)
- [11] J. G. Bednorz and K. A. Müller. Possible High T_c Superconductivity in the Ba-La-Cu-O System. *Z. Phys. B*, 64:189, 1986. [XI](#), [5](#)
- [12] D. Bessis, P. Moussa, and M. Villani. Monotonic Converging Variational Approximations to the Functional Integrals in Quantum Statistical Mechanics. *J. Math. Phys.*, 16:2318, 1975. [122](#)
- [13] N. E. Bickers, D. J. Scalapino, and S. R. White. Conserving Approximations for Strongly Correlated Electron Systems: Bethe-Salpeter Equation and Dynamics for the Two Dimensional Hubbard Model. *Phys. Rev. Lett.*, 62:961, 1989. [X](#), [4](#)
- [14] R. Blankenbecler, D. J. Scalapino, and R. L. Sugar. Monte Carlo Calculations of Coupled Boson-Fermion Systems. *Phys. Rev. D*, 24:2278, 1981. [XIII](#), [6](#), [11](#), [33](#), [98](#)
- [15] W. Brinkman and T. M. Rice. Single-Particle Excitations in Magnetic Insulators. *Phys. Rev. B*, 2:1324, 1970. [X](#), [4](#), [54](#)
- [16] M. Brunner, F. F. Assaad, and A. Muramatsu. Single Hole Dynamics in the $t - J$ Model on a Square Lattice. *Phys. Rev. B*, 66:15480, 2000. [68](#)
- [17] C. M. Canali and M. Wallin. Spin-Spin Correlation Functions for the Square - Lattice Heisenberg Antiferromagnet at Zero Temperature. *Phys. Rev. B*, 48:3264, 1993. [125](#)
- [18] S. Capponi and F. F. Assaad. Spin and Charge Dynamics of the Ferromagnetic and Antiferromagnetic Two-Dimensional Half-Filled Kondo Lattice Model. *Phys. Rev. B*, 63:155114, 2001. [54](#), [58](#), [65](#), [79](#)
- [19] P. Coleman. New Approach to the Mixed Valence Problem. *Phys. Rev. B*, 29:3035, 1984. [X](#), [4](#)

- [20] S. Doniach. *Physica B*, 91:231, 1977. 53, 65
- [21] E. N. Economou. *Green's Functions in Quantum Physics*. Springer Series in Solid-State Sciences Vol.7. Springer, Berlin, 1983. VIII, 2
- [22] R. Eder, O. Rogojanu, and G. A. Sawatzky. Many-Body Band Structure and Fermi Surface of the Kondo Lattice. *Phys. Rev. B*, 58:7599, 1998. 60
- [23] R. Eder, O. Stoica, and G. A. Sawatzky. Single-Particle Excitations of the Kondo Lattice. *Phys. Rev. B*, 55:6109, 1997. 60
- [24] B. Efron. *The Jackknife, the Bootstrap and Other Resampling Plans*. CBMS-NSF Conference Series in Applied Mathematics, No.38 SIAM. Arrowsmith Ltd., Bristol, 1982. 13
- [25] H. G. Evertz. The Loop Algorithm. *cond-mat/9707221*. 11
- [26] H. G. Evertz, G. Lana, and M. Marcu. *Phys. Rev. Lett.*, 70:875, 1993. 11
- [27] M. Feldbacher and F. F. Assaad. Efficient Calculation of Imaginary Time Displaced Correlation Functions in the Projector Auxiliary Field Quantum Monte-Carlo Algorithm. *Phys. Rev. B*, 65:073105, 2001. 42
- [28] M. Feldbacher, C. Jurecka, F. F. Assaad, and W. Brenig. Single Hole Dynamics in the Half-Filled Two-Dimensional Kondo-Hubbard Model. *Phys. Rev. B*, 66:045103, 2002. XIII, 7, 47, 98
- [29] A. L. Fetter and J. Walecka. *Quantum Theory of Many-Particle Systems*. McGraw-Hill, New York, 1971. 30, 72
- [30] R. P. Feynman. *Statistical Mechanics: A Set of Lectures*, volume 36 of *Frontiers in Physics*. Addison-Wesley, New York, 1972. 121
- [31] A. Fortunelli and A. Painelli. Ab Initio Estimate of Hubbard Model Parameters: A Simple Procedure Applied to BEDT-TTF Salts. *Phys. Rev. B*, 55:16088, 1997. 76
- [32] H. Frahm and V. E. Korepin. Correlation Functions of the One-Dimensional Hubbard Model in a Magnetic Field. *Phys. Rev. B*, 43:5653, 1991. IX, 3

- [33] J. Franck, F. Manchester, and D. Martin. *Proc. Roy. Soc.*, A263:494, 1961. 49
- [34] R. M. Fye. New Results on Trotter-Like Approximations. *Phys. Rev. B*, 33:6271, 1986. 16
- [35] A. Georges, G. Kotliar, W. Krauth, and M. J. Rozenberg. Dynamical Mean-Field Theory of Strongly Correlated Fermion Systems and the Limit of Infinite Dimensions. *Rev. Mod. Phys.*, 68:13, 1996. X, 4
- [36] A. Girlando, M. Masino, A. Brillante, R. G. D. Valle, and E. Venuti. BEDT-TTF Organic Superconductors: The Role of Phonons. *Phys. Rev. B*, 66:100507(R), 2002. 75
- [37] N. Goldenfeld. *Lectures on Phase Transitions and the Renormalization Group*, volume 85 of *Frontiers in Physics*. Addison-Wesley, New York, 1992. 118
- [38] M. C. Gutzwiller. Correlations of Electrons in a Narrow s Band. *Phys. Rev.*, 137:A1726, 1965. X, 4
- [39] C. J. Halboth and W. Metzner. Renormalization-Group Analysis of the Two-Dimensional Hubbard Model. *Phys. Rev. B*, 61:7364, 2000. X, 4
- [40] F. Hébert, G. G. Batrouni, R. T. Scalettar, G. Schmid, M. Troyer, and A. Dorneich. Nature of the Quantum Phase Transitions in the Two Dimensional Hard-Core Boson Model. *Phys. Rev. B*, 65:014513, 2002. 92
- [41] J. Hirsch. Discrete Hubbard-Stratonovich Transformation for Fermion Lattice Models. *Phys. Rev. B*, 28:4059, 1983. 18, 21
- [42] J. E. Hirsch. Antiferromagnetic Singlet Pairs, High-Frequency Phonons, and Superconductivity. *Phys. Rev. B*, 35:8726, 1987. 78, 79
- [43] J. E. Hirsch. Stable Monte Carlo Algorithm for Fermion Lattice Systems at Low Temperatures. *Phys. Rev. B*, 38:12023, 1988. 31, 37
- [44] J. E. Hirsch and R. M. Fye. Monte Carlo Method for Magnetic Impurities in Metals. *Phys. Rev. Lett.*, 56:2521, 1986. 38

- [45] C. Hotta and H. Fukuyama. Classification of the Ground States of Two-Dimensional Quarter-Filled Organic Conductors with Strong Dimerization. *J. Phys. Soc. Jpn.*, 70:321, 2001. 77
- [46] J. Hubbard. Calculation of Partition Functions. *Phys. Rev. Lett.*, 3:77, 1959. 18
- [47] J. Hubbard. Electron Correlations in Narrow Energy Bands. *Proc. R. Soc. London, Ser. A*, 276:238, 1963. IX, 3
- [48] C. M. Hurd. Further Evidence of Nagaoka's Bound State for Conduction Electrons in Dilute Alloys. *Phys. Rev. Lett.*, 18:1127, 1967. 49
- [49] M. Imada, A. Fujimori, and Y. Tokura. Metal-Insulator Transitions. *Rev. Mod. Phys.*, 70:1039, 1998. 54
- [50] M. Jarrell and J. Gubernatis. Bayesian Inference and the Analytic Continuation of Imaginary-Time Quantum Monte Carlo Data. *Phys. Rep.*, 269:133, 1996. 7, 67
- [51] C. Jurecka and W. Brenig. Bond-Operator Mean-Field Theory of the Half-Filled Kondo Lattice Model. *Phys. Rev. B*, 64:092406, 2001. 58, 59, 62, 63
- [52] K. Kanoda, K. Miyagawa, A. Kawamoto, and Y. Nakazawa. NMR Relaxation Rate in the Superconducting State of the Organic Conductor κ -(BEDT-TTF)₂Cu(N(CN)₂)Br. *Phys. Rev. B*, 54:76, 1996. 75
- [53] K. Kini, K. Carlson, H. Wang, J. Schlueter, J. Dudek, S. Sirchio, U. Geiser, K. Lykke, and J. Williams. Determination of Mass Isotope Effect on T_c in an Electron-Donor-Based Organic Superconductor, κ -(ET)₂Cu(NCS)₂, Where ET Represents Bis(Ethylenedithio)Tetrathiafulvalene. *Physica C*, 264:81, 1996. 75
- [54] H. Kino and H. Fukuyama. Phase Diagram of Two-Dimensional Organic Conductors: κ -(ET)₂X. *J. Phys. Soc. Jpn.*, 65:2158, 1996. 76, 77
- [55] W. Kohn and J. M. Luttinger. Ground-State Energy of a Many-Fermion System. *Phys. Rev.*, 118:41, 1960. 51
- [56] W. Kohn and J. M. Luttinger. New Mechanism for Superconductivity. *Phys. Rev. Lett.*, 15:524, 1965. 2

- [57] J. Kondo. *Prog. Theor. Phys.*, 32:37, 1964. 47
- [58] C. Lacroix. Some Exact Results for the Kondo Lattice with Infinite Exchange Interaction. *Solid State Commun.*, 54:991, 1985. 72
- [59] L. D. Landau. *Sov. Phys. JETP*, 3:920, 1957. VII, 1
- [60] M. Lang and J. Müller. Organic Superconductors. *cond-mat/0302157*, 2003. XI, 5, 73
- [61] S. Lefebvre, P. Wzietek, S. Brown, C. Bourbonnais, , D. Jérôme, C. Mézière, M. Fourmigué, and P. Batail. Mott Transition, Antiferromagnetism, and Unconventional Superconductivity in Layered Organic Superconductors. *Phys. Rev. Lett.*, 85:5420, 2000. XV, 8, 73, 74, 75, 100
- [62] E. H. Lieb. Two Theorems on the Hubbard Model. *Phys. Rev. Lett.*, 62:1201, 1989. 14
- [63] E. H. Lieb and R. Seiringer. Equivalent Forms of the Bessis-Moussa-Villani Conjecture. *preprint*, math-ph:0210027, 2002. 123
- [64] E. Y. Loh and J. Gubernatis. Stable Numerical Simulations of Models of Interacting Electrons in Condensed-Matter Physics. In W. Hanke and Y. V. Kopayev, editors, *Modern Problems of Condensed Matter Physics*, volume 32, page 177. North Holland, Amsterdam, 1992. 11, 13, 24, 32, 107
- [65] H. Löhneysen. Non-Fermi-Liquid Behaviour in the Heavy-Fermion System $\text{CeCu}_{6-x}\text{Au}_x$. *J. Phys. Cond. Mat.*, 8:9689, 1996. 53
- [66] J. M. Luttinger. Fermi Surface and some Simple Equilibrium Properties of a System of Interacting Electrons. *Phys. Rev.*, 119:1153, 1960. VIII, 2, 51
- [67] J. M. Luttinger. Analytic Properties of Single Particle Propagators for Many-Fermion Systems. *Phys. Rev.*, 121:942, 1961. VIII, 2
- [68] J. M. Luttinger. *J. Math. Phys.*, 4:1154, 1963. IX, 3
- [69] J. M. Luttinger and J. C. Ward. Ground-State Energy of a Many-Fermion System. II. *Phys. Rev.*, 118:1417, 1960. 51

- [70] R. Markiewicz and M. Vaughn. Classification of the Van Hove Scenario as an $SO(8)$ Spectrum-Generating Algebra. *Phys. Rev. B*, 57:14052, 1998. 81
- [71] N. Mathur, F. Grosche, S. Julian, I. Walker, D. Freye, R. Haselwimmer, and G. Lonzarich. Magnetically Mediated Superconductivity in Heavy Fermion Compounds. *Nature*, 394:39, 1998. 53
- [72] Y. Matsushita, M. P. Gelfand, and C. Ishii. Phase Transitions in Bilayer Heisenberg Model with General Couplings. *J. Phys. Soc. Jpn.*, 66:3648, 1997. 66
- [73] D. C. Mattis and E. H. Lieb. *J. Math. Phys.*, 6:304, 1963. IX, 3
- [74] N. D. Mermin. Thermal Properties of the Inhomogeneous Electron Gas. *Phys. Rev.*, 137:A1441, 1965. 122
- [75] K. Miyagawa, A. Kawamoto, K. Uchido, and K. Kanoda. Commensurate Magnetic Structure in κ -(BEDT-TTF)₂X. *Physica B*, 284:1589, 2000. 75
- [76] K. Miyagawa, A. Kawamoto, Y. Nakazawa, and K. Kanoda. Antiferromagnetic Ordering and Spin Structure in the Organic Conductor, κ -(BEDT-TTF)₂Cu[N(CN)₂]Cl. *Phys. Rev. Lett.*, 75:1174, 1995. 75
- [77] N. F. Mott. *Proc. Phys. Soc. London, Ser. A*, 62:416, 1949. IX, 3
- [78] J. Müller, M. Lang, R. Helfrich, F. Steglich, and T. Sasaki. High-Resolution Ac-Calorimetry Studies of the Quasi-Two-Dimensional Organic Superconductor κ -(BEDT-TTF)₂Cu(NCS)₂. *Phys. Rev. B*, 65:140509, 2002. 75
- [79] J. Müller, M. Lang, F. Steglich, J. Schlueter, A. Kini, and T. Sasaki. Evidence for Structural and Electronic Instabilities at Intermediate Temperatures in κ -(BEDT-TTF)₂ X for X=Cu(N(CN)₂) Cl, Cu(N(CN)₂) Br and Cu(NCS)₂ : Implications for the Phase Diagram of These Quasi-Two-Dimensional Organic Superconductors. *Phys. Rev. B*, 65:144521, 2002. 73, 74
- [80] J. Negele and H. Orland. *Quantum Many-Particle Systems*. Addison-Wesley, New York, 1987. 107, 114
- [81] E. Nelson. *J. Math. Phys.*, 5:332, 1964. 14, 105

- [82] A. Nowack, M. Weger, D. Schweitzer, and H. Keller. *Solid State Commun.*, 60:199, 1986. 75
- [83] M. Oshikawa. Topological Approach to Luttinger's Theorem and the Fermi Surface of a Kondo Lattice. *Phys. Rev. Lett.*, 84:3370, 2000. 51
- [84] K. Oshima, T. Mori, H. Inokuchi, H. Urayama, H. Yamochi, and G. Saito. Shubnikov-de Haas Effect and the Fermi Surface in an Ambient Pressure Organic Superconductor κ -(BEDT-TTF)-Cu(NCS)₂. *Phys. Rev. B.*, 38:938, 1988. 75
- [85] L. Pintschovius, H. Rietschel, T. Sasaki, H. Mori, S. Tanaka, N. Toyota, M. Lang, and F. Steglich. Observation of Superconductivity-Induced Phonon Frequency Changes in the Organic Superconductor κ -(BEDT-TTF)₂-Cu(NCS)₂. *Europhys. Lett.*, 37:627, 1997. 75
- [86] W. H. Press, B. P. Flannery, S. A. Teukolsky, and W. T. Vetterling. *Numerical Recipes: The Art of Scientific Computing*. Cambridge University Press, Cambridge, 1988. 36, 40
- [87] R. Preuss, W. Hanke, and W. von der Linden. Quasiparticle Dispersion of the 2D Hubbard Model: From an Insulator to a Metal. *Phys. Rev. Lett.*, 75:1344, 1995. 68
- [88] S. Sachdev. *Quantum Phase Transitions*. Cambridge University Press, Cambridge, 1999. 123
- [89] S. Sachdev and R. N. Bhatt. Bond-Operator Representation of Quantum Spins: Mean-Field Theory of Frustrated Quantum Heisenberg Antiferromagnets. *Phys. Rev. B*, 41:9323–29, 1990. 59
- [90] G. Schmidt, S. Todo, M. Troyer, and A. Dorneich. Finite-Temperature Phase Diagram of Hard-Core Bosons in Two Dimensions. *Phys. Rev. Lett.*, 88:167208, 2002. 92
- [91] L. S. Schulman. *Techniques and Applications of Path Integration*. Wiley, New York, 1981. 14, 16

- [92] H. Schulz. Fermi-Surface Instabilities of a Generalized Two-Dimensional Hubbard Model. *Phys. Rev. B*, 39:2940, 1989. 81
- [93] P. Sinjukow and W. Nolting. Exact Mapping of Periodic Anderson Model to Kondo Lattice Model. *Phys. Rev. B*, 65:212303, 2002. 51
- [94] A. Sokal. Monte Carlo Methods in Statistical Mechanics: Foundations and New Algorithms. *Cours de Troisieme Cycle de la Physique en Suisse Romande*, page citeseer.nj.nec.com/sokal96monte.html, 1989. 13
- [95] S. Sorella, S. Baroni, R. Car, and M. Parrinello. *Europhys. Lett.*, 8:663, 1989. 40
- [96] S. Sorella, E. Tosatti, S. Baroni, R. Car, and M. Parrinello. *Int. J. Mod. Phys. B*, 1:993, 1989. 40
- [97] N. Straumann. *Thermodynamik*. Springer, Berlin, 1986. 117
- [98] W. P. Su, J. R. Schrieffer, and A. J. Heeger. Soliton Excitations in Polyacetylene. *Phys. Rev. B*, 22:2099, 1980. XV, 8, 75, 78, 100
- [99] A. Sumiyama, Y. Oda, H. Nagano, Y. Onuki, K. Shibusaki, and T. Komatsubara. 50
- [100] M. Suzuki. *Commun. Math. Phys.*, 51:183, 1976. 15
- [101] M. Tanatar, T. Ishiguro, H. Ito, M. Kubota, and G. Saito. Hall Effect and Magnetic Viscosity Phenomena in κ -(BEDT-TTF)₂Cu[N(CN)₂]X (X=Cl,Br). *Phys. Rev. B*, 55:12529, 1997. 75
- [102] H. F. Trotter. *Proc. Am. Math. Soc.*, 10:545, 1959. 14
- [103] H. Tsunetsugu, M. Sigrist, and K. Ueda. The Ground-State Phase Diagram of the One-Dimensional Kondo Lattice Model. *Rev. Mod. Phys.*, 69:809, 1997. 54, 55, 57, 58, 63
- [104] G. Visentini, A. Painelli, A. Girlando, and A. Fortunelli. The Dimer Model for κ -Phase Organic Superconductors. *Europhys. Lett.*, 42:467, 1998. 76

- [105] V. Viswanath, S. Zhang, J. Stolze, and G. Müller. Ordering and Fluctuations in the Ground State of the One-Dimensional and Two-Dimensional $\frac{1}{2}XXZ$ Antiferromagnets: A Study of Dynamical Properties Based on the Recursion Method. *Phys. Rev. B*, 49:9702, 1994. [125](#), [126](#)
- [106] M. Vojta and K. W. Becker. Doped Bilayer Antiferromagnets: Hole Dynamics on Both Sides of a Magnetic Ordering Transition. *Phys. Rev. B*, 60:15201–213, 1999. [72](#)
- [107] S. R. White, D. J. Scalapino, R. L. Sugar, E. Y. Loh, J. E. Gubernatis, and R. T. Scalettar. Numerical Study of the Two-Dimensional Hubbard Model. *Phys. Rev. B*, 40:506–516, 1989. [40](#)
- [108] K. Wilson. The Renormalization Group: Critical Phenomena and the Kondo Problem. *Rev. Mod. Phys.*, 47:773, 1975. [48](#)
- [109] J. Wosnitza. *Fermi Surfaces of Low-Dimensional Organic Metals and Superconductors*. Springer, Berlin, 1996. [75](#)
- [110] M. Yamanaka, M. Oshikawa, and I. Affleck. Nonperturbative Approach to Luttinger’s Theorem in One Dimension. *Phys. Rev. Lett.*, 79:1110, 1997. [51](#)
- [111] C. N. Yang and S. C. Zhang. Eta Operator Introduced Bla. *Mod. Phys. Lett.*, B 4:759, 1990. [79](#)
- [112] K. Yosida. Bound State Due to the $s-d$ Exchange Interaction. *Phys. Rev.*, 147:223, 1966. [48](#)
- [113] G.-M. Zhang, Q. Gu, and L. Yu. Kondo Spin Liquid and Magnetically Long-Range Ordered States in the Kondo Necklace Model. *Phys. Rev. B*, 62:69–72, 2000. [53](#)
- [114] G.-M. Zhang and L. Yu. Kondo Singlet State Coexisting with Antiferromagnetic Long-Range Order: A Possible Ground State for Kondo Insulators. *Phys. Rev. B*, 62:76, 2000. [58](#), [70](#)

Publications

Parts of this thesis were published in the following articles:

M. Feldbacher and F. F. Assaad. Efficient Calculation of Imaginary Time Displaced Correlation Functions in the Projector Auxiliary Field Quantum Monte-Carlo Algorithm. *Phys. Rev. B*, 65:073105, 2001.

M. Feldbacher, C. Jurecka, F. F. Assaad, and W. Brenig. Single Hole Dynamics in the Half-Filled Two-Dimensional Kondo-Hubbard Model. *Phys. Rev. B*, 66:045103, 2002.

M. Brunner, C. Lavallo, S. Capponi, M. Feldbacher, F. F. Assaad, and A. Muramatsu. Single Hole Dynamics in Correlated Insulators. In E. Krause and W. Jäger, editors, *High Performance Computing in Science and Engineering '01*, Berlin, 2002. Springer-Verlag.

F. F. Assaad, V. Rousseau, F. Hebert, M. Feldbacher, G. G. Batrouni. Spin and charge dynamics of stripes in doped Mott insulators. *Europhys. Lett.*, 63:569,2003.

M. Feldbacher, F. F. Assaad, F. Hebert, G. G. Batrouni. Coexistence of s-wave Superconductivity and Antiferromagnetism . *Phys. Rev. Lett.*, 91:056401, 2003

C. Lavallo, M. Rigol, M. Feldbacher, F. F. Assaad, and A. Muramatsu. Thermodynamics and dynamics of correlated electron system. In E. Krause and W. Jäger, editors, *High Performance Computing in Science and Engineering '02*, Berlin, 2003. Springer-Verlag.

Curriculum Vitae

Surname: Feldbacher
First name: Martin
Nationality: Austrian
Date of birth: December 3rd, 1970
Place of birth: Graz, Austria
Marital status: unmarried

1977-1981: Primary school: *Volkschule Andritz*, Graz

1981-1989: Secondary school: *Bundesgymnasium Carnerig.*, Graz

1989-1989: University: Diplom (Auszeichnung) at University “Karl-Franzens”, Graz
Diploma work: *Two Magnon Raman Scattering in Cuprates:*
Supervisors: Prof. Ewald Schachinger (Technical University of Graz)
and Prof. Peter Knoll (University “Karl-Franzens”, Graz)

1991-1992 Exchange student at the University of Utah, USA

1999-2003 PhD work at Universität Stuttgart:
Hubbard and Kondo lattice Models in two dimensions:
A QMC study
Supervisor: Prof. Dr. Fakhher Assaad

5/2001,8/2001 Research Visits at INLN, Nice

10-12/2001 Visit at “Laboratoire de Physique Quantique”, Toulouse, France

9/2002 Research Visit at INLN, Nice

Acknowledgments

It is four years ago that I decided to come to Stuttgart in order to continue physics as a Ph.D. student in the group of Prof. Muramatsu. Today I have written my thesis and passed the exam so it is time to thank all the people who have directly and indirectly contributed to this thesis.

First of all I would like to thank my supervisor Prof. Fakher Assaad. More a friend than a boss he has been a constant source of encouragement throughout my work. He has provided the intellectual background and many of the interesting questions discussed in this thesis. Furthermore, I could tap the vast repository of his QMC programs which was an invaluable help. Furthermore Dr. Assaad had incredulous patience with my stubborn and sometimes misguided questions. I am deeply indebted to him for keeping me on track when I was going in the wrong direction.

I would also like to thank Prof. Alejandro Muramatsu for his enduring support and giving precise and critical comments at every stage. Prof. Muramatsu is also responsible for the very pleasant atmosphere at the institute where I had the chance to work with a number of nice collaborators. Dr. Sylvain Capponi joined our group for a year as a postdoc and had been a wonderful person to work with. I had the chance to meet him again during a three month visit at the university of Toulouse, where I want to thank Prof. Didier Poilblanc for his hospitality. I very much enjoyed the time in Toulouse, not the least because I shared office with Fabian Alet and Alex Lefèvre, at the time Ph.D. students who welcomed me very warmly.

At home in Stuttgart I would specially like to mention Lorenzo Campos-Venuti. We spent a lot of time discussing physics and he never lost his patience (unlike me). I also want to thank Catia Lavallo and Marcos Rigol who spent many extra hours keeping our computer system up and running. I am glad to thank Mitsuhiro Arikawa for his time and friendship. And special thanks to Fr. Poljak who solved all the bureaucratic problems I

encountered.

I also want to thank Prof. Roland Zeyher for taking the burden of being referee and examiner for my Ph.D. examination.

I enjoyed very much collaboration with Christoph Jurecka and Wolfram Brenig on the UKLM. Thanks to the joint Franco-German cooperative grant (PROCOPE) I had the opportunity to pay several visits to ILNL in Nice. Prof. Batrouni and Frederic Hébert were very warm and welcoming hosts. The calculations were carried out on the Cray T3E of the HLRS (Stuttgart) and I thank the DFG for financial support under the grant numbers MU 820/10-1 and AS 120/1-3.

Of the many people who made my time in Stuttgart more enjoyable I want to thank Ruth Gaier, Andrea Hause and many others. A warm “Thank You” goes to Ute Crummenauer.

I want to dedicate this work to my parents. It is their support and love that made it possible.